Behaviour of Monazite and Evolution of Polymetamorphic Pelites from the Monte Rosa Nappe, Western Central Alps, Italy.

Inauguraldissertation
der Philosophisch-naturwissenschaftlichen Fakultät
der Universität Bern

vorgelegt von

Nadim C. Scherrer

von Nesslau SG

Leiter der Arbeit:

Prof. M. Engi

Mineralogisch-petrographisches Institut, Universität Bern

Behaviour of Monazite and Evolution of Polymetamorphic Pelites from the Monte Rosa Nappe, Western Central Alps, Italy.

Inauguraldissertation
der Philosophisch-naturwissenschaftlichen Fakultät
der Universität Bern

vorgelegt von

Nadim C. Scherrer

von Nesslau SG

Leiter der Arbeit:

Prof. Dr. M. Engi

Mineralogisch-petrographisches Institut, Universität Bern

Von der Philosophisch-naturwissenschaftlichen Fakultät angenommen.

Bern, 8. Februar 2001

Der Dekan
Prof. Dr. P. Bochsler

P. Bochsler

Foreword

This thesis has developed over the course of the past four years - seemingly a never-ending story. The conversion from a quaternary geomorphologist and master of palaeomagnetism of speleothems to an Alpine hardrock petrologist with geochronologic features, was tougher than expected back in the enthusiastic days of my return to the much beloved Alpine world. The attractive fieldwork let me explore the Monte Rosa massif with much joy and keenness, but when it got down to the nitty gritty, work wasn't always as motivating. Somewhere along the way I found myself lost in the labyrinth of the secrets of monazite. The struggle went on, culminating in a serious midlife crisis. It was time to learn how to swim properly and progress followed shortly after the first few lessons in the pool.

Now that it has come to an end, it looks short and simple. One wonders how time has been wasted to get only this far. But since it is all that easy, why didn't anyone tell me before? Things rarely work on first try, and if they do, one only learns half as much as if they don't. In this regard I went through a rather steep learning curve... And be reminded that to all theory there is a practical side to it.... doing rarely matches the ease of saying and some things are more of an art than simple routine.

The XRF-microprobe, originally planned to become a basic working tool for my PhD by the end of my second year, had its initiation well into my fourth year. It has been an intensive but rewarding burst since.

Late at night I often wondered why and what for, but giving up stayed out of question. As long as there is this persisting quest to find out, there is energy and patience to learn and try. The relieving 'yes, it works'is ample satisfaction.

In the days of interactive communication, a homepage seemed an appealing way to make the colours of research accessible to a wider community beyond the working and scientific environment. The reader is invited to a surf along the shores of http://www.earthsci.unibe.ch/people/scherrer/Main.htm. Take it as a complementary to this thesis.

Acknowledgements

This project has been fully funded by the Swiss National Fonds. I am extremely grateful to all those people who helped in any way or other in the making of this thesis. Special thanks go to:

Claudia for all her love and care and enjoyment she has been giving me. Her assistance, persistence and patience going through a bit of a tough time... and for never stopping believe in me.

My parents on the other side of the globe, far off the beautiful Swiss mountains, for their never ending support with natural Aussie power and love.

Gotte and Eddie Frey-Schwyn for their invaluable support with natural Swiss power (chestnut honey and goat's cheese...) and their much appreciated hospitality any time during my fieldwork.

Bärnu for all those spontaneous and most enjoyable powder thrills and scenic training rides over the last four years of living in Bern - brain recovery is an essential part of life.

My supervisor Prof Martin Engi who let me discover the Monte Rosa in a most enjoyable way. His care for all those supplements during the more hungry moments of life has always been much appreciated. I bet it has taken a fair bit of patience over the last four years...

Prof Larryn Diamond for his moral support and the deadly possum stories. He has been a great teacher, not just in microprobing.

Dr Andriy Cheburkin and Dr Alfons Berger for their efforts in getting the XRF-microprobe running before my time ran out...

Prof Randy Parrish and Dr Gavin Foster for their hospitality in Nottingham and time and help with the LA-PIMMS analysis at BGS Nottingham.

Prof Christian Chopin for his interest and easy communication concerning the bearthite story.

Dr Dieter Rhede and Prof Wilhelm Heinrich of GFZ Potsdam for scientific exchange and their hospitality at an earlier stage of my PhD.

Dr Greg Roselle for introducing me to the production of synthetic standard minerals.

Dr Edwin Gnos who very often was the best address for a quick answer... a favourite for efficient teamwork.

Prof Tjerk Peters for finally agreeing on the benefits of a smoke-free working environment...

Dr Urs Eggenberger, Ulli Linden and Werner Zaugg for passing on their computing experience and assistance whenever it was needed.

Vreni Jakob, Ruth Mäder, Jürg Megert and Adrian Liechti who were always helpful with impeccable thin sections, chemically related supplies or technical solutions. Extra compliments go to Vreni for her special service of an unknown number of immaculate thin sections polished lead free.

Lina Bobade and Isabelle Jobin for efficient support with any administrative questions.

Thomas Burri for the good teamwork in the field, the lab and many other aspects leading to a fruitful learning environment. Discussions in skier's latin always brought relief when nothing else lead to success...

More thanks go to Andreas Jenni as a master of the SEM buttons, Daniel Traber for EMP problem solving, Valérie Grandjean for the odd exchange on petrographic questions, Giancarlo Rizzoli for XRD related questions, Marc Hauser for the swimming lessons, Mathias Rickli for the odd midnight chat and Rico Senti for his unforgettable company on the most thrilling fieldtrip.

And, of course, anyone who slipped through my memory.

Abstract

Despite the recognised importance of monazite in geochronology, the contextural information is lost when using standard mineral separation techniques. To overcome this problem, new techniques were developped to date monazite in thin section or as grains drilled out from thin sections.

Chemical Th-U-Pb dating of monazite on the microprobe is limited to grains older than 200 Ma, due to the high detection limit. Moreover, a range of fundamental analytical and preparational problems remains. For example, for monazite containing 12% Th, the commonly disregarded interference of Th Mz on Pb Ma causes an overestimation of 11% (relative) in Pb. This propagates to an age overestimation of ~50 Ma for a sample of 400 to 500 Ma in age. A judicious choice of X-ray peaks used in quantitative EMP analysis avoids or minimises peak overlap for all elements, including REE.

A newly developped XRF-microprobe achieves superior performance, permitting to date small grains (< 100 µm) as young as Miocene in age. As an example, the precision achieved with the XRF-microprobe for a well characterised monazite age standard FC-1 (TIMS age 54.3 Ma; µ-XRF age 55.3 ± 2.6 Ma), doubly polished to 30 µm in thickness, is below 5 % (2 sigma) after 90 minutes integration time (50 kV; 30 mA) at a spatial resolution of 90 µm. Special sample preparation techniques using a PE-polishing disk permit the sequential use of thermobarometric and geochronometric analytical tools and thus the potential to derive time-calibrated P-T paths. The first two papers describe methods for sample preparation, analysis techniques and data interpretation for electron microprobe and XRF-microprobe dating.

In the other two papers the techniques are tested on pelitic rocks of the Monte Rosa nappe, western Central Alps, which is believed to have played a key role in the tectono-metamorphic evolution of the Central and Western Alps. In these rocks monazite occurs in different textures. Similarities to the better known Adula - Cima Lunga nappes further east hint at a potentially equivalent late emplacement history from depths in excess of 70 km during Alpine orogenesis. Studying the polymetamorphic basement rocks of the Monte Rosa nappe successfully revealed new insight into the complex history of this fragment of continental crust with European affinity. Careful analysis applying the chemical Th-U-Pb dating technique unveiled two distinct phases of monazite growth in these rocks: a Permian one around 280 Ma, believed to be associated with the intrusion

of the Monte Rosa granite; and an Alpine one around 35 Ma, attributed to the timing of high pressure metamorphism when maximum depths were reached during continental subduction. The combination of geochronometry and thermobarometry, sequentially applied ‘in-situ’ demonstrates the potential of this new technique.

While monazite dating is frequently used for geochronometry, there exists also a relative lack of knowledge of monazite-forming reactions which is commonly fundamental for an age interpretation. Fine-grained symplectites of monazite, apatite and corundum within allanite of the Monte Rosa nappe have been recognized as breackdown product from bearthite. Similar textures have also been observed in the Dora-Maira high pressure terrane. Bearthite $Ca_2Al[PO_4]_2(OH)$, an aluminium phosphate contains up to ~10 wt% of light rare-earth elements (LREE) + Th. The documented symplectitic textures are assumed to be related to rapid decompression, following high to ultra-high pressure conditions during Tertiary subduction. The systematic study of bearthite from the Monte Rosa type locality and the Dora Maira area revealed that bearthite fractionates LREE, Th and U similar as monazite. This indictes a potential use of bearthite for age dating of ultra-high pressure rocks.

Contents

General introduction

This thesis consists of four self-contained components, each presented in the style of a journal publication.

The objective of this project was to contribute to the understanding of the evolution of pelitic rocks from the polymetamorphic Monte Rosa nappe. Part four may be regarded as the synthesis of this research, combining newly developed techniques along the way to a field related geologic question.

Precise geochronology is fundamental to the understanding of many processes of the Earth system. Thus, the development of an affordable 'in-situ' dating technique is of considerable value, certainly to petrologists in their quest for time-calibrated P-T paths. Particular emphasis of this project was to be given on exploring and exploiting the potential of chemical Th-U-Pb geochronometry on the thorium bearing phosphate mineral monazite $(REE)PO_4$ by applying a promising new and low cost XRF technique. This technique is presented in part three, which gives information on the details of the instrument, dating methodology, and a direct comparison of performance of the XRF-microprobe based on independent mass spectrometry.

Since there has been a relative lack of knowledge concerning the metamorphic processes causing the growth and decay of monazite, much effort has gone into the full (chemical and textural) documentation of this mineral phase as it occurs in the pelitic rocks of the Monte Rosa paragneisses. Few monazite-forming reactions are known to date despite their relative importance to the interpretation of geochronometric information. Part two constitutes a documentation of a previously unknown monazite-forming reaction and as such contributes to a better understanding of monazite behaviour in pelitic rocks.

The non-trivial nature of the full chemical characterisation of this rare-earth element bearing mineral by electron microprobe led to a major analytical effort, culminating in the published first part of this thesis which already has received much appreciation as a practical guide to many other researchers in this field of Earth science.

SCHWEIZ. MINERAL. PETROGR. MITT. 80, 93-105, 2000

Monazite analysis; from sample preparation to microprobe age dating and REE quantification

by *N.C. Scherrer , M. Engi*[1]*, E. Gnos, V. Jakob* and *A. Liechti*

Abstract

Despite the recongnized importance of monazite in geochronology and petrology, a range of fundamental analytical and preparational problems remains. For example, chemical Th-U-Pb dating of monazite requires special lead-free sample preparation. This is achieved efficiently and at high quality with specially developped grooved ND-PE polyethylene polishing disks. Techniques useful in locating and characterizing monazite are evaluated. Back scattered electron imaging is an effective way to determine zonation patterns, particularly with respect to thorium. Quantitative analysis of monazite by EMP is delicate and time consuming. A whole series of X-ray peak interferences has been ignored in published work. For example, for monazite containing 12% Th, the commonly disregarded interference of Th Mz on Pb Ma causes an overestimation of 11% (relative) in Pb. This propagates to an age overestimation of ~50 Ma for a sample of 400 to 500 Ma in age. A judicious choice of X-ray peaks used in quantitative EMP analysis avoids or minimises peak overlap for all elements, including REE. Only for U a correction factor is required: $U\ wt\%_{corrected} = U\ wt\%_{measured} - (0.0052 * Th\ wt\%_{measured})$ based on the analytical lines U Mb and Th Ma.

Keywords: EMPA, REE, monazite, polishing, sample preparation, chemical dating, Th-U-Pb dating

Introduction

Monazite is increasingly recognized as a powerful mineral for age dating in a wide variety of igneous (MOUGEOT et al., 1997), metamorphic (BINGEN AND VAN BREEMEN, 1998; BRAUN et al., 1998; KINGSBURY et al., 1993; PAQUETTE et al., 1999; PARRISH, 1990; SUZUKI AND ADACHI, 1994) and even diagenetic (EVANS AND ZALASIEWICZ, 1996) environments. Monazite does not "incorporate" appreciable common lead during growth and thus all of its lead is radiogenic, from the decay of Th and U. This eliminates the need for an isotopic correction for common lead. The possibility to date monazite older than ~200 Ma with the electron microprobe (EMP), a non-destructive, in-situ, high-resolution, and accessible method, has enhanced the mineral's popularity as a chronometer. Various other methods (e.g. ion microprobe, LA-ICP-MS, XRF) allow dating of geologically young monazite, giving this mineral good potential for solving geochronological problems over a wide range of time. Problems identified in monazite geochronology range from sample preparation (contamination with lead) to analytical complications (X-ray line interference) to complex processes during and following the formation of monazite (^{230}Th disequilibrium, Pb loss, U excess, single grain zoning).

Relatively little is known about monazite forming reactions despite its importance for a better interpretation of P-T-t data. To decipher such reactions, quantitative microanalysis of monazite in thin section is indispensible. ANDREHS AND HEINRICH (1998) demonstrated the use of monazite in temperature-calibrated geochronology, requiring complete quantitative analysis of coexisting xenotime and monazite. On reviewing published EMP analyses of monazite, considerable differences in the quality of the analyses have become apparent.

The present paper addresses mainly technical aspects of finding, analysing and chemically dating monazite. We report techniques specifically deve-

[1] Mineralogisch-petrographisches Institut, Universität Bern, Baltzerstrasse 1, CH-3012 Bern, Switzerland.
<engi@mpi.unibe.ch>

lopped for sample preparation, characterization and analysis of monazite. While monazite is a frequent accessory in various rock types, it is by no means easy to find and identify by the untrained eye. We evaluated a range of techniques to locate this mineral in context and present information on their relative merits.

Sample preparation

Th-U-Pb dating by the EMP requires lead-free polishing. While this can be time consuming for large series, a method is presented to achieve excellent polish with an efficiency competitive to conventional polishing techniques.

Conventional lead disks are unsuitable for the production of thin sections for Th-U-Pb analysis on the EMP because they deposit lead at grain boundaries, filling in surface irregularities and thus contaminating the sample. Lead-free polishing disks made of ND-PE Polyethylene have achieved astonishing results, though only after special treatment of the abrasive surface. Using a Schaublin lathe, a spiral groove of 0.1 mm depth was cut at 75 rotations per minute and 150 mm/min radial progression (Fig. 1). This reduced the total polishing time from days to less than 3 hours. It proved necessary to make adjustments to the sequence of abrasives used; the currently most successful procedure is listed in table 1. The quality of surface polish achieved by this method is equivalent to conventional techniques (using a lead disk), with comparable preparation efficiency.

Finding monazite

A range of methods has been tried with variable success. Cathode luminescence and UV luminescence, applicable to zircon, are unsuitable. Monazite does not luminesce with either technique. By far the most efficient and practical method is scanning (lead-free) polished thin sections in BSE-mode, using the EMP. The methods evaluated are outlined and detailed recommendations are given.

OPTICAL MICROSCOPY

Petrographic microscopy of thin sections provides an efficient way to find heavy minerals in their textural context. Detecting monazite with reasonable certainty, however, requires experience, and even with all that, monazite is not always clearly distinguishable from zircon, allanite, xenotime or titanite. Some practical hints are given on distinctive characteristics of the various phases, always in comparison with monazite.

Zircon: in reflected light, zircon is distinctly brighter than monazite; zircon is often euhedral with elongate shapes and occurs mostly as single grains whereas monazite tends to show rounded or irregular shapes and often occurs as clusters or in trails; the low uranium and thorium content in zircon implies that radiation damage to the host minerals becomes visible only if the rocks exceed several hundred million years in age.

Allanite has low interference colors (1st order grey to brown) whereas monazite generally shows

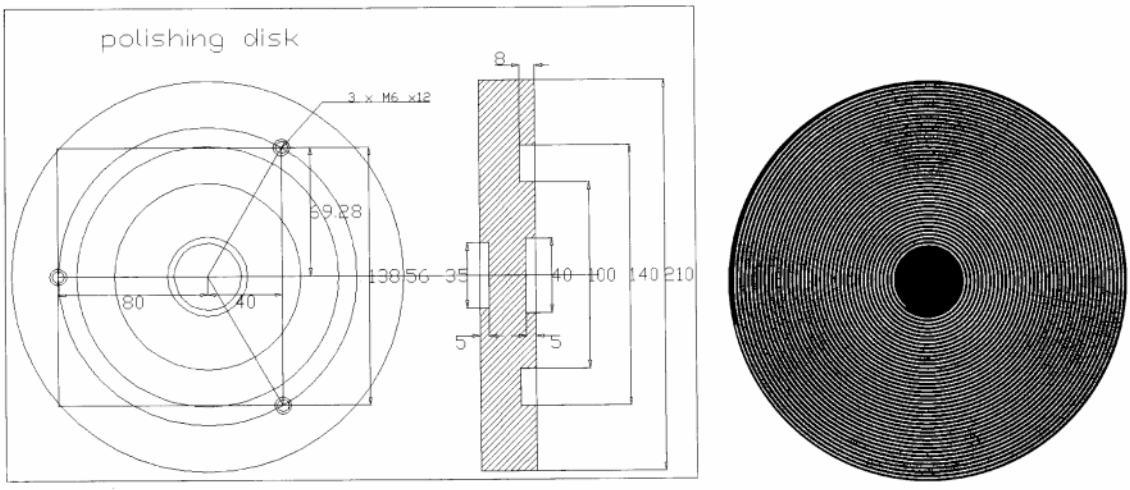

Fig. 1 Plan of the ND-PE Polyethylene disks with spiral groove pattern developed for lead-free thin section preparation at the University of Bern. Measurements are in mm.

Tab. 1 Overview of lapping and polishing procedure.

LAPPING			
Steps	**Disk**	**Abrasive**	**Time in min**
1	Cast iron	SiC 600 plus water	30
2	Glass plate (by hand)	SiC 800 plus water	1 to 2
POLISHING			
Steps	**Disk**	**Abrasive**	**Time in min**
1*	PE disk with spiral grooves	Stähli AWS-WS-4-8/19 plus AWS-DS-5-8 10.0	2 x 30
2*	PE disk with spiral grooves	Stähli AWS-WS-2-3/20 plus AWS-DS-2-4 10.0	2 x 30
3*	PE disk with spiral grooves	Stähli AWS-WS-1/20 plus AWS-DS-0.75-1.5 10.0	1-2 x 30
* after each step, the PE disks are roughened with a diamond ring			

distinctly higher ones (third order blue to fourth order green or yellow); simple twinning is common in allanite, not so in monazite which may exhibit multiple twinning. Euhedral grain shapes and color zoning are typical features of allanite, and grain sizes exceeding 100 m are common; pleochroic halos around allanite (and monazite!) are common in biotite and chlorite, even in rocks younger than 50 Ma.

Xenotime is virtually indistinguishable from monazite, apart from the lack of halos due to low uranium and low thorium contents.

Titanite similarly occurs as trails; in general, it is easily distinguished in transmitted light showing darker body colors.

Monazite is colorless or faintly colored from yellow to brown, but is clearly distinguishable from rutile. Pleochroic halos in biotite, chlorite and cordierite are a characteristic but non-exclusive feature; interference colors (3rd order) may resemble epidote, zircon or small titanite. Grain shapes and textural relations of monazite vary widely, especially in metamorphic rocks (Fig. 2). Petrographic observation supplemented by electronic imaging (SEM, EMP, see below) provide the best means to identify likely interpretations of geochronologic data. Understanding local phase relations and reaction textures (e.g. BEA and MONTERO, 1999; BINGEN and VAN BREEMEN, 1998; FINGER et al., 1998; SPEAR and PARRISH, 1996) is crucial in linking metamorphic processes to monazite ages.

OPTICAL SPECTROSCOPY

A technique applied to identify gemstones, each having characteristic absorption bands within the visible spectrum. Neodymium, a common constituent in monazite, has absorption lines at 580, 525 and 514 nm (BERNSTEIN, 1982) and these are visible to the trained eye, provided monazite grains have diameters in excess of 60 m. The method is applicable to grain mounts or thick sections.

ALPHA SPUTTERING

This method relies on the emission of alpha particles from the radioactive decay of uranium and thorium. Since monazite may contain up to 30 wt% thorium, sufficient alpha particles are emitted to produce alpha tracks on an alpha emission sensitive film. This is achieved by exposing lightly polished rock sections to Kodak LR115 type 1 film for two weeks or longer. Development times are up to six hours. Unfortunately, metamorphic monazite commonly has Th contents of around 2 to 15 wt%, which is insufficient to produce visible alpha tracks within a month. The method is better suited for minerals such as uraninite (Fig. 3) or thorianite.

SCANNING ELECTRON MICROSCOPE (SEM)

Prerequisites are lead-free polished thin sections coated with either carbon, aluminum or beryllium. The SEM allows complete thin sections to be scanned quite efficiently (magnification 20 x) and provides positive identification of monazite by EDS (energy dispersive spectrometry) analysis. By adjusting the brightness and contrast on the screen, zircon and other bright phases such as ilmenite are easily filtered out such that the remaining bright spots can be examined to distinguish monazite from xenotime with a quick EDS analysis. The imaging features can produce quick digital images at various scales for recognition under the optical microscope. A major drawback of the SEM is the missing optical microscope.

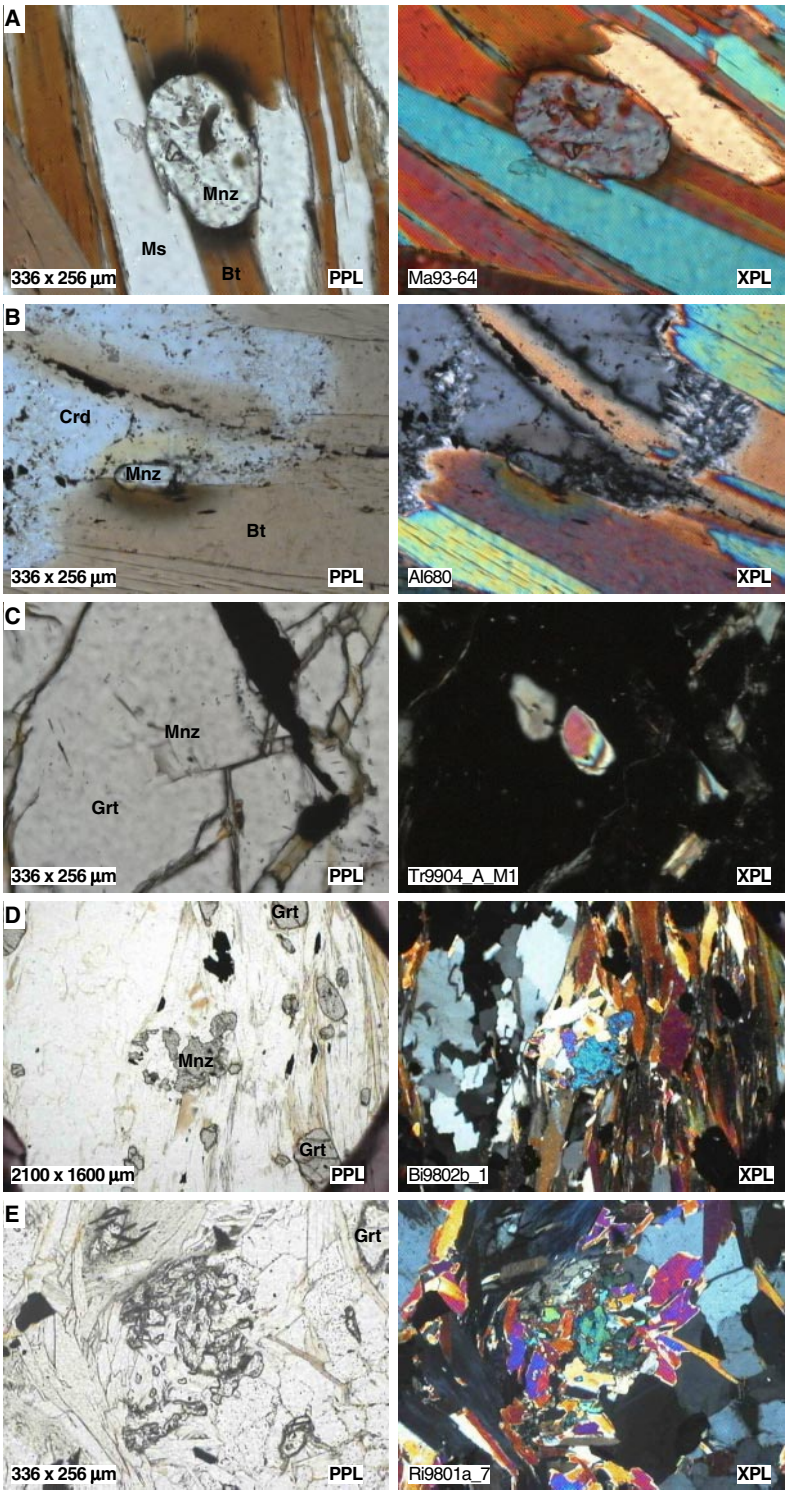

Fig. 2 Monazites in metapelitic rocks under the optical microscope: typical morphologies. Left column: plain polarizers; on right: crossed nicols, same scale.
(A) Single grain monazite with typical rounded shape and pleochroic halo in biotite. (B) Characteristic yellowish pleochroic halo in cordierite and dark halo in biotite. (C) Monazite inclusion in garnet. (D) Pre-kinematic monazite

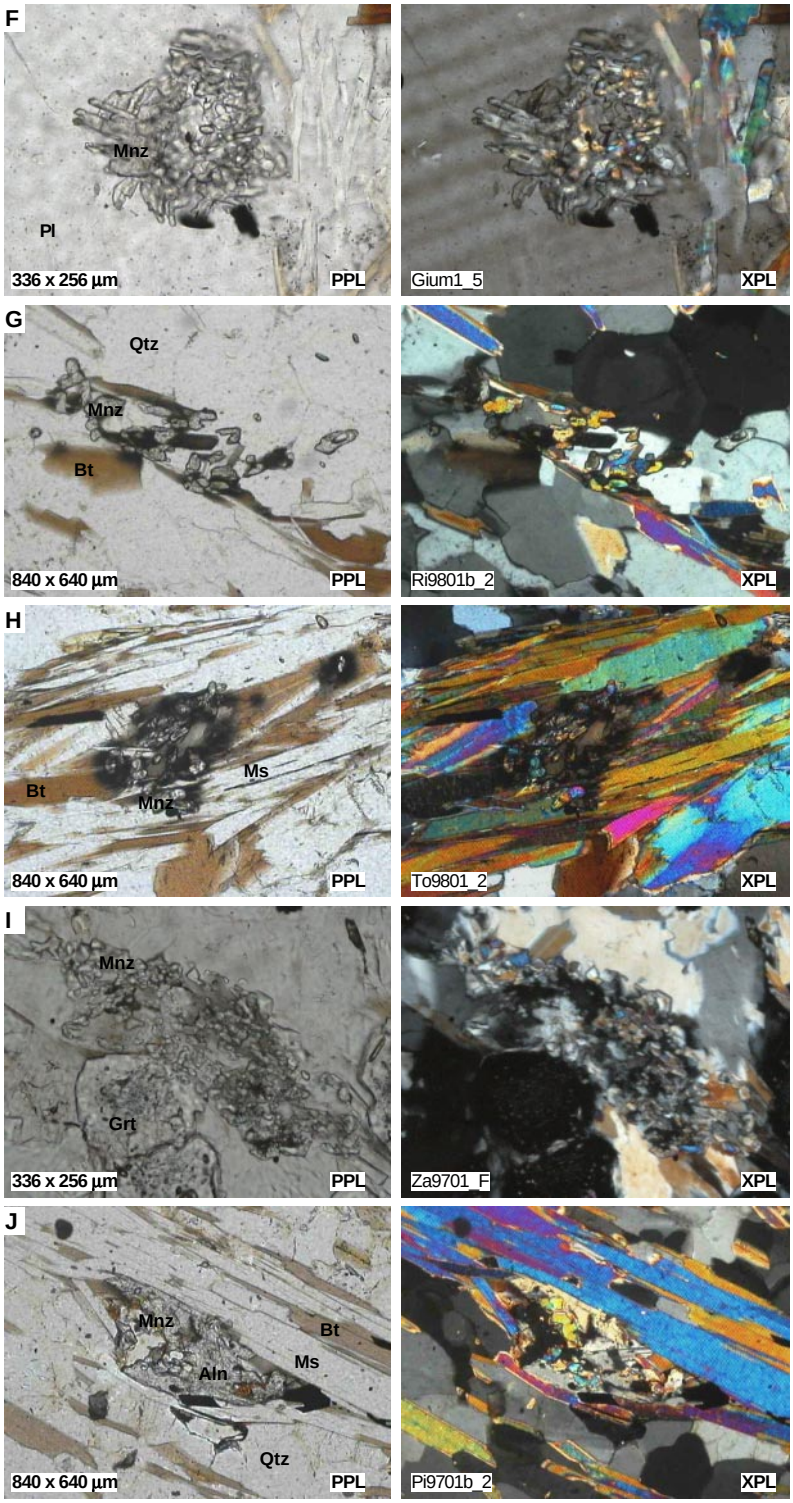

blast in garnet-bearing mica schist. (E) Monazite relic. (F) Vermicular monazite: close arrangement of round or elongated fine-grained monazite. (G) Monazite "trail": "stretched" cluster of small rounded monazite grains. (H) Loose cluster of small rounded monazite grains in biotite. (I) Large cluster of monazite with larger fragments. (J) Monazite associated with allanite

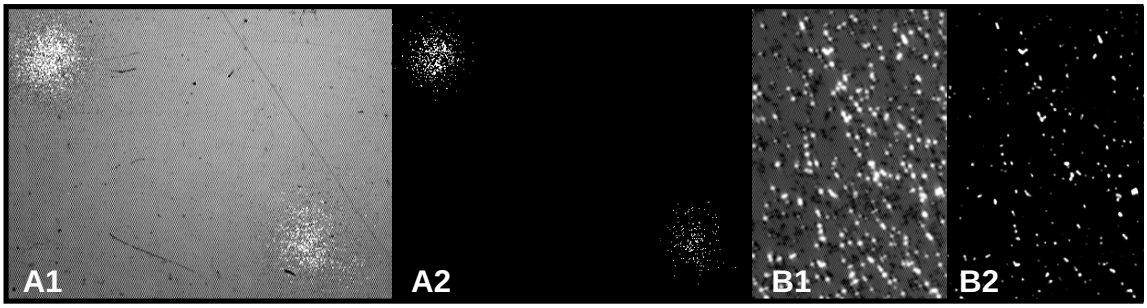

Fig. 3 Alpha tracks emitted from a uraninite bearing sample recorded on Kodak LR115 type 1 film. The tracks can be viewed under a normal petrographic microscope (A1, B1). A2 and B2 are contrast-enhanced images (b&w).

ELECTRON MICROPROBE (EMP)

Again, thin sections must be prepared with lead-free polishing and carbon coated. The EMP combines all of the advantages of finding monazite, imaging zonation patterns, quantification and chemical Th-U-Pb dating of old monazite (>200 Ma, or younger if thorium contents are exceptionally high). Monazite is easily and efficiently localized and mapped using the BSE feature on an electron microprobe.

Tab. 2 Electron microprobe settings from the literature applied to the quantitative analysis of monazite. Note that the critical ionisation energies of the L-lines of elements La to Lu range from 6 keV to 11 keV. Ideally, the accelerating voltage should be 3 to 5 times the ionisation energy, i.e. at least 20 kV.

kV	nA	Reference
15	10	Gratz and Heinrich, 1997; Podor and Cuney, 1997
15	20	Della Ventura et al., 1996; De Parseval et al., 1997
15	40	Van Emden et al., 1997
15	100	Bingen and Van Breemen, 1998
15	150	Suzuki and Adachi, 1994; Crowley and Ghent, 1999
15	250	Finger and Helmy, 1998; Finger and Broska, 1999
15	100	Montel et al., 1996
20	10	Mannucci et al., 1986; Demartin et al., 1991
20	20	Fialin et al., 1997
20	40	Franz et al., 1996; Rhede, GFZ Potsdam, 1999
20	50	Kingsbury et al., 1993; Simmat, Uni Bonn, 1999
20	75	Rapp and Watson, 1986
20	100	Cocherie et al. , 1998
25	130	Montel et al., 1994

EMP quantitative analysis of monazite and xenotime

Quantitative analysis of monazite and xenotime is not trivial and should be planned with care. The considerable number of Rare Earth elements occurring in monazite and xenotime requires careful selection of X-ray lines such that interferences can be kept to a minimum. On examining the recent literature to find EMP settings suitable for monazite analysis, one finds a whole range of analytical strategies (Tab. 2). While there exist several methods to correct for peak overlaps (ÅMLI AND GRIFFIN, 1975; DONOVAN et al., 1993; FIALIN et al., 1997; ROEDER, 1985), it appears to be more sensible to choose lines with negligible interference (EXLEY, 1980), even at the cost of some extra analysis time. Well characterized standard materials are essential and, ideally, synthesized REE-phospates should be used (refer to JAROSEWICH AND BOATNER, 1991). Synthesized glass standards by DRAKE AND WEILL (1972) may be used for minor elements or as secondary standards. With respect to Th-U-Pb dating, ThP_2O_7, a synthesized thorium phosphate, achieved better results than ThO_2, while UO_2 is preferable to

Tab. 3 Absolute background positions recommended by WILLIAMS (1996) for Rare Earth element analysis. Additional positions (this study) are marked with an asterisk *.

LiF	PET
38500	29775
41336*	30735
45400	40970*
51700	45865*
55650	50890*
64750	62510*
67170	

Tab. 4 Critical elements in monazite and xenotime analysis. Data is based on compositions for monazite and xenotime listed in table 5, and on the program VIRTUAL WDS (REED AND BUCKLEY, 1996). Problematic X-ray lines are highlighted. Interference ratios have been calculated for the given mineral compositions and will vary with differing monazite or xenotime compositions (more or less significant). Interference can be ignored if none of the overlapping elements are present, but not otherwise. Xenotime has been included to point at potential problems with Gd thermometry after GRATZ AND HEINRICH (1997). References: 1) ANDREHS AND HEINRICH, 1998; 2) COCHERIE et al., 1998; 3) CROWLEY AND GHENT, 1999; 4) DELLA VENTURA et al., 1996; DEMARTIN et al., 1996; 5) DEMARTIN et al., 1991; 6) FIALIN et al., 1997; 7) FINGER AND BROSKA, 1999; 8) FINGER AND HELMY, 1998; 9) FRANZ et al., 1996; 10) GRATZ AND HEINRICH, 1997; 11) MANNUCCI et al., 1986; 12) MONTEL et al., 1994; 13) PODOR AND CUNEY, 1997; 14) RAPP AND WATSON, 1986; 15) WILLIAMS et al., 1999.

Favored line	X-tal	Wave	I cps	Inferior lines	X-tal	Wave	I cps	Interferences (order)	Wave	I cps	Ratio†	wt % overl.	Elem. wt %	Significance	References (refer to caption)
P Ka1 Mnz	PET	70343	124329					Y Lb1 (1)	71005	36	0.0003	0.004	12.373	-	4); 9); 13); 14)
				P Ka1	TAP	23956	540638	Y Lb1 (1)	24182	2046	0.0038	0.047		-	6)
P Ka1 Xe	PET	70343	158956					Y Lb1 (1)	71005	619	0.0039	0.06	15.521	-	
				P Ka1	TAP	23956	691209	Y Lb1 (1)	24182	35449	0.0513	0.796		**	
La La1 Mnz	LiF	66202	10046									0	9.757	-	9); 14)
				La La1	PET	30468	65962	Nd Ll (1)	30600	839	0.0127	0.124		*	4); 5); 11); 13)
Pr Lb1 Mnz	LiF	56091	2267					La Lb2_15 (1)	57216	16	0.0146	0.031	2.155	*	2); 9)
								Ce Lb6 (1)	56662	17					
				Pr Lb1	PET	25819	8120	La Lb2_15 (1)	26334	74	0.0507	0.109		**	4)
								Ce Lb3 (1)	26407	338					
				Pr La1	PET	28152	15214	La Lb1 (1)	28106	25671	1.6873	3.636		***	5); 11)
Nd Lb1 Mnz	LiF	53809	8093					Dy Ll1 (1)	53615	5	0.0101	0.069	6.806	-	2); 9)
								Ce Lb2 (1)	54855	77					
				Nd La1	LiF	58863	9956	Ce Lb1 (1)	58515	153	0.0154	0.105		*	4); 6)
								Ce Lb4 (1)	58356	0					
				Nd La1	PET	27094	56434	La Lb3 (1)	27571	359	0.0684	0.465		**	5); 11)
								Ce Lb1_4 (1)	26917	3500					
				Nd Lb1	PET	24768	22081	La Lg1 (1)	24505	45	0.0251	0.171		*	
								Ce Lb2_15 (1)	25241	371					
								Sm La1 (1)	25140	139					
Sm Lb1 Mnz	LiF	49623	2989					Er Ll1 (1)	50044	0	0.011	0.021	1.927	*	4); 6); 9)
								Ce Lg1 (1)	50881	15					
								Nd Lb2 (1)	50565	15					
								Tb La1 (1)	49088	3					
				Sm La1	LiF	54624	3702	Ce Lb2 (1)	54855	312	0.0867	0.167		**	2); 14)
								Pr Lb3 (1)	55066	9					
Gd Lb1 Mnz	LiF	45864	2415					Ho La1 (1)	45822	75	0.0311	0.042	1.351	Ho dependent	1); 9); 10)
				Gd La1	LiF	50831	3289	Ce Lg1 (1)	50881	1926	0.6564	0.887		***	4)
								La Lg3 (1)	50709	135					
								Nd Lb2 (1)	50565	98					
Gd La1 Xe	LiF	50831	3655					Ce Lg1 (1)	50881	3	0.0011	0.002	1.471	-	
								La Lg3 (1)	50709	0					
								Nd Lb2 (1)	50565	1					
				Gd Lb1	LiF	45864	2683	Ho La1 (1)	45822	2860	1.066	1.568		***	1); 9); 10)
Tb Lb1 Mnz	LiF	44128	351					Er La1 (1)	44313	19	0.0769	0.014	0.178	Er dependent	1); 9); 10)
								Sm Lg5 (1)	44202	8				**	
				Tb La1	LiF	49085	490	Sm Lb1 (1)	49623	18	0.1469	0.026		**	
								La Lg4 (1)	49277	16					
								Ce Lg10 (1)	48796	30					
								Pr Lg1 (1)	48700	8					
Tb La1 Xe	LiF	49085	2137					Sm Lb1 (1)	49623	1	0.0005	0	0.79	-	
								La Lg4 (1)	49277	0					
								Ce Lg10 (1)	48796	0					
								Pr Lg1 (1)	48700	0					
				Tb Lb1	LiF	44128	1530	Er La1 (1)	44313	493	0.3222	0.255		***	1); 9); 10)
								Sm Lg5 (1)	44202	0					
Er La1 Mnz	LiF	44314	378					Tb Lb1 (1)	44128	51	0.1561	0.021	0.132	Tb dependent	
								Sm Lg5 (1)	44202	6				**	
								Nd Lg3 (1)	44613	2					
				Er Lb1	LiF	39426	243	Gd Lg1 (1)	39548	99	0.4239	0.056		***	9)
								Dy Lb5 (1)	39468	4					
Lu				Lu La1	LiF	40222	60	Sm Lg4 (1)	39907	2	3.4667	0.055	0.016	***	1); 9)
								Gd Lg1 (1)	39548	1					
unresolved!								Ho Lb3 (1)	40241	12					
								Dy Lb2 (1)	40325	193					
				Lu Lb1	LiF	35356	31	Yb Lb2 (1)	35155	2	1.6774	0.027		***	
								Ho Lb1 (1)	35202	2					
								Dy Lg3 (1)	35187	45					
								Tb Lg4 (1)	35427	3					
Pb Mb1 Mnz	PET	58020	561					U Mz2	57707	2	0.0036	0.001	0.269	-	
				Pb Ma1	PET	60393	805	Y Lg2_3	60367	22	0.1106	0.03		**	2); 3); 7); 8); 12); 14); 15)
								Th Mz1,2	59968	67					
U Mb1 Mnz	PET	42475	3795					Th Mg1 (1)	42052	286	0.0754	0.042	0.555	**	9); 12)
				U Ma1	PET	44692	2656	Th Mb1 (1)	45046	791	0.2997	0.166		***	2); 7); 8)
								Ce Lg2-3 (2)	44695	5					

* ratio derived from (sum of interfering counts)/(peak counts of line of interest)*100 = overlap in percent

= overestimation of element in wt% for the composition given from mineral composition table

-- no overlap; - overlap ≤ 1%; * overlap 1 to 4% ; ** overlap 4 to 29%; *** overlap ≥ 30%

elemental U. Concerning the calibration of Pb, either a well characterized crocoite or vanadinite should be given preference over galena, avoiding interference of S on Pb.

Though rarely published, background positions are critical. Because of the very closely spaced X-ray lines of the REE, it is preferable to use global rather than local background positions free of interferences, as suggested by WILLIAMS (1996). Experimentation has shown that for elements from Pr to U it is best to measure upper and lower background on the two closest overlap-free positions (according to Tab. 3) surrounding the peak of interest.

Table 4 summarizes the most relevant overlaps, pointing at the relative overestimation induced by analysis of the inferior line(s). With respect to Th-U-Pb dating of monazite by means of the EMP, it should be interesting to know that neither U Ma nor U Mb are free of significant peak interference related to the Th content. None of the referenced papers indicate correction procedures. To derive a simple correction procedure based on the analytical lines Th Ma and U Mb, theoretical counts were simulated on VIRTUAL WDS (REED AND BUCKLEY, 1996), using monazite compositions with varying amounts of Th. The ratio of interest, determined to be 0.0052 (Tab. 7), is the intensity of Th Mg at the peak position of U Mb over the intensity of the analyzed line Th Ma. Even more relevant with respect to Th-U-Pb dating is the choice between Pb Ma and Pb Mb. While no correction is required to Pb Mb, Pb Ma should be corrected for interfering Th Mz and Y Lg, the former being the more relevant to monazite, commonly being high in Th and low in Y (Fig. 4, Tab. 4). This tends to be neglected (i.e. COCHERIE et al., 1998; CROWLEY AND GHENT, 1999; FINGER AND BROSKA, 1999; FINGER AND HELMY, 1998; MONTEL et al., 1994; SUZUKI AND ADACHI, 1994; WILLIAMS et al., 1999). Uncertainties are relatively high in Th-U-Pb age determinations by EMP, being quite sensitive to variations in Pb. It is thus essential to select the most favorable lines.

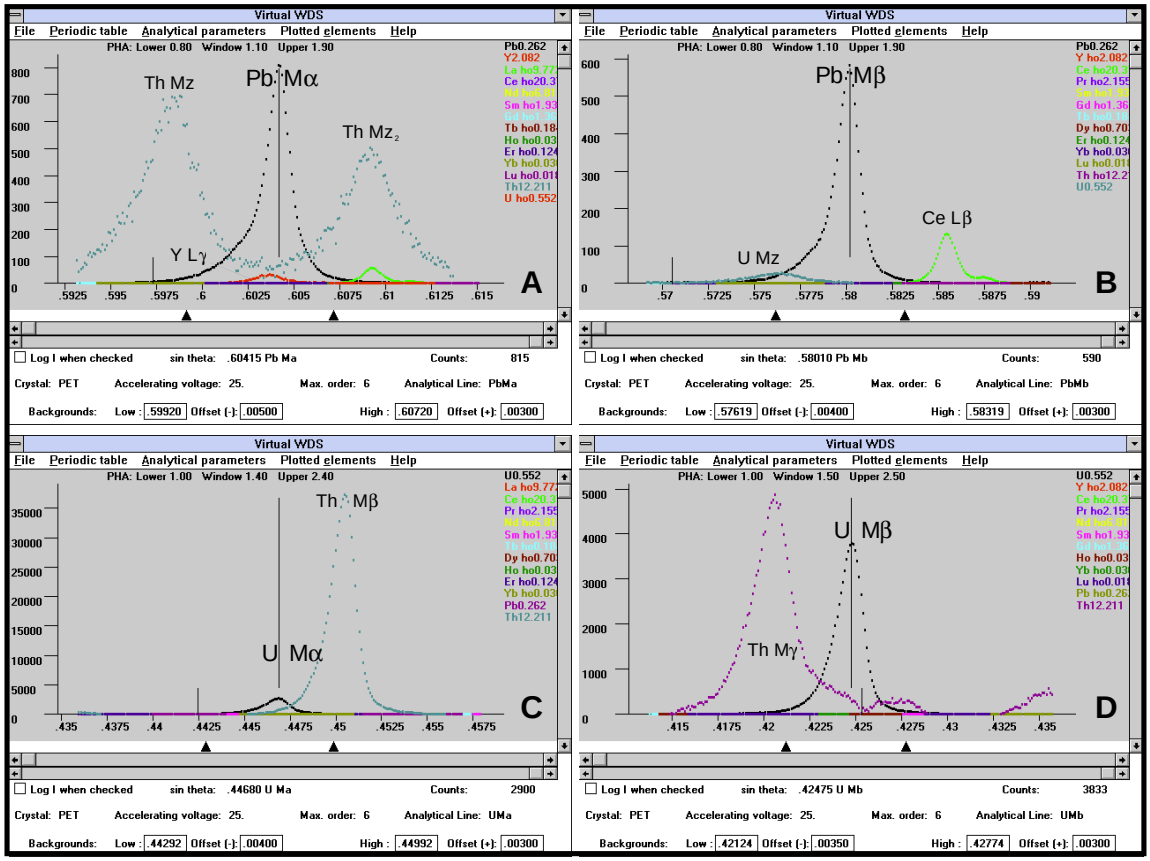

Fig. 4 Peak overlap simulations applying the program VIRTUAL WDS by REED AND BUCKLEY (1996). These simulations were run with the monazite composition given in table 5. The figure visualizes the critical interferences relevant to Th-U-Pb dating of monazite with the EMP. Peak counts of the element of interest and interfering counts are listed in table 4.

Tab. 5 Reference composition of monazite and xenotime used for the calculations on table 4 and 6.

Monazite:			Xenotime:		
Elem.	Ions	wt%	Elem.	Ions	wt%
P	3.774	12.373	P	4.024	15.521
Si	0.278	0.825	Si	0.007	0.025
Ca	0.289	1.225	Ca	0.003	0.016
Y	0.222	2.076	Y	3.207	35.324
La	0.667	9.757	La	0.001	0.01
Ce	1.379	20.352	Ce	0.002	0.031
Pr	0.145	2.155	Pr	-	-
Nd	0.448	6.806	Nd	0.004	0.075
Sm	0.122	1.927	Sm	0.004	0.078
Gd	0.082	1.351	Gd	0.076	1.471
Tb	0.011	0.178	Tb	0.04	0.79
Dy	0.041	0.709	Dy	0.336	6.76
Ho	0.002	0.038	Ho	0.064	1.317
Er	0.007	0.132	Er	0.155	3.215
Yb	0.002	0.028	Yb	0.076	1.627
Lu	0.001	0.016	Lu	-	-
Pb	0.012	0.269	Pb	-	-
Th	0.499	12.251	Th	-	-
U	0.022	0.555	U	0.002	0.06
O	16	27.098	O	16	32.019
Sum	8.003	100.121	Sum	8.001	98.339

Tab.6 This table demonstrates the effect of the overlaps on Pb Ma (Th Mz) and U Mb (Th Mg) with respect to Th-U-Pb age calculation. The monazite composition is listed on table 5. The ages have been calculated according to MONTEL et al. (1996).

PbO	ThO2	UO2	Analytical X-ray lines	Age Ma
0.290	13.941	0.630	Th Ma, Pb Mb, U Mb corr	426
0.290	13.941	0.677	Th Ma, Pb Mb, U Mb uncorr	422
0.290	13.941	0.818	Th Ma, Pb Mb, U Ma uncorr	411
0.322	*13.941*	*0.630*	*Th Ma, Pb Ma, U Mb corr*	*473*
0.322	*13.941*	*0.677*	*Th Ma, Pb Ma, U Mb uncorr*	*468*
0.322	*13.941*	*0.818*	*Th Ma, Pb Ma, U Ma uncorr*	*456*

Table 6 demonstrates the effect arising from the neglect of interferences, using the monazite composition listed in table 5. Even though overlaps on Pb Ma and U Ma are counteracting, the calculated age is still 30 Ma off the best approximation (426 Ma) by using Pb Mb and correcting for interferences on U Mb.

Recommended settings for the quantification of monazite by electron microprobe are listed in table 8. These contain the full information on best lines, background positions, and integration times - optimized for a monazite composition as given in table 5. For compositions deviating considerably from the given example, adjustments may become necessary, as, for example, a simulation on VIRTUAL WDS would elucidate. Note that the integration times and background positions are different for calibration on standards and measurement on monazite. All lines and background positions have been checked for interferences by means of wavelength dispersive scans and by applying the program VIRTUAL WDS, using the compositions of the natural monazite listed on table 5 and respective standard materials. Employing the settings outlined, correction procedures as introduced by ÅMLI AND GRIFFIN (1975) are only applicable to the interference of Th Mg on U Mb (Tab. 7). All other elements listed using the respective lines and background positions have minimal overlaps or none for monazite similar to the reference sample. The elements Fe and Al are measured to have a control on the influence of adjacent minerals, and for good monazite analyses should fall below the detection limit of the EMP. With the recommended settings, 95% of 1000 analyses achieved totals of 98.00 to 101.00%, and 75% had cation sums within 7.99 and 8.02, normalizing to 16 oxygens.

Tab. 7 Simulation of the Th Mg overlap on U Mb using the program VIRTUAL WDS for varying Th amounts in monazite for the determination of a correction factor based on Th Ma. The correction should be applied as follows:
$U\ wt\%_{corrected} = U\ wt\%_{measured} - (0.0052 * Th\ wt\%_{measured})$.

Th wt%	I Th Mg at U Mb cps	I Th Ma pk cps	I Th shoulder / I Th Ma pk
5	117	22411	0.005221
10	235	44821	0.005243
11	258	49304	0.005233
25	587	112054	0.005239
30	704	134464	0.005236
		Correction factor	0.00523

BSE imaging and X-ray mapping

Monazite may show complex zonation patterns with domains of distinctive origin (COCHERIE et al., 1998; HAWKINS AND BOWRING, 1997). Heterogeneity in the Th/Pb ratio is crucial to Th-U-Pb age interpretation and may reveal multi-stage growth, possible Pb diffusion, or partial recrystallization of a monazite grain. Thus, if monazite is to provide geochronological information, they ought to be tested for their growth topology. This is easily

Tab. 8 Recommended settings for the quantitative analysis of monazite by EMP. Note that background positions and integration times are different for standardization and measurement. Ideally, standard materials for elements Y to Yb should be REE-phosphates (e.g. JAROSEWICH AND BOATNER, 1991). U Mb and Th Mg are overlapping and adjustments should be made according to table 7.

Electron Microprobe: MPI Bern, Cameca SX 50 Accelerating Voltage: 25 kV; Beam Current: 50 nA												
Monazite analysis:				Measurement settings				Calibration settings				
Element	Val.	Line	X-tal	+ Bkg	- Bkg	Pk time	Bkg total	+ Bkg	- Bkg	Pk time	Bkg total	#Standard
P	5+	Ka	PET	1150	-1150	30	30	1150	-1150	30	30	CePO4
Al	3+	Ka	TAP	500	-500	30	30	500	-500	30	30	anorthite
Si	4+	Ka	TAP	500	-500	30	30	500	-500	30	30	almandine
Ca	2+	Ka	PET	500	-500	30	30	500	-500	30	30	anorthite
Y	3+	La	PET	500	-500	60	60	500	-500	60	60	Y2O3
La	3+	La	LiF2	700	-500	100	100	700	-500	100	100	La0.95Nd0.05TiO3
Ce	3+	La	LiF2	650	-550	100	100	650	-550	100	100	CePO4
Pr	3+	Lb	LiF	8659	-441	50	50	500	-500	80	80	PrAlO3
Nd	3+	Lb	LiF2	1841	-2104	100	100	300	-350	80	80	†REE2
Sm	3+	Lb	LiF	2082	-4223	50	50	500	-500	80	80	†REE2
Gd*	3+	Lb	LiF	5841	-464	50	50	350	-300	80	80	†REE1
Tb*	3+	Lb	LiF	1272	-5628	50	50	400	-300	80	80	†REE1
Dy	3+	Lb	LiF	2919	-1145	50	50	450	-300	80	80	†REE4
Ho	3+	Lb	LiF	4483	-2417	50	50	500	-300	80	80	†REE4
Er	3+	La	LiF	1086	-2980	50	50	500	-500	80	80	†REE4
Yb	3+	La	LiF	none	-200	50	50	450	-300	80	80	†REE2
Lu	no ideal line											
Pb	2+	Mb	PET	4490	-7130	300	300	500	-500	50	50	crocoite
Th	4+	Ma	PET	400	-500	100	100	400	-500	50	50	ThP2O7
U	4+	Mb	PET	3390	-1505	150	150	500	-500	50	50	UO2
Fe	2+	Ka	LiF2	500	-500	30	30	500	-500	50	50	almandine
* Xenotime analysis:												
Gd	3+	La	LiF	869	-5431	50	50	500	-500	50	50	†REE1
Tb	3+	La	LiF	2615	-3685	50	50	450	-300	80	80	†REE1
† standards by Drake & Weill (1972) # Note that ideal standards for the elements Y to Yb are REE PO4, eg. by Jarosewich & Boatner (1991).												

accomplished through BSE imaging of each grain prior or after quantitative analysis. The video settings for best imaging quality of zonation patterns vary from microprobe to microprobe and from grain to grain within one thin section. Recommended electron beam settings for BSE_Z imaging are 15 kV and 20 nA, whereas for X-ray mapping of heavy elements, higher voltages and currents are preferable (e.g. 25 kV and 100 nA). While X-ray mapping can provide element specific maps within hours rather than seconds, BSE_Z images show the variation of the mean atomic number across the grain within a few seconds. Experience shows that patterns visible in BSE_Z images closely match X-ray maps of the element Th. Very little contrast is visible in X-ray maps of the elements Ce, La, Nd, Sm or Gd, mainly because the variation in Th is being compensated by several LREE (light rare earth elements). Monazite grains with no visible zonation in BSE_Z mode may thus be assumed as being homogeneous in chemistry and age within geologic times. Heterogeneity may potentially hint at multi-stage growth, even though this must not always be the case, an example being shown in figure 5.

Conclusions

Several conclusions regarding technical aspects of monazite analysis can be drawn from this research:

Lead-free thin sections required for Th-U-Pb analysis can be prepared using specially treated polyethylene disks for polishing - at no compromise in quality or efficiency.

Monazite is most easily analyzed by means of an electron microprobe which offers the combination of efficient searching, zonation imaging, quantification, and Th-U-Pb chemical dating capabilities. Neither optical microscopy, optical spectroscopy, alpha sputtering, cathode luminescence, UV luminescence or scanning electron microscope techniques can match the

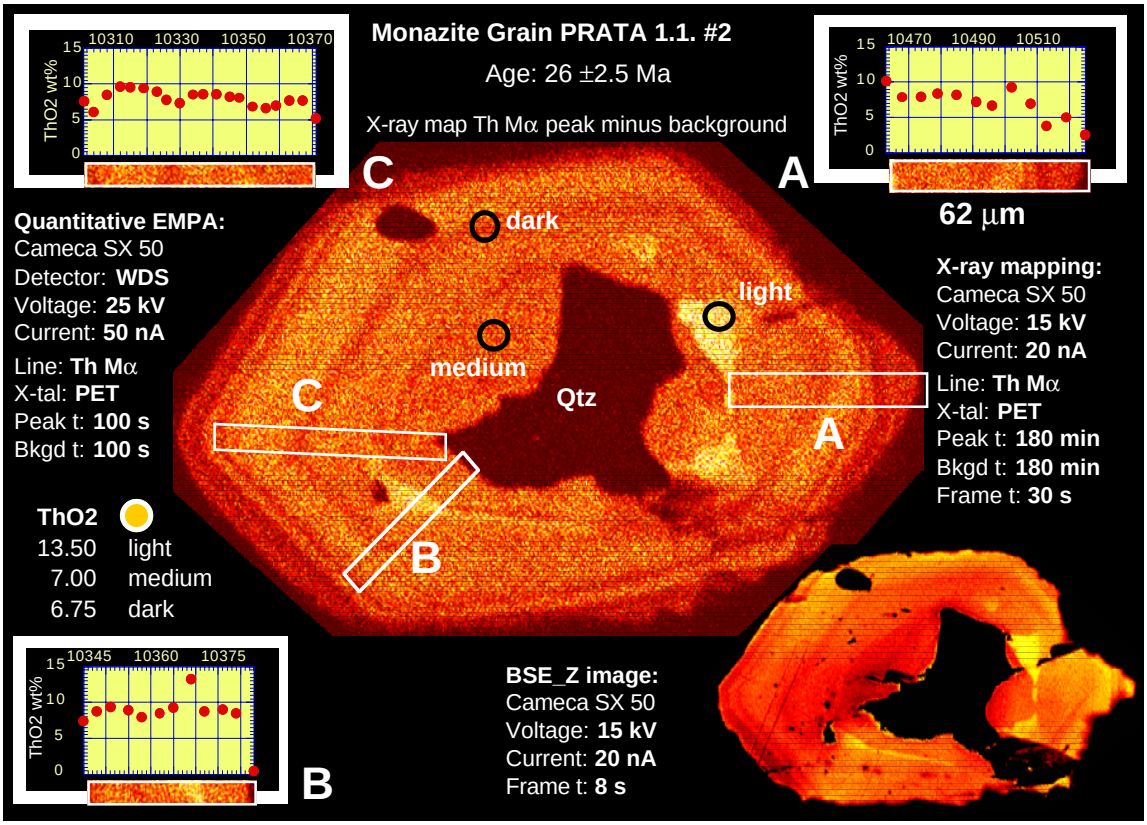

Fig. 5 Comparison of visualization methods to demonstrate variable Th contents within a zoned monazite grain. The grain (supplied by V. Köppel) has been dated by XRF-microprobe to 26±2.5 Ma.

efficiency and the combination of tasks available on an electron microprobe.

Age information on monazite should only be interpreted upon tests on homogeneity using BSE_Z imaging facilities.

Quantification of monazite using wavelength dispersive spectrometry is time consuming and requires careful selection of analytical settings. Several misconceptions from the literature have been outlined and discussed, and for the first time a complete analytical strategy has been presented. Of particular interest to Th-U-Pb dating should be the common neglect of interferences on Pb Ma and U Mb.

Acknowledgements

This study is part of a PhD project supported by Schweizerischer Nationalfonds (Credit 20-49671.96/1 and 2000-055306.98/1). L.W. Diamond is thanked for passing on his valuable knowhow on EMPA. T. Burri provided the alpha autoradiographs. Scientific exchange with the EMP laboratory at GFZ Potsdam has been made possible through W. Heinrich, with special thanks going to D. Rhede and O. Appelt. J. Spratt and C.T. Williams of NHM London are thanked for valuable discussions and for UO_2 standard material. Comments by V. Köppel, E. Reusser and U. Schaltegger are gratefully acknowledged. The EMP laboratory at the MPI Bern has been funded by Schweizerischer Nationalfonds (Credit 21-26579.89).

References

ÅMLI, R. and GRIFFIN, W.L. (1975): Microprobe analysis of REE minerals using empirical correction factors. American Mineralogist, 60(7-8), 599-606.

ANDREHS, G. and HEINRICH, W. (1998): Experimental determination of REE distributions between monazite and xenotime: potential for temperature-calibrated geochronology. Chemical Geology, 149(1-2), 83-96.

BEA, F. and MONTERO, P. (1999): Behavior of accessory phases and redistribution of Zr, REE, Y, Th, and U during metamorphism and partial melting of metapelites in the lower crust: An example from the Kinzigite Formation of Ivrea-Verbano, NW Italy. Geochimica et Cosmochimica Acta, 63(7-8), 1133-1153.

BERNSTEIN, L.R. (1982): Monazite from North Carolina having the alexandrite effect. American Mineralogist, 67(3-4), 356-359.

BINGEN, B. and VAN BREEMEN, O. (1998): U-Pb monazite ages in amphibolite- to granulite-facies orthogneiss reflect hydrous mineral breakdown reactions: Sveconorwegian Province of SW Norway.

Contributions to Mineralogy and Petrology, 132(4), 336-353.

BRAUN, I., MONTEL, J.M. and NICOLLET, C. (1998): Electron microprobe dating of monazites from high-grade gneisses and pegmatites of the Kerala Khondalite Belt, southern India . Chemical Geology , 146 (1-2), 65-85.

COCHERIE, A., LEGENDRE, O., PEUCAT, J.J. and KOUAMELAN, A.N. (1998): Geochronology of polygenetic monazites constrained by in situ electron microprobe Th-U total lead determination: Implications for lead behaviour in monazite. Geochimica et Cosmochimica Acta, 62(14), 2475-2497.

CROWLEY, J.L. and GHENT, E.D. (1999): An electron microprobe study of the U-Th-Pb systematics of metamorphosed monazite: the role of Ph diffusion versus overgrowth and recrystallization. Chemical Geology, 157(3-4), 285-302.

DELLA VENTURA, G., MOTTANA , A., PARODI, G.C., RAUDSEPP, M., BELLATRECCIA , F., CAPRILLI, E., ROSSI, P. and FIORI, S. (1996): Monazite-huttonite solid-solutions from the Vico Volcanic Complex, Latium, Italy . Mineralogical Magazine , 60 (402), 751-758.

DEMARTIN, F., PILATI, T., DIELLA, V., DONZELLI, S. and GRAMACCIOLI, C.M. (1991): Alpine monazite; further data. The Canadian Mineralogist, 29(Part 1), 61-67.

DONOVAN , J.J., SNYDER, D.A. and RIVERS, M.L. (1993): An improved interference correction for trace element analysis. Microbeam Analysis, 2, 23-28.

DRAKE, M.J. and WEILL, D.F. (1972): New rare earth element standards for electron microprobe analysis. Chemical Geology, 10(2), 179-181.

EVANS , J. and ZALASIEWICZ, J. (1996): U-Pb, Pb-Pb and Sm-Nd dating of authigenic monazite: Implications for the diagenetic evolution of the Welsh Basin . Earth and Planetary Science Letters , 144 (3-4), 421-433.

EXLEY, R.A. (1980): Microprobe studies on REE-rich accessory minerals; implications for Skye granite petrogenesis and REE mobility in hydrothermal systems. Earth and Planetary Science Letters, 48(1), 97-110.

FIALIN, M., OUTREQUIN, M. and STAUB , P.F. (1997): A new tool to treat peak overlaps in electron-probe microanalysis of rare-earth-element L-series X-rays. European Journal of Mineralogy, 9 (5), 965-968.

FINGER, F. and BROSKA, I. (1999): The Gemeric S-type granites in southeastern Slovakia: Late Palaeozoic or Alpine intrusions? Evidence from electron-microprobe dating of monazite. Schweizerische Mineralogische und Petrographische Mitteilungen, 79(3), 439-443.

FINGER, F., BROSKA, I., ROBERTS , M.P. and SCHERMAIER, A. (1998): Replacement of primary monazite by apatite-allanite-epidote coronas in an amphibolite facies granite gneiss from the eastern Alps . American Mineralogist , 83 (3-4), 248-258.

FINGER, F. and HELMY, H.M. (1998): Composition and total-Pb model ages of monazite from high-grade paragneisses in the Abu Swayel area, southern Eastern Desert, Egypt. Mineralogy and Petrology , 62 (3-4), 269-289.

FRANZ, G., ANDREHS, G. and RHEDE, D. (1996) Crystal chemistry of monazite and xenotime from Saxothuringian-Moldanubian metapelites, NE Bavaria, Germany. In C. Ayora, Ed. Fluid inclusions., 8, p. 1097-1118. Schweizerbart'sche Verlagsbuchhandlung (Naegele u. Obermiller), Stuttgart, Federal Republic of Germany.

GRATZ , R. and HEINRICH, W. (1997): Monazite-xenotime thermo-barometry: Experimental calibration of the miscibility gap in the binary system CePO4-YPO4 . American Mineralogist , 82 (7-8), 772-780 .

HAWKINS, D.P. and BOWRING, S.A. (1997): U-Pb systematics of monazite and xenotime: Case studies from the Paleoproterozoic of the Grand Canyon, Arizona. Con-tributions to Mineralogy and Petrology, 127 (1-2), 87-103.

JAROSEWICH, E. and BOATNER , L.A. (1991): Rare-earth element reference samples for electron microprobe analysis. Geostandards Newsletter, 15(2), 397-399.

KINGSBURY, J.A., MILLER, C.F., WOODEN, J.L. and HARRISON, T.M. (1993) Monazite paragenesis and U-Pb systematics in rocks of the eastern Mojave Desert, California, U.S.A.; implications for thermochronometry. In E.B. Watson, T.M. Harrison, C.F. Miller, and F.J. Ryerson, Eds. Geochemistry of accessory minerals; papers presented at the Third V. M. Goldschmidt conference., 110, p. 147-167. Elsevier, Amsterdam, Netherlands.

MANNUCCI, G., DIELLA, V., GRAMACCIOLI, C.M. and PILATI, T. (1986) A comparative study of monazite specimens from the Alpine region. In C.T. Prewitt, Ed. Abstracts with program 1986; the Fourteenth general meeting of the International Mineralogical Association., p. 166. International Mineralogical Association, International.

MONTEL, J.M., VESCHAMBRE, M. and NICOLLET, C. (1994): Dating Monazite with the Electron Microprobe . Comptes Rendus de L Academie Des Sciences Serie II , 318 (11 Part 2), 1489-1495.

MOUGEOT, R., RESPAUT, J.P., LEDRU, P. and MARIGNAC, C. (1997): U-Pb chronology on accessory minerals of the Velay anatectic dome (French Massif Central) . European Journal of Mineralogy , 9 (1), 141-156.

PAQUETTE, J.L., MONTEL, J.M. and CHOPIN, C. (1999): U-Th-Pb dating of the Brossasco ultrahigh-pressure metagranite, Dora-Maira massif, western Alps. European Journal of Mineralogy, 11(1), 69-77.

PARRISH, R.R. (1990): U-Pb dating of monazite and its application to geological problems. Canadian Journal of Earth Sciences = Journal Canadien des Sciences de la Terre, 27(11), 1431-1450.

PODOR, R. and CUNEY, M. (1997): Experimental study of Th-bearing LaPO4(780 degrees C, 200 MPa): Implications for monazite and actinide orthophosphate stability. American Mineralogist , 82 (7-8), 765-771.

RAPP, R.P. and WATSON , E.B. (1986): Monazite solubility and dissolution kinetics; implications for the thorium and light rare earth chemistry of felsic magmas. Contributions to Mineralogy and Petrology, 94(3), 304-316.

REED, S.J.B. and BUCKLEY, A. (1996): Virtual WDS. Mikrochim. Acta [Suppl.], 13, 479-483.

ROEDER, P.L. (1985): Electron-microprobe analysis of minerals for rare-earth elements; use of calculated peak-overlap corrections. The Canadian Mineralogist, 23(Part 2), 263-271.

SPEAR, F.S. and PARRISH, R.R. (1996): Petrology and cooling rates of the Valhalla complex, British Columbia, Canada. Journal of Petrology , 37 (4), 733-765.

STÄHLI Flathoning AG, Sägestrasse 10, CH-2542 Pieterlen/Biel, Switzerland. Facsimile: +41 (0)32 376 0509.

SUZUKI, K. and ADACHI, M. (1994): Middle Precambrian detrital monazite and zircon from the Hida Gneiss on Oki-Dogo Island, Japan; their origin and implications for the correlation of basement gneiss of Southwest Japan and Korea. Tectonophysics, 235(3), 277-292.

WILLIAMS, C.T. (1996) Analysis of rare earth minerals. In A.P. Jones, F. Wall, and C.T. Williams, Eds. Rare Earth Minerals: Chemistry, origin and ore deposits, p. 327-348. Chapman and Hall, London.

WILLIAMS, M.L., JERCINOVIC, M.J. and TERRY, M.P. (1999): Age mapping and dating of monazite on the electron microprobe: Deconvoluting multistage tectonic histories. Geology, 27(11), 1023-1026.

Manuscript received January 25, 2000; minor revision accepted February 10, 2000.

Appendix

FINDING MONAZITE WITH THE CAMECA SX50 ELECTRON MICROPROBE

The following procedure, based on the setup of the SX50 microprobe laboratory at MPI Bern (SP1: (hP) LiF/PET; SP2: (lP) LiF/TAP; SP3: (hP) LiF/PET; SP4: (lP) TAP/PC1; SP5: EDS), has crystallized to be very efficient and effective:

- *Generate a focused beam with a voltage of 25 kV and a beam current of 50 nA.*
- *Change the detectors to BSE Z mode.*
  SX>m1 vs1
  SX>vs1 bse z
- *Adjust the magnification to mag 400. This sets the field of view on M1 in BSE mode equal to the field of view of the optical image.*
  SX>mag 400
- *Set the beam to scanning mode TV.*
  SX>mode tv
- *Ensure the orientation of the optical image is equivalent to the one of the BSE image. If not, rotate it such that the two images are identical.*
  SX>rota
- *Move the spectrometers to the following lines:*
  SX>mov sp1 ce la
  SX>mov sp2 fe ka
  SX>mov sp3 p ka
  SX>mov sp4 y la
- *Adjust the contrast/brightness settings of M1:*
  SX>vs1 manu
- *Use the following settings:*
  Offset: 270 (470) Dark level: 50
  Contrast Difference: 1 Gain: 60
- *Turn the reflected light source back on.*
  SX>light samp 5
- *The transmitted light source should be off at all times while running in BSE mode. When the beam is in fixed spot size mode (SX>mode fix), the transmitted light source may be quickly turned on to check the context of the grain of interest. Turn it off before you switch back to scanning mode (SX>mode tv).*
- *Now systematically scan the thin section using the x-y-z-stage control. Thanks to the high sensitivity of the BSE detector and screen, the stage can be moved at full speed without missing out on any potential candidates. Scanning of a round 1" thin section takes about 15 minutes, including the programming of the positions of the monazite and xenotime grains of interest.*
  SX>move stage [a-z] save

The above settings filter out any other phases (black) and show monazite as bright spots or areas, with the complete outline of the grain luminescing. Xenotime (YPO4) is just detectable on the screen with the above settings, is however not quite as bright as monazite. Pyrite (FeS2) shows equivalent brightness to monazite but is immediately identified in reflected light (slightly golden reflectance). Zircon (ZrSiO4) may luminesce similarly to monazite in some samples (you may lower the offset to 260), however, it can be easily distinguished from monazite: (1) from its typical morphology showing elongate idiomorphic shapes; (2) luminescence on the screen may show only part of the grain; (3) in reflected light, zircon is brighter than monazite (monazite is similar to garnet in reflected light); (4) by quickly changing the beam to fixed spot size.

SX>mode fix

If the beam spot is luminescing on the grain, it is either a xenotime or a zircon. High counts on P and Y indicate a xenotime, low counts on any of the spectrometers set as above indicate a zircon. Note that the fixed beam spot is slightly offset to the top right of the cross.

submitted to SCHWEIZ. MINERAL. PETROGR. MITT.

Retrograde monazite-forming reaction in bearthite-bearing high-pressure rocks

by *N.C. Scherrer[1], E. Gnos and C. Chopin*

Abstract

Bearthite $Ca_2Al[PO_4]_2(OH)$, an aluminium phosphate containing up to ~10 wt% of light rare-earth elements (LREE) + Th, has been observed to break down to apatite + monazite + Al-rich phase + H_2O ± Sr-bearthite. Two cases are described: Case A concerns a pyrope-bearing kyanite-phengite-quartz (coesite) schist from the high-pressure Dora-Maira terrane, Italy, where bearthite displays a symplectitic rim consisting of apatite + monazite; Case B deals with a garnet-bearing muscovite-biotite gneiss of the Monte Rosa nappe, Italy, in which a symplectitic pseudomorph of apatite + corundum + monazite was found included in allanite. We suggest a petrogenetic sequence of LREE minerals: bearthite represents the stable phase in a pressure dominated regime (subduction) in rocks with a high Al/Ca ratio and decomposes to symplectitic monazite + apatite + Al-rich phase upon rapid decompression. Bearthite coexisting with HREE dominated minerals like xenotime does not show increased HREE contents. Because of its Th contents, bearthite has a geochronological potential to constrain the time of high-pressure metamorphism.

Keywords: bearthite, monazite, metamorphic reaction, EMPA, LREE

Introduction

Monazite is widely used for age dating in a variety of igneous, metamorphic and diagenetic rocks. There is, however, relatively little knowledge of its origin in metamorphic rocks and, so far, there are only few monazite-forming reactions described in the literature (AKERS, 1993; BINGEN, 1996; BROSKA, 1998; FINGER, 1998; PAN, 1997; SMITH, 1990), despite their importance with respect to the interpretation of monazite age data.

Bearthite, $Ca_2Al[PO_4]_2(OH)$, was first observed in rocks of the Monte Rosa Massif by BEARTH (1952). CHOPIN et al. (1993) found bearthite with symplectitic rims (Fig. 1) of *"apatite containing highly refringent blebs of a rare-earth phosphate (monazite?)"* in metapelites and magnesian schists of the coesite-bearing Dora-Maira terrane. Recent studies on metapelitic rocks of the Monte Rosa nappe revealed patches of fine-grained and closely intergrown apatite + monazite + corundum, making up the core of a millimetre-sized allanite grain (Fig. 2). Reintegration of microprobe data from the three different minerals that formed the fine-grained areas suggests a precursor rich in LREE with Al as a major component to account for the formation of corundum. The above observations led to the idea that the phosphate bearthite could be a major reactant in a monazite-forming reaction in high- or ultra-high-pressure rocks. For this purpose we re-investigated the symplectitic reaction rim described in CHOPIN et al. (1993), as well as samples from other bearthite localities.

Occurrence

The original type locality of bearthite (BEARTH, 1952; CHOPIN et al. 1993) is situated on the western ridge of the Stockhorn southeast of Zermatt within the frontal part of the Monte Rosa nappe, where it has been observed associated with lazulite $MgAl_2(PO_4)_2(OH)_2$, fluor-apatite $(Ca_{4.95},Sr_{0.05})_5(PO_4)_3(F_{0.54},OH_{0.43},Cl_{0.03})$, and paragonite $NaAl_2[AlSi_3O_{10}](OH)_2$.

[1] Mineralogisch-petrographisches Institut, Universität Bern, Baltzerstrasse 1, CH-3012 Bern, Switzerland. <scherrer@mpi.unibe.ch>

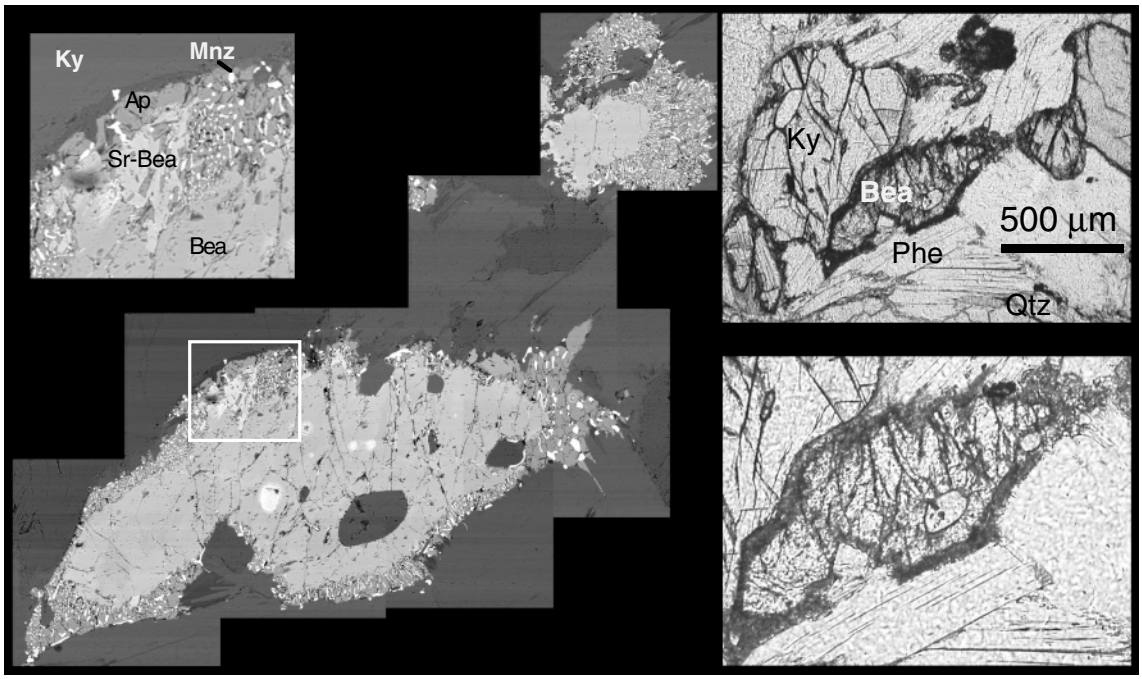

Fig. 1a: Documentation of symplectitic rim of apatite + monazite on a bearthite grain within garnet-kyanite-phenghite-quartz schist from Dora-Maira (BSE images on left; plane polarised light on right). The zoom-window of the BSE-map (top left) highlights the presence of Sr-bearthite, which appears to be restricted to the resorbing edge of bearthite, against the symplectite rim. Electron microprobe analyses are listed in table 1.

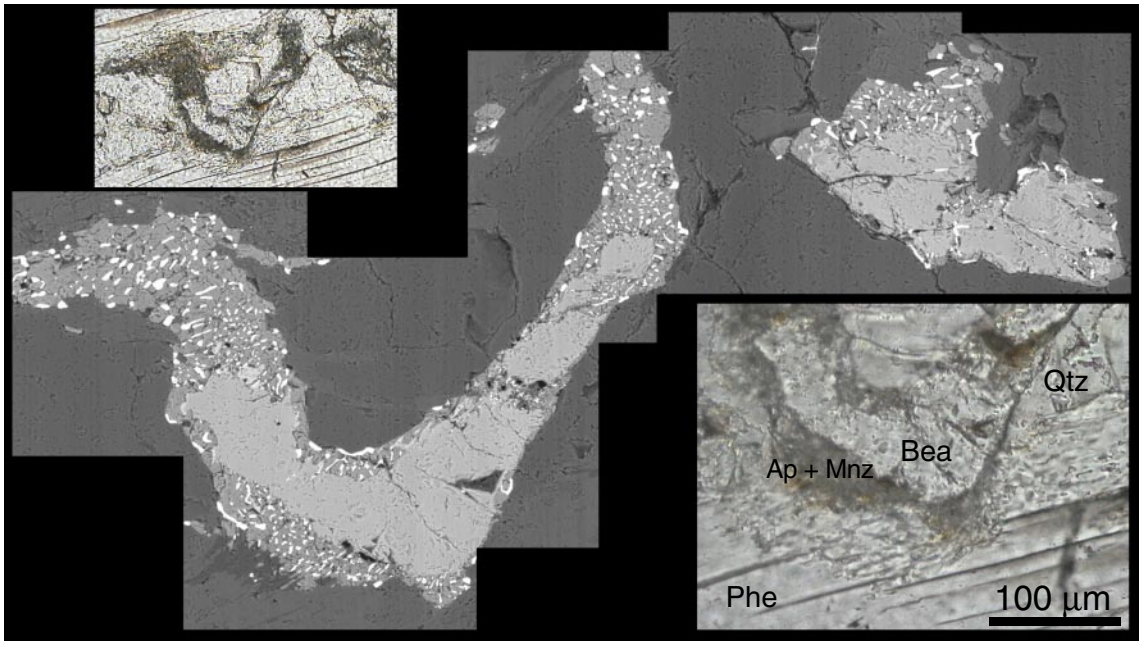

Fig. 1b: Images documenting a second bearthite grain within section 85DM45a showing exactly the same symplectite reaction as figure 1a.

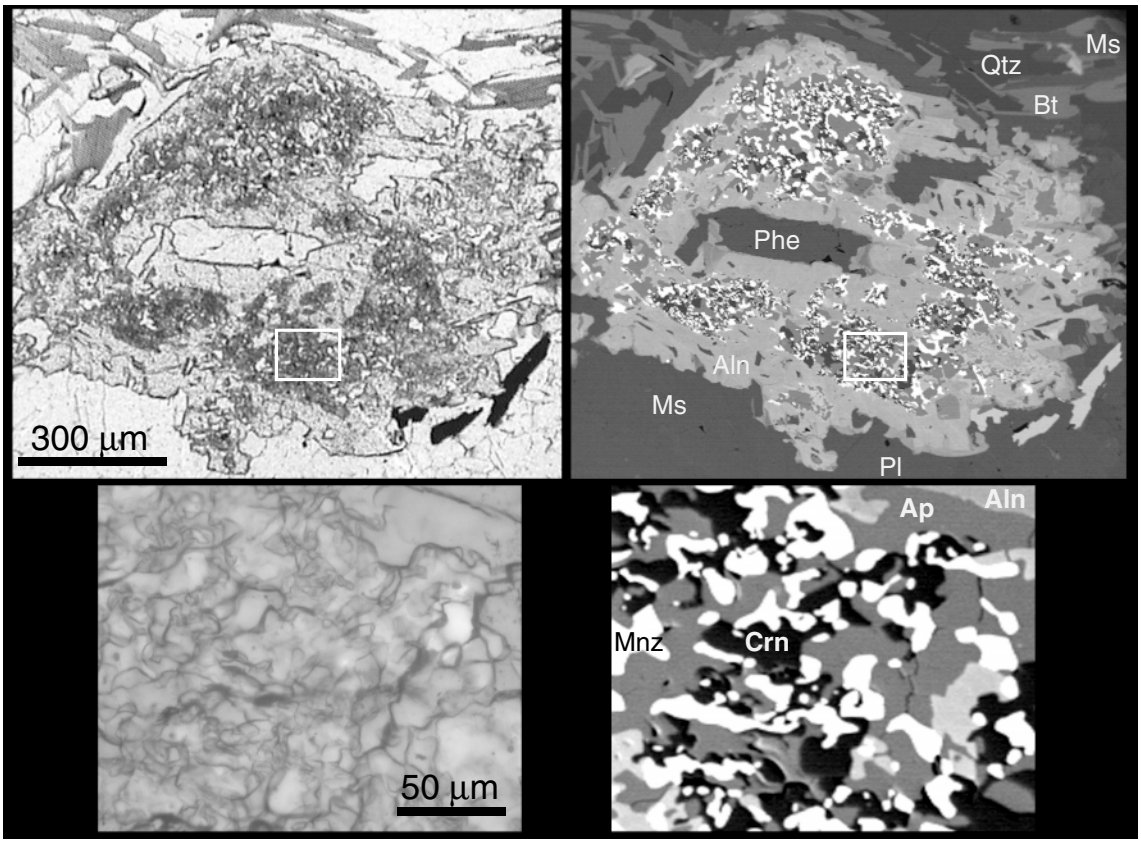

Fig. 2: Optical (left) and BSE images (right) of sample Mo9801 showing the fine-grained reaction texture with apatite + monazite + corundum within a large grain of allanite. The close-up view of the BSE image shows that within the reaction zones, allanite is virtually absent. These textural relationships as well as the lack of Si, Fe and Mg within the product phase assemblage suggest that allanite was not involved in the symplectite-forming breakdown reaction of bearthite. Note that the white mica enclosed in the symplectite has a phengitic composition ($Mg_{0.29}Si_{3.40}Al_{2.20}$), whereas only muscovite is present in the matrix ($Mg_{0.07}Si_{3.05}Al_{2.80}$).

CHOPIN et al. (1991; 1993, sample 85DM45a) discovered bearthite in coesite-bearing rocks of the Dora-Maira massif. Bearthite occurs as an accessory rock-forming mineral in metapelitic rocks as well as in pyrope-bearing kyanite-phengite-quartz (coesite) schists. The symplectitic rim (Fig. 1) composed of apatite + monazite (Tab. 1) has been interpreted as a retrogressive and decompression-related feature.

No bearthite relic was observed in the Monte Rosa nappe sample (Psso. del Mottone, south of Antronapiana, sample Mo9801) collected by the first author. However, the garnet-bearing mica gneiss belonging to the metapelitic pre-granitic, pre-Permian basement, hosts an interesting reaction texture of symplectitic apatite + monazite + corundum, surrounded by allanite. While sillimanite has been observed elsewhere in this rock unit (BEARTH, 1957), no Al-silicate is apparent in our sample. The petrography of the sample shows a typical garnet-bearing muscovite-biotite gneiss with plagioclase ($Ab_{70}An_{30}$), K-feldspar, quartz and late chlorite as the main constituents. Rutile rimmed by ilmenite is observed mainly as inclusions in garnet, rarely in the matrix. Phengitic mica ($Mg_{0.29}Si_{3.40}Al_{2.20}$) has been observed as inclusion in allanite (Fig. 2), but not within the matrix where only muscovite ($Mg_{0.07}Si_{3.05}Al_{2.80}$) is found. Several large allanite grains as well as minor apatite and rare monazite have been observed throughout the matrix. The samples are derived from the lowest part of the

Monte Rosa nappe within a few metres of the contact to the Antrona trough units (ophiolitic sequence).

Methods

The electron microprobe (Cameca SX50, MPI Bern and IMP Lausanne) was used to produce BSE images, X-ray maps and quantitative analyses. Monazite analysis was performed using beam conditions of 25 kV and 50 nA. For a detailed description of analytical settings, refer to SCHERRER et al. (2000). Because neither bearthite nor apatite are stable under the beam conditions necessary for full rare-earth quantification as above, the beam settings were reduced to 15 kV at 20 nA with a defocused beam (~20 μm). A full rare-earth quantification on bearthite is thus not easily achieved by electron microprobe.

The software NIH Image was applied for semi-quantitative analysis of X-ray maps and BSE images to determine the relative amounts of apatite, monazite and corundum within the reaction texture. BSE imaging turned out to be more suitable and efficient than time-consuming element maps. Several representative areas were selected to calculate the amount of each phase in 2D.

The fine-grained nature of the symplectitic textures was an additional problem for good analyses to be achieved. Nevertheless, the original suggestion of CHOPIN et al. (1993) of a symplectite of apatite plus monazite has now been confirmed by quantitative analyses for such monazite (Tab. 1).

Results

Case A (Sample 85DM45a): Two bearthite grains within sample 85DM45a, a pyrope-bearing kyanite-phengite-quartz schist (CHOPIN et al. 1993), were mapped in BSE mode to display the different phases present in the reaction. The reaction zones surrounding the bearthite nicely show symplectitic textures (Fig. 1a and 1b). The image also revealed an additional phase produced (Fig. 1a) during the symplectite-forming reaction. This phase appears to be Sr-bearthite (Tab. 1). The texture clearly shows that bearthite can be a reactant in a monazite-forming reaction. The REE (+ Y, Th, U) ratios of bearthite are identical to the REE (+ Y, Th, U) ratios of monazite and, in trace amounts, in apatite within the symplectite, whereby (L)REE are strongly fractionated into monazite (Fig. 3a). REE and Th concentrations in bearthite are generally 10 - 20% of the amount in monazite. Sr-bearthite forms overgrowth patches along the inner side of the symplectite (Fig. 1a). From the BSE image, it is apparent that Sr-bearthite is present only in direct contact with bearthite and is lacking further out, towards the edge of the symplectite. This suggests that excess strontium from the bearthite breakdown apparently cannot be accommodated by apatite (SrO in Ap ranging from 1.7 to 3.5 wt%), nor is it completely resorbed by bearthite. It forms isolated Sr-bearthite patches instead (Fig. 1a). This observation indicates very slow Ca/Sr interdiffusion or the existence of compositional gaps between bearthite and Sr-bearthite under conditions of symplectite formation (Fig. 4). The REE (+ Y, Th, U) concentrations in Sr-bearthite and bearthite (Tab. 1; Fig. 3a) are similar. Since neither monazite nor apatite contain Al and no additional Al-phase is present within the symplectite, it appears that excess Al (± Mg) is removed with the fluid (e.g. to form phengitic white mica) or reacting with quartz to form kyanite, as suggested by BRUNET and CHOPIN (1995). Estimated volume proportions derived from image analysis are 70-80% apatite and 20-30% monazite. In combination with the microprobe data the reaction coefficients are estimated at

$$7\ \mathrm{Bea} \Rightarrow \sim 2.8\ \mathrm{Ap} + 2\ \mathrm{Mnz} + \sim 4.4\ \mathrm{Al_2O_3} + \mathrm{Ca_1Sr_1Al(PO_4)_2(OH)} + \mathrm{H_2O}.$$

Case B (Mo9801): In sample Mo9801, a garnet-bearing mica gneiss free of Al-silicates, a one millimetre sized allanite porphyroblast displays regions within the core consisting of apatite + monazite + corundum (Fig. 2). Allanite is virtually absent within those zones. For mass balance estimations, ten areas essentially free of allanite were selected within those reaction zones and approximate volume ratios of 50-70 % apatite to 20% monazite to 10-30 % corundum were determined. This seems to be similar to *Case A*, except for the presence of corundum. An explanation for this may be that the allanite-forming reaction occurred prior to the breakdown of relic bearthite to the observed symplectite. The REE and Th concentrations in allanite are typically

Tab. 1: Electron microprobe analyses of samples Mo9801, 85DM45a, and B8485A. Mg and Nd values marked with an asterisk * were calculated from the relationship displayed in figure 4b.

Location	Psso. del Mottone, S of Antronapiana					Dora Maira							Stockhorngrat, SE of Zermatt		
Sample	**Mo9801**					**85DM45a**							**B8485A**		
Mineral	Ap	Aln	Monazite			Apatite		Bearthite			Sr-Bea	Mnz	Bea	Sr-Bea	Xen.
Point#	#19	#20	#22	#28	#34	#8#9	publ. '93	#1	#4	publ. '93	#6	#1	#18	#8	#24
P2O5	41.97	0.05	29.99	29.64	29.49	41.34	40.67	39.42	39.65	39.85	37.21	31.05	43.18	40.75	35.36
SiO2	0.01	34.16	0.23	0.42	0.93	0.08	0.14	0.43	0.53	0.27	0.27	0.23	0.02	0.01	0
TiO2	n.a.	0	n.a.	n.a.	n.a.	n.a.	n.a.	n.a.	n.a.	n.a.	n.a.	n.a.	n.a.	n.a.	n.a.
Al2O3	0.02	23.67	0	0	0	0.01	0.05	9.32	10.01	10.36	8.13	0	15.55	14.61	0
FeO	0.04	7.28	0	0	0	0	0.05	0	0	0.03	0	0	0.07	0.04	0
MnO	n.a.	0	n.a.	n.a.	n.a.	n.a.	n.a.	n.a.	n.a.	n.a.	n.a.	n.a.	n.a.	n.a.	n.a.
MgO	n.a.	0.76	n.a.	n.a.	n.a.	2.09	0.16	3.65*	2.80*	3.13	3.47*	n.a.	0.30	0.12	0
CaO	54.16	13.92	0.33	1.01	1.65	50.91	51.36	23.78	23.12	23.95	16.11	1.69	22.82	16.25	0.07
SrO	n.a.	n.a.	n.a.	n.a.	n.a.	1.65	3.49	4.26	7.41	5.72	17.19	n.a.	16.07	26.46	0
Y2O3	0	0	0	0	0	n.a.	n.a.	n.a.	n.a.	n.a.	n.a.	0.91	0	0	46.77
La2O3	0.08	4.08	18.09	14.39	11.58	0.13	0.04	3.56	2.59	2.95	3.58	15.08	0.05	0	0
Ce2O3	0.13	8.15	34.23	30.39	26.95	0.24	0.18	6.83	5.40	5.97	6.32	29.12	0.10	0.07	0.01
Pr2O3	0.03	0.89	3.40	3.45	3.35	0.06	n.a.	0.65	0.51	n.a.	0.64	3.07	0.05	0.02	0.03
Nd2O3	0.15	3.23	11.03	13.27	14.04	0.10	0.08	1.83*	1.41*	1.57	1.74*	10.85	0.06	0.05	0
Sm2O3	0.05	0.51	1.20	1.73	2.24	0.16	n.a.	0.41	0.40	n.a.	0.24	2.02	0	0.01	0
Gd2O3	0.01	0.13	0.33	0.46	0.65	0.01	n.a.	0.30	0.23	n.a.	0.05	1.29	0.07	0.02	0.26
Tb2O3	0	0.07	0	0.02	0	n.a.	n.a.	n.a.	n.a.	n.a.	n.a.	0.16	0	0	0.24
Dy2O3	0	0	0	0	0	n.a.	n.a.	n.a.	n.a.	n.a.	n.a.	0.30	0	0.01	3.74
Ho2O3	0.01	0	0	0	0.01	n.a.	n.a.	n.a.	n.a.	n.a.	n.a.	0	0	0.02	1.43
Er2O3	0	0.02	0.01	0.01	0.02	n.a.	n.a.	n.a.	n.a.	n.a.	n.a.	0.04	0.01	0.01	4.53
Tm2O3	n.a.	n.a.	n.a.	n.a.	n.a.	n.a.	n.a.	n.a.	n.a.	n.a.	n.a.	n.a.	n.a.	n.a.	0.51
Yb2O3	0	0.00	0	0	0	n.a.	n.a.	n.a.	n.a.	n.a.	n.a.	0	0	0	4.19
PbO	0	0.09	0	0	0	n.a.	n.a.	n.a.	n.a.	n.a.	n.a.	0	0.10	0.13	0
ThO2	0	0.30	0.76	4.23	8.77	0.03	n.a.	0.16	0.69	n.a.	0.09	4.01	0.01	0.01	0
UO2	0	0.04	0.01	0.07	0.11	n.a.	n.a.	n.a.	n.a.	n.a.	n.a.	0.94	0.01	0	0.06
F	n.a.	n.a.	n.a.	n.a.	n.a.	3.95	3.20	0.66	0.56	0.64	0.72	n.a.	1.00	0.81	n.a.
Cl	n.a.	n.a.	n.a.	n.a.	n.a.	0.18	0.19	0.02	0.01	0.01	0.03	n.a.	0.03	0.06	n.a.
Total	96.65	97.38	99.61	99.09	99.77	*99.21*	*98.22*	*95.01*	*95.09*	*94.18*	*95.50*	100.76	*99.05*	*99.10*	97.19
Mineral	Ap	Aln	Monazite			Apatite		Bearthite			Sr-Bea	Mnz	Bea	Sr-Bea	Xen.
Normalised to	25 O	25 O	16 O			25 O		17 O			17 O	16 O	17 O	17 O	16 O
P	6.035	0.008	3.983	3.960	3.911	5.987	5.976	3.949	3.937	3.968	3.966	4.017	3.997	3.999	4.014
Si	0.002	6.017	0.035	0.066	0.146	0.013	0.024	0.051	0.063	0.032	0.034	0.035	0.003	0.001	0
Ti	n.a.	0.007	n.a.	n.a.	n.a.	n.a.	n.a.	n.a.	n.a.	n.a.	n.a.	n.a.	n.a.	n.a.	n.a.
Al	0.004	4.939	0	0	0	0.001	0.007	1.307	1.391	1.443	1.213	0	2.014	2.006	0
Fe	0.006	1.073	0	0	0	0	0.007	0	0	0.003	0	0	0.006	0.003	0
Mn	n.a.	0	n.a.	n.a.	n.a.	n.a.	n.a.	n.a.	n.a.	n.a.	n.a.	n.a.	n.a.	n.a.	n.a.
Mg	n.a.	0.199	n.a.	n.a.	n.a.	0.533	0.041	0.643	0.490	0.549	0.652	n.a.	0.049	0.020	0
Ca	9.856	2.628	0.055	0.171	0.277	9.333	9.550	3.015	2.906	3.018	2.172	0.276	2.673	2.018	0.010
Sr	n.a.	n.a.	n.a.	n.a.	n.a.	0.164	0.351	0.293	0.504	0.390	1.254	n.a.	1.019	1.779	0
Y	0	0	0	0	0	0.000	0.000	0.000	0.000	n.a.	0.000	0.074	0	0	3.355
La	0.005	0.266	1.052	0.842	0.672	0.008	n.a.	0.156	0.112	0.129	0.167	0.854	0.002	0	0
Ce	0.008	0.529	1.976	1.764	1.554	0.015	0.012	0.298	0.233	0.259	0.293	1.637	0.004	0.003	0
Pr	0.002	0.057	0.195	0.199	0.192	0.003	0.000	0.028	0.022	n.a.	0.030	0.172	0.002	0.001	0.002
Nd	0.009	0.207	0.621	0.752	0.790	0.006	0.005	0.079	0.060	0.067	0.080	0.595	0.002	0.002	0
Sm	0.003	0.031	0.065	0.094	0.122	0.009	n.a.	0.017	0.016	n.a.	0.011	0.107	0	0	0
Gd	0.001	0.008	0.017	0.024	0.034	0	n.a.	0.012	0.009	n.a.	0.002	0.066	0.002	0.001	0.011
Tb	0	0.004	0	0.001	0	n.a.	n.a.	n.a.	n.a.	n.a.	n.a.	0.008	0	0	0.011
Dy	0	0	0	0	0	n.a.	n.a.	n.a.	n.a.	n.a.	n.a.	0.015	0	0	0.161
Ho	0	0	0	0	0	n.a.	n.a.	n.a.	n.a.	n.a.	n.a.	0	0	0.001	0.061
Er	0	0.001	0.001	0.001	0.001	n.a.	n.a.	n.a.	n.a.	n.a.	n.a.	0.002	0	0	0.193
Tm	n.a.	n.a.	n.a.	n.a.	n.a.	n.a.	n.a.	n.a.	n.a.	n.a.	n.a.	n.a.	n.a.	n.a.	0.021
Yb	0	0.000	0	0	0	n.a.	n.a.	n.a.	n.a.	n.a.	n.a.	0	0	0	0.171
Pb	0	0.004	0	0	0	n.a.	n.a.	n.a.	n.a.	n.a.	n.a.	0	0.003	0.004	0
Th	0	0.012	0.027	0.152	0.313	0.001	0	0.004	0.018	0	0.003	0.140	0	0	0
U	0	0.002	0	0.003	0.004	0.000	0.000	n.a.	n.a.	n.a.	n.a.	0.032	0	0	0.002
F	n.a.	n.a.				1.113	0.912	0.126	0.106	0.121	0.146		0.18	0.152	
Cl	n.a.	n.a.				0.027	0.029	0.002	0.001	0.001	0.003		0	0.006	
OH						0.860	1.059	1.871	1.893	1.877	1.851		1.82	1.842	
Sum Cations	15.930	15.990	8.028	8.028	8.014	16.074	15.976	9.851	9.763	9.858	9.876	8.029	9.78	9.840	8.013
						P+Si = 6		P + Si = 4					P + Si = 4		
						OH+F+Cl = 2		OH + F + Cl = 2					OH+F+Cl = 2		

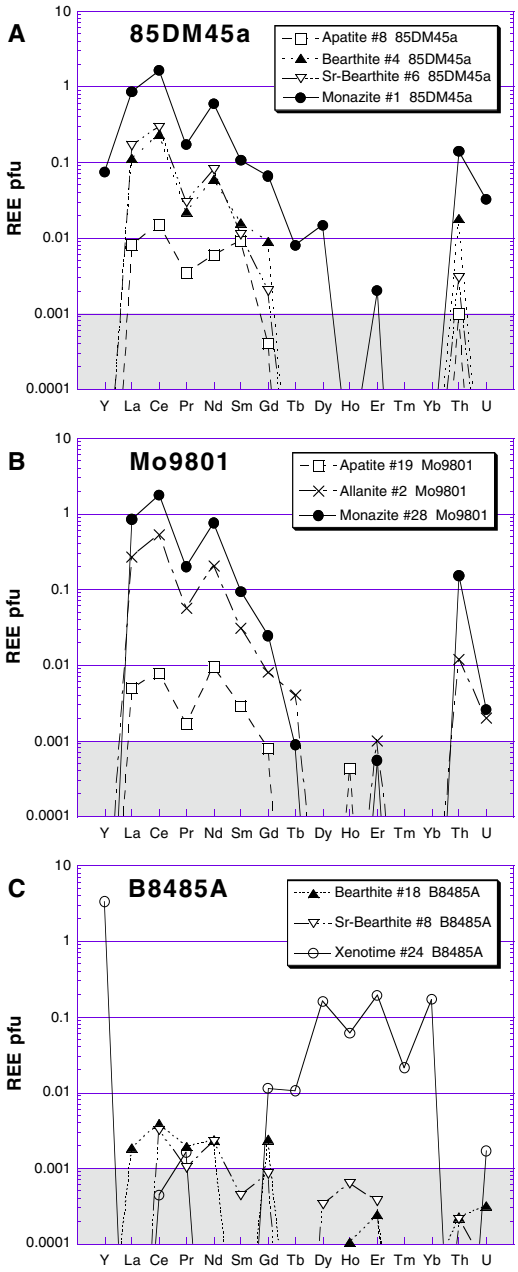

Fig. 3: REE (+ Y, Th, U) concentrations of coexisting phases in samples 85DM45a, Mo9801 and B8485A (values per formula unit as in table 1). Note the similarity of the mineral patterns in the first two examples, and the completely different element distribution of xenotime to bearthite and Sr-bearthite in B8485A. No monazite was detected in this latter sample. Shaded area marks the range at or below the detection limit of EMPA.

a quarter to one third of that in monazite (Fig. 3b). Both minerals show similar distribution patterns suggesting the allanite pattern is likely inherited from bearthite. Both REE patterns are very similar to the Dora-Maira sample (Fig. 3a).

We also included in this study a sample B8485A from the Stockhorngrat (BEARTH, 1952) in which two compositionally different Sr-bearthites coexist with xenotime (Tab. 1; Fig. 4a), but monazite is absent (Fig. 5). The existence of either Ca-enriched (dark) versus Sr-enriched (light) zones with distinct boundaries within the Sr-bearthite (Fig. 5) match the observation made in the Dora-Maira sample 85DM45a (Fig. 1a), where bearthite and Sr-bearthite coexist side by side. We propose potential compositional or miscibility gaps to exist between bearthite and $Ca_1Sr_1Al(PO_4)_2(OH)$ (Fig. 4a). Xenotime YPO_4 is known to be enriched in HREE as opposed to LREE dominant monazite (HEINRICH et al., 1997). Bearthite and Sr-bearthite from the Stockhorn locality show very low REE and Mg concentrations (Fig. 3c and Fig. 4b). In contrast, bearthite and Sr-bearthite from the Dora-Maira sample (85DM45a) have higher Mg contents and display a REE pattern similar to monazite. This hints at an allanite-type substitution of $Ca_{-1}Al_{-1}MgREE$ (Fig. 4b) in the bearthite/Sr-bearthite structure. Furthermore, we suggest that neither bearthite nor Sr-bearthite in the Stockhorn sample (B8485A) originated as a result of monazite breakdown. Whether there is potential preference of LREE over HREE within the bearthite or Sr-bearthite crystal structure seems feasible but may not be concluded from current data.

Discussion

CHOPIN et al. (1993) suggested the symplectitic rim around bearthite to be a retrogressive decompression-related feature, with bearthite to be considered a very high-pressure phase because of its occurrence in coesite hosting rocks. However, subsequent experimental studies on bearthite (BRUNET and CHOPIN, 1995) showed that endmember bearthite is stable over a very wide range in pressure in the $CaO\text{-}Al_2O_3\text{-}P_2O_5\text{-}H_2O$ system, from ultra-high down to very low pressures. With increasing temperatures, bearthite breaks down to apatite + α-berlinite ($AlPO_4$) + corundum + vapour, with a positive Clapeyron

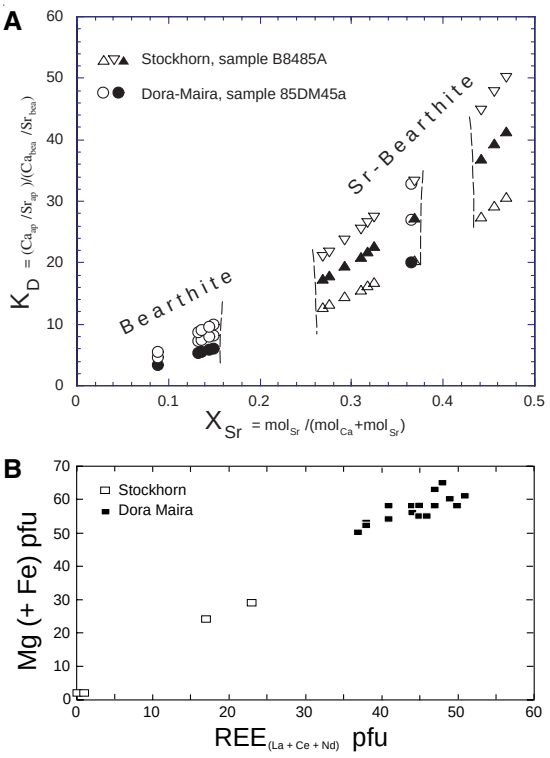

Fig. 4: (**A**) X_{Sr} of coexisting pairs of bearthite - Sr-bearthite (85DM45a) and (B8485A) hinting at possible compositional gaps between coexisting Ca- versus Sr-enriched members. The data represents analyses made on contrasting shades of the BSE image seen within the $(Ca,Sr)_2Al(PO_4)_2(OH)$ phase (Fig. 1a and 5). (**B**) This figure demonstrates the clear relationship between Mg and La + Ce + Nd, suggestive of an allanite-type $Ca_{-1}Al_{-1}MgREE$ substitution.

slope, from approximately 550°C at near-atmospheric pressure to 800°C at 8 kbar. P-T estimates for the Dora-Maira occurrence are about 725°C, 30 kbar (talc + pyrope + coesite/quartz). Peak metamorphic estimates for the Monte Rosa nappe are 550°C at >20 kbar (presence of talc + chloritoid + kyanite assemblages, e.g. LE BAYON et al., 2000 unpubl.). This suggests that increasing REE in the system causes the reaction curve to shift to lower temperatures. Sample Mo9801 is likely to have gone through high- to ultra-high-pressure at initially low temperature conditions during continental subduction of the Monte Rosa nappe (e.g. DAL PIAZ and LOMBARDO, 1986; LE BAYON et al., 2000 unpubl.). Since the assemblage

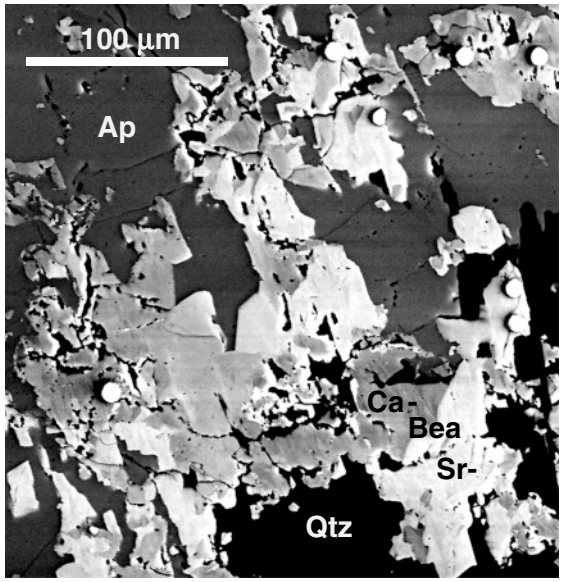

Fig. 5: Contrasting BSE image of the Stockhorn sample B8485A displaying the patchy character of bearthite in this sample with Ca- versus Sr-enriched zones.

contains abundant quartz it is likely that bearthite relics survived only as inclusions in allanite. Bearthite then broke down to the Ap + Mnz + Crn symplectite during decompression, similar to the Dora-Maira sample. The occurrence of corundum is limited to these inclusions, where the Al-phase is isolated from quartz.

ZHANG et al. (1997) and LIOU and ZHANG (1998) observed that monazite exsolution lamellae are common in apatite in the Dabie Shan ultra-high-pressure terrane. Similar exsolutions of monazite (?) in apatite were also observed by the third author in coesite-bearing rocks of Dora-Maira. This may signify a limited solid solution between monazite and apatite (Fig. 6). Moreover, these authors also describe monazite as matrix grains, suggesting that either the Ca/Al ratio of the whole rock or the local Ca/Al ratio is controlling the presence of the phosphate assemblage (Fig. 6). In calcium-rich environments, apatite or $apatite_{ss}$ + $monazite_{ss}$ form, whereas in aluminium-rich lithologies (pelitic rocks, and granitic gneisses) bearthite is expected (Fig. 6). If bearthite forms under ultra-high pressure conditions and the mineral $(REECaMg(PO_4)_2OH$ - "bearthite" component) takes up U and Th from the monazite, as

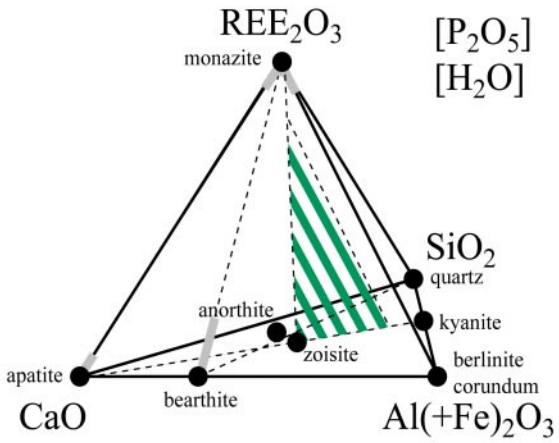

Fig. 6: Phase relations in the CaO-Al_2O_3-SiO_2-REE_2O_3-P_2O_5-H_2O system projected from the H_2O and P_2O_5 apices. Shaded area indicates allanite solid-solution field.

indicated by the data in table 1, this offers an interesting possibility to constrain the time when ultra-high-pressure conditions were reached. Referring to sample 85DM45, the chondrite normalised REE pattern of bearthite and of monazite formed by its breakdown are similar and both are LREE dominated (Fig. 3a). Since REE patterns of allanite are variable, and may either be LREE or HREE dominated (SMULIKOWSKI & KOZLOWSKI, 1994; DUDA & NAGY, 1995; PETRIK et al., 1995), it cannot be strictly excluded that allanite could also have been involved in the prograde formation of bearthite.

Conclusions

A previously documented symplectite rim around a rare-earth-bearing bearthite has been reinvestigated to confirm that 1) the product phase is monazite and 2) bearthite is a potential precursor of a fine-grained reaction texture, with the product phase assemblage apatite + monazite + corundum. Both bearthite and its Sr-bearthite are shown to be LREE-fractionating phases.

Considering the large number of studies based on radiometric dating of monazite, compared to the paucity of knowledge on monazite-forming reactions, this documentation contributes to the understanding of the genesis of this rare-earth phosphate. Specifically, dating of bearthite and symplectitic monazite offers the interesting possibility to constrain the time (1) when ultra-high-pressure conditions were attained (prograde), and (2) when decompression and/or heating set in.

Acknowledgements

This study is part of a PhD project supported by Schweizerischer Nationalfonds (Credit 20-49671.96/1 and 2000-055306.98/1). The EMP laboratory at the MPI Bern has been funded by Schweizerischer Nationalfonds (Credit 21-26579.89). Beda Hofmann, Natural History Museum Bern, is thanked for providing the bearthite sample B8485A from the Stockhorngrat type locality. Open doors for use of the EMP facility at IMP Lausanne are also acknowledged. Andreas Jenni is thanked for his assistance with the SEM of the Geological Institute Bern.

References

AKERS, W. T., GROVE, M., HARRISON, T. M. & RYERSON, F. J. (1993): The instability of rhabdophane and its unimportance in monazite paragenesis. In: Geochemistry of accessory minerals; papers presented at the Third V. M. Goldschmidt conference. Chem. Geol. (eds Watson, E. B., Harrison, T. M., Miller, C. F. & Ryerson, F. J.), pp. 169-176, Elsevier. Amsterdam Netherlands. 1993.

BEARTH, P. (1952): Geologie und Petrographie des Monte Rosa. Beitr. geol. Karte Schweiz 96; Kümmerly & Frey AG, Bern.

BEARTH, P. (1957): Erläuterungen zu Blätter Saas und Monte Moro. Geologischer Atlas der Schweiz 1:25 000; Blätter 30 & 31. Schweiz. Geol. Kommission, 1-20.

BINGEN, B., DEMAIFFE, D. & HERTOGEN, J. (1996): Redistribution of rare earth elements, thorium, and uranium over accessory minerals in the course of amphibolite to granulite facies metamorphism: The role of apatite and monazite in orthogneisses from southwestern Norway. Geochimica et Cosmochimica Acta, 60, 1341-1354.

BORGHI, A., COMPAGNONI, R., SANDRONE, R. (1996): Composite P-T paths in the internal Penninic massifs of the western Alps: Petrological constraints to their thermo-mechanical evolution. Eclogae Geologicae Helvetiae, 89, 345-367.

BROSKA, I. & SIMAN, P. (1998): The breakdown of monazite in the West-Carpathian Veporic orthogneisses and tatric granites. Geologica Carpathica, 49, 161-167.

BRUNET, F. and CHOPIN, C. (1995): Bearthite, $Ca_2Al(PO_4)_2OH$: stability, thermodynamic properties and phase relations. Contrib. Mineral. Petrol., 121, 258-266.

CHOPIN, C., BRUNET, F., GEBERT, W., MEDENBACH, O. and TILLMANNS, E. (1993): Bearthite, $Ca_2Al[PO_4]_2(OH)$, a new mineral from high-pressure terranes of the western Alps. Schweiz. Mineral. Petrogr. Mitt., 73, 1-9.

DAL PIAZ, G.V., LOMBARDO, B. (1986): Early Alpine eclogite metamorphism in the Penninic Monte Rosa - Gran Paradiso basement nappes of the northwestern Alps. In: EVANS, B.W. and BROWN, E.H. (eds) *Blueschists and eclogites.* Memoir - Geological Society of America, Boulder, 164, 249-265.

DUDA, G., NAGY, G. (1995): Some REE-bearing accessory minerals in two types of Variscan granitoids, Hungary. Geologica Carpathica, 46, 67-78.

FINGER, F., BROSKA, I., ROBERTS, M. P. & SCHERMAIER, A. (1998): Replacement of primary monazite by apatite-allanite-epidote coronas in an amphibolite facies granite gneiss from the eastern Alps. American Mineralogist, 83, 248-258.

HEINRICH, W., ANDREHS, G., FRANZ, G. (1997): Monazite-xenotime miscibility gap thermometry. 1. An empirical calibration. Journal of Metamorphic Geology, 15, 3-16.

LE BAYON, R., DE CAPITANI, C.; CHOPIN, C. AND FREY, M. (2000): Modelling of the sequential evolution of whiteschist assemblages: HP in Monte Rosa (Western Alps). 2000 Annual Meeting in Winterthur, Swiss Society for Mineralogy and Petrology. Winterthur, 12-13 October 2000, unpublished.

LIOU, J.G. & ZHANG, R.Y. (1998): Petrogenesis of ultrahigh-P garnet-bearing ultramafic body from Maowu, the Dabie Mountains, Central China. Island Arc, 7, 115-134.

PAN, Y. M. (1997): Zircon- and monazite-forming metamorphic reactions at Manitouwadge, Ontario. Canadian Mineralogist, 35, 105-118.

PETRIK, I., BROSKA, I., LIPKA, J., SIMAN, P. (1995): Granitoid allanite-(Ce): Substitution relations, redox conditions and REE distributions (on an example of I-type granitoids, Western Carpathians, Slovakia). Geologica Carpathica, 46, 79-94.

SCHERRER, N.C., ENGI, M., GNOS, E., JAKOB, V. and LIECHTI, A. (2000): Monazite analysis; from sample preparation to microprobe age dating and REE quantification. Schweizerische Mineralogische und Petrographische Mitteilungen, 80, 93-105.

SMITH, H. A. & BARREIRO, B. (1990): Monazite U-Pb dating of staurolite grade metamorphism in pelitic schists. Contributions to Mineralogy and Petrology, 105, 602-615.

SMULIKOWSKI, W., KOZLOWSKI, A. (1994): Distribution of Cerium, Lanthanum and Yttrium in Allanites and Associated Epidotes of Metavolcanic Rocks in Hornsund Area, Vestspitsbergen. Neues Jahrbuch Fur Mineralogie - Abhandlungen, 166, 295-324.

ZHANG, R.Y., HACKER, B. & LIOU, J.G. (1997): Exsolution in ultrahigh-pressure rocks from the Dabie-Sulu (China) and Kokchetav (Khazakhstan) terranes. Terra Nova, 9, 43.

Non-destructive micro-dating of monazite by XRF technology

by *N.C. Scherrer[1], M. Engi, A. Cheburkin, R. R. Parrish and A. Berger*

Abstract

A newly developed XRF-microprobe at the Institute of Mineralogy and Petrology, University of Bern, Switzerland, has been applied for precise chemical Th-U-Pb dating of individual monazite grains separated from Pb-free polished petrographic thin sections. The non-destructive nature of the XRF-microprobe permitted a comparative study of dating methods by sequentially applying chemical dating by electron microprobe analysis (EMPA), chemical dating by XRF-microprobe analysis, and isotopic $^{208}Pb/^{232}Th$ dating by LA-PIMMS (**L**aser **A**blation **P**lasma **I**onisation **M**ulti-collector **M**ass **S**pectrometry) analysis. As an example, the precision achieved with the XRF-microprobe for a well characterised monazite age standard FC-1 (TIMS age 54.3 Ma; μ-XRF age 55.3 ± 2.6 Ma), doubly polished to 30 μm in thickness, is below 5 % (2 sigma) after 90 minutes integration time (50 kV; 30 mA) at a spatial resolution of 90 μm. The sample characteristics are: 200-300 ppm of Pb (μ-XRF), 3.8-5.1 wt% of Th (EMPA) and 0.4-1.4 wt% U (EMPA). Combined with an electron microprobe and conventional optical microscopy, the XRF-microprobe is thus a competitive low-cost and non-destructive alternative to more costly isotopic methods. The XRF-microprobe is easy to use and maintain.

Keywords: monazite, EMPA, XRF-microprobe, LA-PIMMS, Th-U-Pb dating

Introduction

Monazite is acclaimed to possibly be one of the most promising accessory phases for dating metamorphism in amphibolite and higher grade granitic and pelitic rocks (FOSTER et al., 2000; FINGER et al., 1998; SPEAR and PARRISH, 1996). In rocks from polymetamorphic terrains, often more than one population of monazite may be distinguished on the basis of textural relationships. So it has been observed that monazite inclusions within garnet preserve ages that are distinctly different from monazite ages found within the matrix (eg. FOSTER et al., 2000; MONTEL et al., 2000; SIMPSON et al., 2000; ENGI et al. in prep.). This window to the past increases chances to time-constrain ancient geothermobarometric conditions of included assemblages, and thus may potentially permit time-calibrated P-T paths.

Monazite rarely incorporates substantial amounts of common lead ^{204}Pb and thus Pb_{total} in most cases, ~equals $Pb_{radiogenic}$. Since Th is a major element in monazite, sufficient $Pb_{radiogenic}$ is produced within 100 to 200 Ma such that Pb_{total} can be quantified by means of easily accessible electron microprobe analysis (SUZUKI and ADACHI, 1991a; MONTEL et al., 1996; SCHERRER et al., 2000), offering the conventional petrologist a somewhat imprecise but useful geochronometer (MONTEL et al., 1996; RHEDE et al., 1996) with high spatial resolution (< 5μm). The fact that chemical age dating approximates isotopic dating in the case of monazite suggests that the lower limitation (minimum age) is mainly set by the analytical detection limit of the element Pb. While the electron microprobe has clear limitations in dating geologically young samples, the new XRF-microprobe technology achieves minimal background interference such that the detection limit of the XRF-microprobe instrument (Fig. 1) with respect to Pb is as low as 10 ppm.

This paper follows up on an earlier publication (SCHERRER et al., 2000) where aspects of sample preparation and full rare-earth element quanti-

[1] Mineralogisch-petrographisches Institut, Universität Bern, Baltzerstrasse 1, CH-3012 Bern, Switzerland. <scherrer@mpi.unibe.ch>

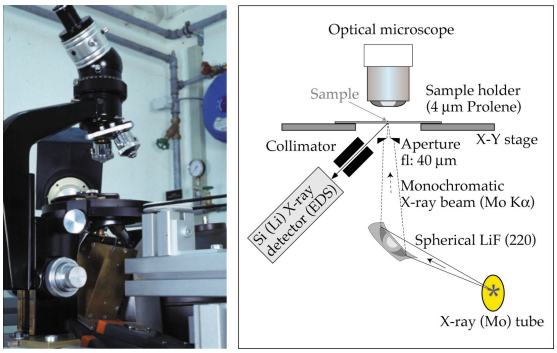

Fig. 1: Schematic and photographic view of the XRF-microprobe layout at the MPI Bern, Switzerland.

fication on monazite - with particular emphasis on chemical Th-U-Pb dating - have been addressed. Here we introduce the non-destructive high-precision chemical dating technique by XRF-microprobe as applied to well-characterised single grains drilled individually from doubly polished petrographic thin sections. The non-destructive nature of the method permitted a comparative study with an independent isotopic dating method LA-PIMMS (Parrish et al. 1999), analysing $^{208}Pb/^{232}Th$ ratios corrected for ^{204}Pb.

Opposed to conventional heavy liquid separation techniques used in geochronology, our aim was to retain the full context information of each single grain we attempted to date. Doubly polished petrographic thin sections are perhaps the most versatile and informative sample preparation method in petrology. Performing age dating of single grains in well characterised thin sections is thus geologically far more powerful and informative. This becomes particularly important when dealing with polymetamorphic rocks where multiple stages of monazite growth may have been preserved. Combining optical and BSE image information with quantitative analysis by EMP and Th-U-Pb dating by EMP, XRF-microprobe and LA-PIMMS in a database provided a very powerful tool for the 'correct' interpretation of age data.

The XRF-microprobe instrument

The principal design elements of the energy-dispersive XRF-microprobe instrument are a conventional X-ray tube (Mo, fine focus, 3 kW), a spherically focussing LiF monochromator, a sample holder (4 micron prolene), and an energy-dispersive Si(Li) X-ray detector cooled with liquid nitrogen (Fig. 1). A pulse-processor converts the detected signal into a spectrum which is easily processed on a conventional PC-computer. An optical microscope with a rotating x-y sample stage permit optical recognition and centring of the grain to be analysed prior to measurement. The system is fed by a generator, cooled by a closed water circuit and operates at normal room conditions (no vacuum). Originally designed as a small desktop system, this instrument is simple to build, operate, maintain and modify according to new needs, if necessary.

The energy resolution for eg. Mn is ~130 eV. Use of monochromatic X-ray radiation achieved low background, with much lower detection limits than in conventional XRF instruments. For a single grain derived from polished thin section (30 µm) as small as Ø 50 µm, the detection limits for U, Th, and Pb are on the order of 10 ppm for analysis times of 60 minutes. Different apertures are available to account for variable needs from high spatial resolution to homogenous average composition: one with a small hole of Ø 35 µm and an estimated interaction volume of ~1150 μm^2 multiplied by the sample thickness; a medium one of Ø 90 µm with an estimated interaction volume of ~7850 μm^2 times the sample thickness; and a large one of Ø 1000 µm for fast and homogenised analyses on larger samples. Since the minimum integration time necessary to achieve sufficient statistics strongly depends on the volume, Th content and age, it is more efficient to use the larger aperture, unless the size of unseparated grains or internal zonation do not permit such low spatial resolutions. Using the small aperture significantly increases the integration time necessary (factor of 9) for achieving equivalent statistics, but on the other hand the original spatial resolution is reduced by about 7 times. Use of doubly polished grains minimises topographic effects such that rotation of the stage during acquisition is not necessary, but is available for homogenised average analyses.

X-ray spectra (Fig. 2) and data analysis: Complete spectra of individual mineral grains or zones are collected at 30 kV and 50 mA by EDS over 5-120 minutes, depending on the age and volume of the sample, spatial resolution and required precision.

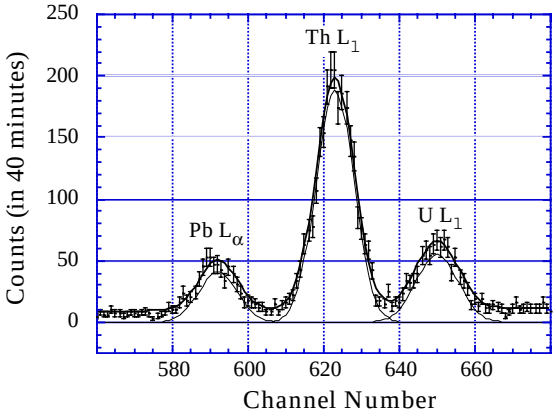

Fig. 2: Close-up view of an EDS spectrum by XRF-microprobe showing the section which is processed for Th-U-Pb age determination.

Since the method is non-destructive, small and young grains can be repeatedly measured for improved statistics (and improved age precision), thus providing a clear advantage over destructive methods using laser-ablation technology - where a failed analysis means no result at all. Spectral peaks (Fig. 2) of all elements to be analysed in monazite including Pb L_a (10.5 eV), Th L_l (11.12 eV), and U L_l (11.62 eV) are normalised by the peak area due to coherent scattering. This normalisation accounts very effectively for differences in grain size (mass) and permits analysis of individual grains as small as 20 µm. For element ratios, such as Pb/Th required to date monazite, this method is thus essentially standard-free. Determining absolute elemental concentrations for any element, however, does require a suitable standard from the same mineral group as the sample material. A well characterised gem quality monazite from Manangotry (Madagascar) was utilised for this calibration. Ages are calculated in a simple iteration, based on the measured Pb/Th ratio and accounting for the contribution of U and Pb derivatives thereof (CHEBURKIN et al., 1997), like in chemical dating by electron microprobe (SUZUKI and ADACHI, 1991b; MONTEL et al., 1996).

From optical microscopy to µ-XRF dating

The preparation of lead-free polished thin sections, an essential precondition for chemical Th-U-Pb dating, is described in SCHERRER et al. (2000). Apart from SHRIMP analysis, most high-precision methods still have a spatial resolution, which may exceed the resolution required to avoid mixing of distinct growth zones in small or internally heterogeneous grains. Similarly, interference from adjacent minerals in thin section is often a problem where monazite grain sizes are smaller than 60 microns. An additional problem is the penetration depth of different analytical techniques. With XRF-microprobe analysis, where the penetration depth exceeds several tenths of microns, traces of Pb within the glass substrate of a petrographic thin section will interfere with the monazite signal. We thus prepare our thin sections using an acetone-soluble glue so as to permit removal of doubly polished grains from the thin section by use of a diamond micro-drill (Fig. 3), acetone and a preparation needle. The separated grains are then mounted on a substrate producing minimal interference to the XRF signal. A 4 µm thick prolene foil and Canada balsam offer easy handling with no interference within the detection limit of the XRF-microprobe.

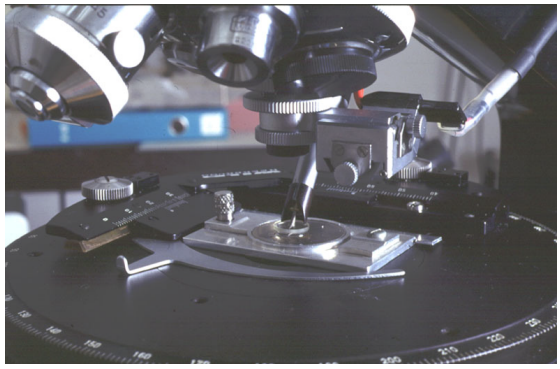

Fig. 3: Photograph showing the diamond micro-drill mounted on a conventional optical petrographic microscope.

For successful chemical Th-U-Pb dating by XRF-microprobe, the following aspects should thus be considered in the sample preparation:

- *thin sections should be prepared with an acetone soluble glue (easy removal)*
- *polishing should be performed on a Pb-free polyethylene disk to avoid contamination of the Th-U-Pb ratio with common lead*

Since individual grains are removed from their original context for µ-XRF analysis, documentation should be as complete as possible and thus the following work is desirable prior to µ-XRF sample preparation:

- *microfiche photocopy of whole thin section (thin section overview)*
- *BSE context image for each monazite (Fig. 4; local context overview)*
- *BSE zonation image (Fig. 4; internal homogeneity versus heterogeneity)*
- *quantitative analysis on monazite (Th contents of > 1 wt% are preferable; chemical Th-U-Pb age by EMP may provide imprecise but useful 'reconnaissance' information)*
- *optical image with parallel and crossed nicols (petrographic overview of the local context)*
- *an optical image of the grain mount provides information on which part of the grain has been successfully removed and whether the separate is clean or still contains other phases attached (potential interference)*
- *combining all available information into a 'grain database' (Fig. 5)*

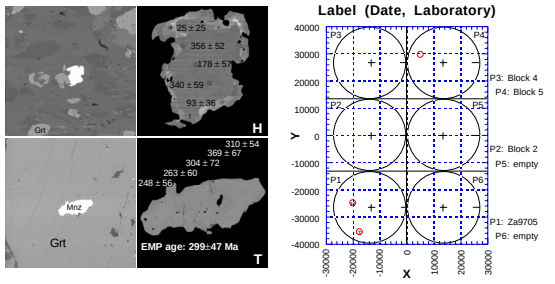

Fig. 4: Searching monazite in BSE mode on an electron microprobe is probably the most efficient way of locating monazite in Pb-free polished thin sections: the EMP combines BSE context and zonation (and optical) views (left) with full quantitative analyses (Tab. 1; chemical Th-U-Pb dating). Furthermore, X-Y coordinates of the position of any analysed grain are very easily transferred to the thin sections (right) for efficient recognition on an optical microscope. This a considerable advantage to people with no experience in the optical recognition of monazite (refer to the appendix in Scherrer et al. 2000) intending to successfully apply micro-dating of monazite.

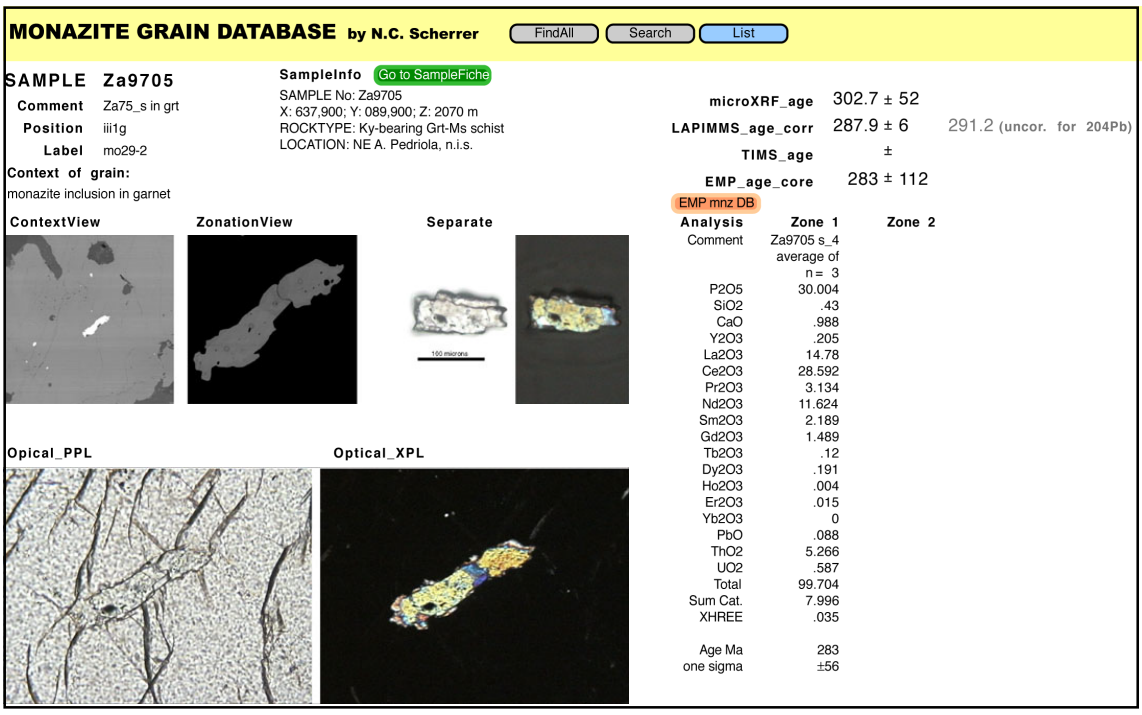

Fig. 5: An example of a Grain-Database entry. The database permits to compare several criteria relevant to the interpretation of age analysis in one clear overview. More examples are discussed on the website.

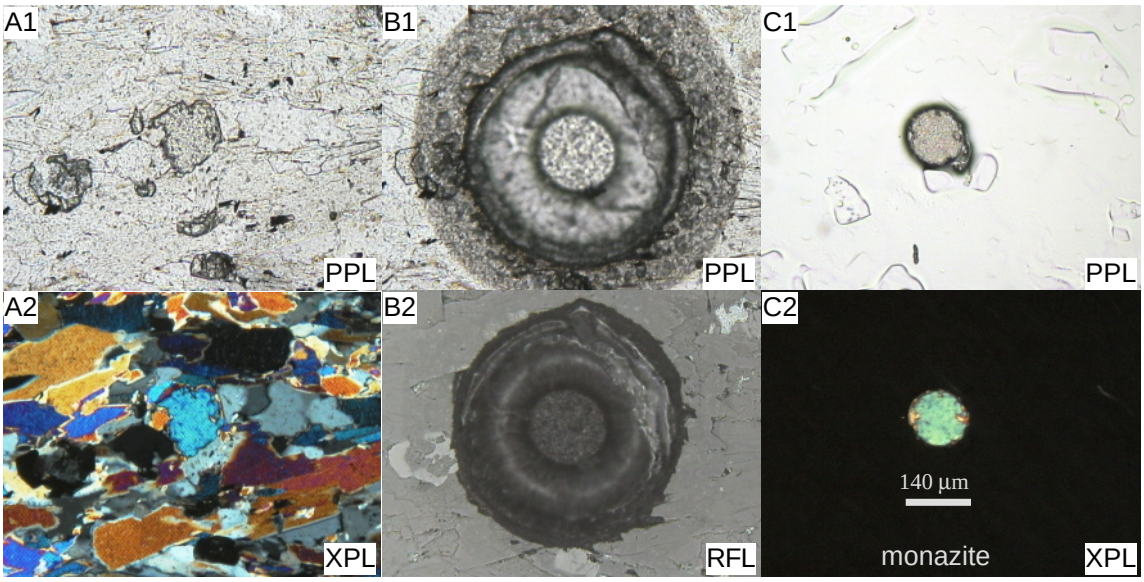

Fig. 6: A) Optical image of a kyanite bearing garnet-mica gneiss with the view centred on a matrix monazite. B) Optical images in transmitted and reflected light mode demonstrating the minimal loss of material at thin section scale by applying a micro diamond drill for the preparation of doubly polished grain mounts with full context control. The micro drill is mounted on a conventional optical microscope (Fig. 3). The cloudy rim in the upper image is the zone of acetone leaching the glue of the thin section. C) The finished grain mount ready for XRF-microprobe analysis. The substrate used is a 4 µm prolene foil and the grains are mounted with Canada balsam. Canada balsam has several useful properties: it contains no common lead; it is non toxic and easily dissolves and redissolves in alcohol; it is optically clear when dry. PPL = plane polarised light; XPL = crossed polarised light; RFL = reflected light.

Zone	**Core**	**Rim**
average of	n = 3	n = 2
Y2O3	**2.20**	**0.34**
La2O3	13.77	9.88
Ce2O3	27.41	25.96
Nd2O3	11.29	13.83
Sm2O3	2.03	3.16
PbO	0.09	0.03
ThO2	**4.99**	**6.79**
UO2	**0.55**	**1.21**
Age Ma	**291±98**	**47±66**

Tab. 1: The use of a full quantitative analysis by EMP of monazite grains to be dated is often underestimated. Even though dating by EMPA has large uncertainties associated with the technique and can only serve as 'reconnaissance' dating, the high spatial resolution is unbeaten and so is the beam positioning control with live BSE imaging. Furthermore, in polymetamorphic rocks, multiple stages of monazite growth can directly be linked to mineral growth topology using the quantitative variation of particular elements like yttrium and others. Thus, age information with such documentation becomes geologically far more relevant.

Once all the documentation is ready, any monazite suitable for µ-XRF analysis, ie. not zoned in age and preferentially larger than ~40 microns in diameter, can be drilled out and prepared for µ-XRF analysis (Fig. 6). Following age determination by µ-XRF, the same grains may be analysed by an independent isotopic technique at higher precision with little additional effort concerning sample preparation.

Chemical Th-U-Pb dating by XRF-microprobe

The µ-XRF of the MPI Bern currently has a maximum spatial resolution of ~38 µm. Larger apertures (90 µm and 1000 µm) are available for better efficiency with homogenous grains (Fig. 7). Using doubly polished separates (derived from thin sections), topographic effects as encountered with measuring irregularly shaped whole grains derived

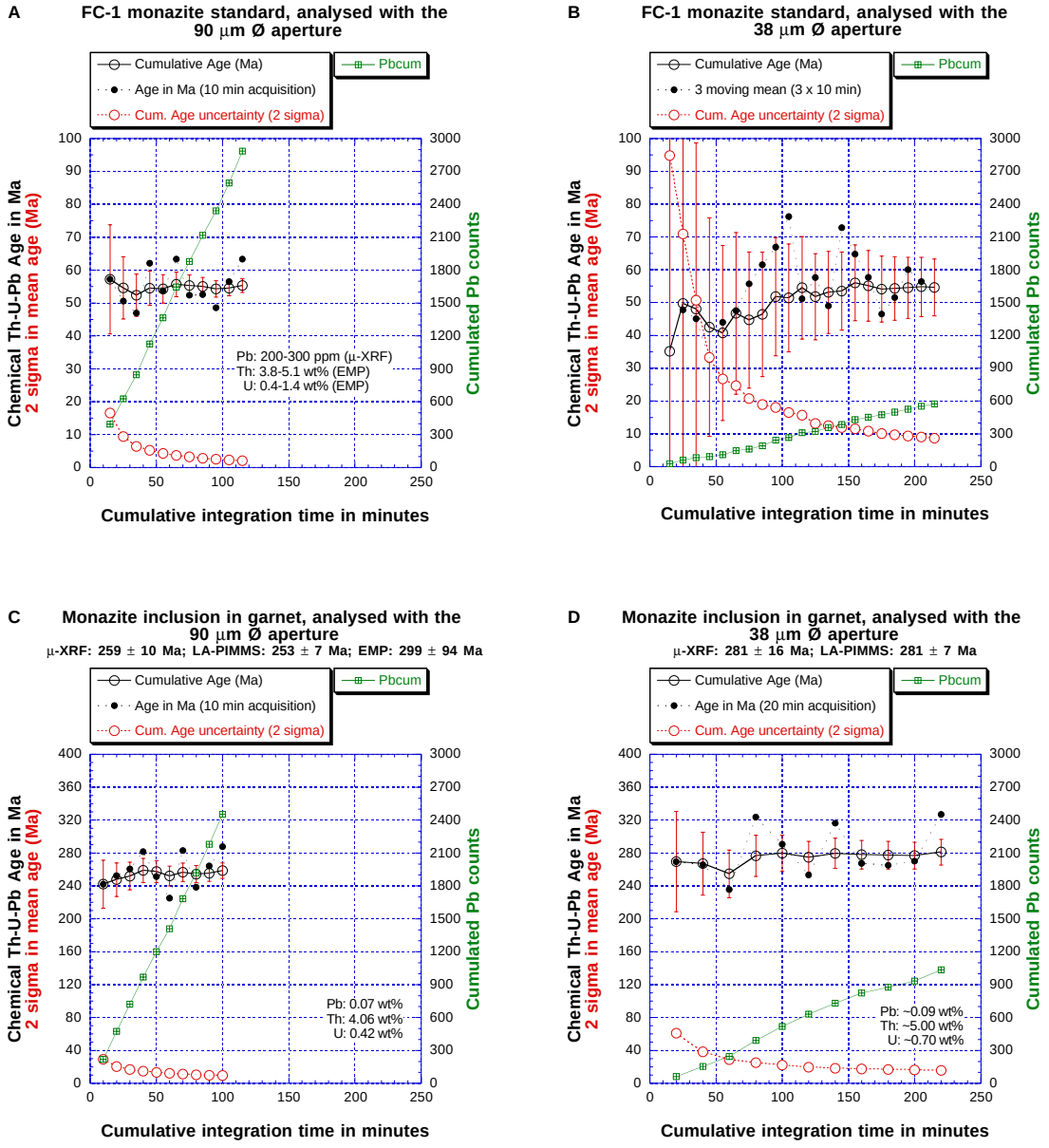

Fig. 7: These plots demonstrate the performance of the XRF-microprobe using two different spatial resolutions: 90 µm versus 38 µm, tested on a Tertiary monazite age standard (FC-1; A and B) and on two Permian monazite grains (C and D). Instrument settings for Th-U-Pb age determination are commonly 30 kV at 50 nA. The plots are indicative of the integration time required and the uncertainties to be expected when analysing single monazite grains separated from thin sections. The age uncertainties are based on the counting statistics of the Pb determination. Note the implications for analysing small (< 50 microns) versus large (> 90 microns) grains: with the small aperture, integration time is 9 times longer to achieve similar counting statistics as with the 90 µm aperture (compare cumulated Pb counts of sample FC-1). Since the technique is non-destructive, analysis can be performed in cumulative mode and integration times can be adjusted individually until a satisfactory level of uncertainty is reached. This leaves the option open to age date young grains smaller than 30 µm, something that may not be achieved easily satisfactorily with destructive TIMS or LA-ICPMS techniques.

from crushed rock separates are negligible. Integration time varies with the volume to be measured and the amount of lead present, which in turn is a function of age and thorium (and uranium) content.

Chemical versus isotopic ages

Chemical ages of monazite are mainly Th/Pb ages (see MONTEL et al. 1994), but a direct comparison between isotopic 232Th/208Pb ages and chemical ages was missing. We used standard material FC-1 derived from a pegmatite in the Canadian Cordillera, which is well characterised by TIMS analysis, using both U-Pb and Th-Pb systems (PARRISH, 1990; 1995). We measured the same material using LA-PIMMS, µ-XRF and EMP. Using high quality µ-XRF data (Fig. 7) the ages agree with the 208Pb/232Th isotope age uncorrected for common Pb (eg. grains FC-1_std, G7_std and G1_std in Fig. 8) within the uncertainty of the analytical precision.

The overlap of ages on standard material give the possibility to directly compare isotope ages with chemical ages of unknown samples (Fig. 8). The samples presented in figure 8 demonstrate that µ-XRF ages are all within the 2-sigma analytical error of the isotopic age. Thus, high-precision ages can be achieved with an XRF-microprobe. The precision, however, depends on integration time as a function of grain size, Th-content and age.

Performance and uncertainty

Figure 7 demonstrates the acquisition time necessary to date an individual grain separated from a polished thin section (approx. volume of 191000 µm^3 with the 90 µm aperture and 34000 µm^3 with the 38 µm aperture) at minimum uncertainty of around 5% at the two sigma level. Since µ-XRF analysis is non-destructive on the separates, there is no limit other than efficiency as to how long a grain may be analysed. With cumulative acquisition measurements, the

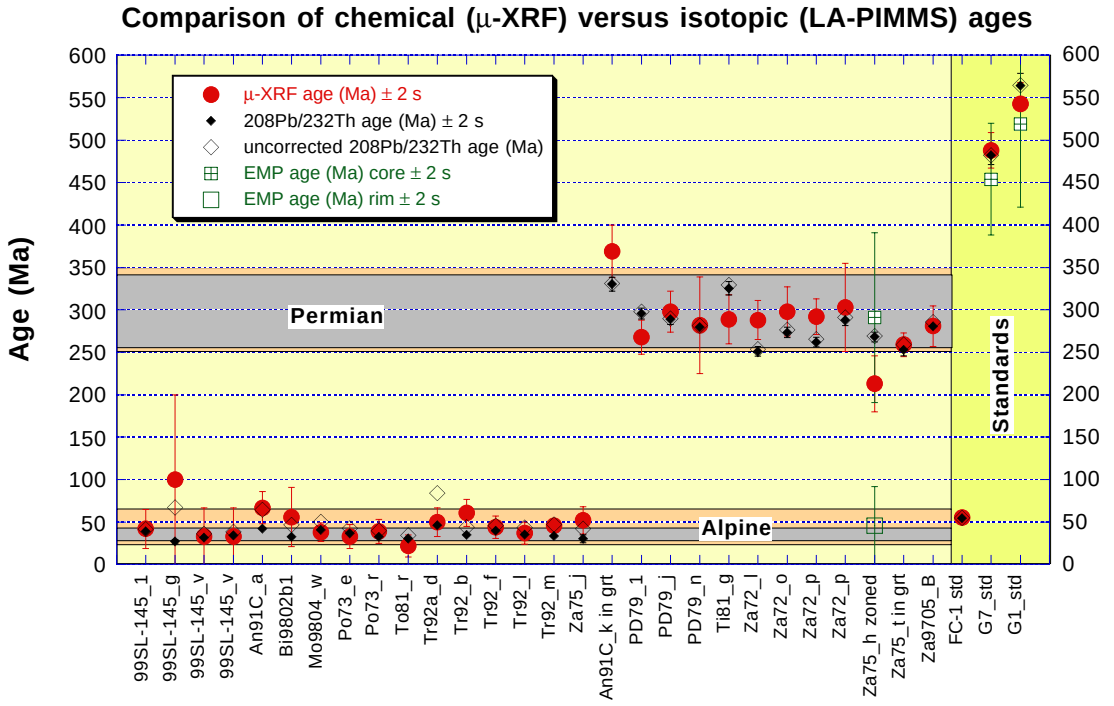

Fig. 8: Direct comparison of chemical Th-U-Pb ages (µ-XRF and EMP) with isotopic $^{208}Pb/^{232}Th$ ages (LA-PIMMS) for a set of sequentially dated single grain separates (doubly polished). Note that with few exceptions, integration time for the XRF analysis was generally 60 minutes and extended to a maximum of 120 minutes per grain, if cumulated Pb counts did not reach 100 after 60 minutes (compare Fig. 7). The colour bands delimit one standard deviation about the mean of µ-XRF versus LA-PIMMS analyses.

precision of an age determination can thus be optimised to a limit from where on it may no longer be economical. This is shown in figure 7, where a well characterised monazite age standard of Tertiary age has been prepared as described above and measured at two different spatial resolutions and a series of equally spaced time intervals. Using the cumulative acquisition mode, the gain in statistics leads to continuously improved precision of the apparent age. At 90 µm spatial resolution a minimum acquisition time of less than 1 hour is sufficient to achieve a maximum uncertainty of ±10% in age at the 2-sigma level. For similar precision with the 38 µm spatial resolution, a nine-fold increase in acquisition time becomes necessary, as can be determined from the cumulated Pb counts over time at the two spatial resolutions (Fig. 7). A choice is thus to be made between precise age data (few grains, long integration times, repeat measurements), or approximate age data (lots of grains, minimal integration times - eg. stopping cumulative acquisition as soon as Pb counts are near 100).

The age uncertainty is derived from the statistical uncertainty associated with the determination of Pb ($\sqrt{N_{Pb}}/N_{Pb}$), propagated to the age calculation. No other correction is currently applied.

Discussion and summary

Table 2 compares EMPA, µ-XRF analysis and LA-PIMMS analysis on the basis of several criteria relevant to dating of monazite.

Summarising capabilities and advantages of the XRF-microprobe:

- *(separated) grains as small as Ø 20 µm may be dated*
- *non-destructive nature of the µ-XRF sets no limitation on integration time to achieve good statistics even for very small and young < 50 Ma monazite grains*
- *since the method is non-destructive, verification can be achieved with an independent dating technique*
- *for a grain of Permian age, an analytical uncertainty of less than ±10% (2 sigma) is achieved with an integration time of ~100 minutes at a spatial resolution of Ø 38 µm (for grains < 90 µm, integration time is one ninth using the 90 µm diameter aperture)*

Criteria	**EMPA**	**µ-XRF**	**LA-PIMMS**
Th-U-Pb dating	chemical	chemical	isotopic
Common lead 204Pb correction	no	no	yes
207Pb/206Pb ages	no	no	yes
Average precision at 2 sigma	± 35 %	< ± 10 %	± 1.5-5 %
Spatial resolution	Ø < 5 µm	Ø 38 or 90 µm	30x30 µm
Beam shape	spot or rectangle	fixed, circular	variable shape
Penetration depth	< 5 µm	> 30 µm	~ 10 µm
Destruction during analysis	none	none	complete
Repeat measurement	possible	unlimited	not on same material
Optical control (real time)	very good	limited	good
BSE imaging (simultaneous)	yes	no	no
transmitted light (simultaneous)	yes	oblique	yes
reflected light (simultaneous)	yes	no	yes
beam visibility (simultaneous)	yes	no	yes
Average analysis time (min)	20	30-240	< 5
Calibration time	3 hours	- *	~30 min
stability of calibration	several days	- *	10-30 analyses
Consumption of standard material	small / unique	small / unique	considerable /continuous

Tab. 2: This table summarises and compares several criteria to be considered when analysing monazite by any or a combination of the presented methods. * The µ-XRF calibration procedure involves a unique effort at the initial setup of the instrument. From then on, each spectrum is normalised by the peak area due to coherent scattering and Th Ll at the other end. Thus, calibration time regarding µ-XRF analysis can essentially be neglected.

Some limitations and disadvantages:

- *beam is invisible on measurement and since it is non-destructive it leaves no markers on analysed spots. This may be considered as a disadvantage relevant to heterogeneous grains only, which are unsuitable for μ-XRF analysis.*
- *lack of isotopic correction for common lead ^{204}Pb leads to slight overestimation of young ages, particularly with Th-poor monazite; overestimation, however, is still within the 2 sigma uncertainty of the μ-XRF analysis.*
- *there is a practical limit with respect to handling very small grains (training)*
- *the method is not suitable to analyse grains with heterogeneous age zones due to limited spatial and temporal resolution*

Conclusions

A new and low cost method for high precision chemical Th-U-Pb dating of monazite has been introduced. Thanks to the non-destructive nature of the technique, we were able to present a direct comparison of performance of the XRF-microprobe with the most accessible but limited chemical dating technique using the electron microprobe, and more precise but destructive and less accessible isotopic dating method, LA-PIMMS. The methodological approach presented is particularly useful and promising to better understand the evolution of polymetamorphic rocks (P-T-t paths) by relying on the petrographer's most versatile research medium - the polished thin section - from initial optical characterisation to thermobarometry and age dating for all data acquisition. Since context information is retained throughout the different steps, there is a clear advantage over conventional dating methods which rely on loose grains picked from crushed whole rock separates.

Acknowledgements

This study is part of a PhD project supported by Schweizerischer Nationalfonds (Credit 20-49671.96/1 and 2000-055306.98/1). The EMP and XRF laboratories at the MPI Bern have been funded by Schweizerischer Nationalfonds (Credit 21-26579.89).

References

CHEBURKIN, A.K., FREI, R., SHOTYK, W. (1997): An energy-dispersive miniprobe multielement analyzer (EMMA) for direct analysis of trace elements and chemical age dating of single mineral grains . Chemical Geology, 135 , 75-87.

CROWLEY, J.L., PARRISH, R.R. (1999): U-Pb isotopic constraints on diachronous metamorphism in the northern Monashee complex, southern Canadian Cordillera. Journal of Metamorphic Geology, 17, 483-502.

FINGER, F., BROSKA, I., ROBERTS, M.P. and SCHERMAIER, A. (1998): Replacement of primary monazite by apatite-allanite-epidote coronas in an amphibolite facies granite gneiss from the eastern Alps. American Mineralogist, 83, 248-258.

FOSTER, G., KINNY, P., VANCE, D., PRINCE, C. and HARRIS, N. (2000): The significance of monazite U-Th-Pb age data in metamorphic assemblages; a combined study of monazite and garnet chronometry. Earth and Planetary Science Letters, 181, 327-340.

MONTEL, J.M., VESCHAMBRE, M., NICOLLET, C. (1994): Dating Monazite with the Electron Microprobe. Comptes Rendus de L Academie Des Sciences Serie II , 318 , 1489-1495.

MONTEL, J.M., FORET, S., VESCHAMBRE, M., NICOLLET, C. and PROVOST, A. (1996): Electron microprobe dating of monazite. Chemical Geology, 131, 37-53.

MONTEL, J.M., KORNPROBST, J. and VIELZEUF, D. (2000): Preservation of old U-Th-Pb ages in shielded monazite: example from the Beni Bousera Hercynian kinzigites (Morocco). Journal of Metamorphic Geology, 18, 335-342.

PARRISH, R.R. (1990): U-Pb dating of monazite and its application to geological problems. Canadian Journal of Earth Sciences = Journal Canadien des Sciences de la Terre, 27, 1431-1450.

PARRISH, R.R. (1995): Thermal evolution of the southeastern Canadian Cordillera. Canadian Journal of Earth Sciences, 32, 1618-1642.

PARRISH, R.R., NOWELL, G., NOBLE, S.R., HORSTWOOD, M., TIMMERMANN, H., SHAW, P., and BOWEN, I. (1999): LA-PIMMS: A new method of U-Th-Pb geochronology using micro-sampling techniques. EUG10, Terra Abstracts, 11, 799.

RHEDE, D., WENDT, I. and FORSTER, H.J. (1996): A three-dimensional method for calculating independent chemical U/Pb- and Th/Pb-ages of accessory minerals. Chemical Geology, 130, 247-253.

SCHERRER, N.C., ENGI, M., GNOS, E., JAKOB, V. and LIECHTI, A. (2000): Monazite analysis; from sample preparation to microprobe age dating and REE quantification. Schweizerische Mineralogische und Petrographische Mitteilungen, 80, 93-105.

SIMPSON, R.L., PARRISH, R.R., SEARLE, M.P. and WATERS, D.J. (2000): Two episodes of monazite crystallization during metamorphism and crustal melting in the Everest region of the Nepalese Himalaya. Geology, 28, 403-406.

SPEAR, F.S. and PARRISH, R.R. (1996): Petrology and cooling rates of the Valhalla complex, British Columbia, Canada. Journal of Petrology, 37, 733-765.

SUZUKI, K. and ADACHI, M. (1991a): The chemical Th-U-total Pb isochron ages of zircon and monazite from the gray granite of the Hida Terrane, Japan. Journal of Earth Sciences, Nagoya University, 38, 11-37.

SUZUKI, K. and ADACHI, M. (1991b): Precambrian provenance and Silurian metamorphism of the Tsubonosawa Paragneiss in the South Kitakami Terrane, Northeast Japan, revealed by the chemical Th-U-total Pb isochron ages of monazite, zircon and xenotime. Geochemical Journal, 25, 357-376.

Metamorphic evolution of pelitic rocks of the Monte Rosa nappe: constraints from petrology and single grain monazite age data

by M. Engi[1], N.C. Scherrer, T. Burri and A. Berger

Abstract

A suite of metapelites from the pre-granitic basement of the Monte Rosa nappe was collected and investigated to gain insight into the evolution of this important upper Pennine unit. Careful sampling at mesoscopic to microscopic scale allowed the identification of mineral assemblages of distinctly pre-Alpine origin, of assemblages formed in the early Alpine high pressure history of the nappe, and of features due to the Meso-Alpine thermal overprint. Variscan structural relics were recognized in the field and at thin section scale, e.g. as large monazite grains with relic cores, or monazite inclusions within garnet porphyroblasts; high pressure and younger thermal phases were not readily separable in the field, but they are usually distinctly identifiable at thin section scale.

Combined chemical Th-U-Pb dating of monazite by EMPA and novel XRF-microprobe analysis, verified and enhanced by isotopic LA-PIMMS analysis, was performed on single monazite grains selected in thin section, with the full context information preserved. P-T-calculations employed electron microprobe data on assemblages from these same thin sections, yielding metamorphic conditions preserved along the P-T-t path of polyorogenic evolution path. Monazite inclusions in old garnet were found in only two samples to record ages of 330 Ma, corresponding to the intrusion of the main Mote Rosa granodiorite mass. High-grade Permian metapelites appear variably affected – in isolated cases even unaffected – by all Alpine activity, retaining mineral assemblages, consistent P-T-information, and monazite grains (even within the sample matrix) formed some 260 Ma ago in response to the intrusion of minor granitic intrusions in the Monte Rosa nappe. This same stage of low to medium pressure metamorphism was detected in monazite inclusions in garnet from numerous samples. It reached sillimanite + K-feldspar grade, is evident in migmatic restites as well, and is suggested to represent either a regional event, at 10-20 km depth, associated with the generation and emplacement of an extensive suite of acid dykes and small stocks; alternatively, and more or less equivalently, one may think of this phase as indicating widespread contact metamorphism.

No evidence whatsoever could be found supporting a questionable Cretaceous high-pressure phase metamorphism. The dominant Alpine overprint documented in many samples containing assemblages kyanite-garnet-phengite±staurolite consistently yielded TWQ pressure estimates near 9-10 kbar, with temperatures ranging from 550° to 600°C, and with monazite single grain dates ranging from 46 to 31 Ma, but with most of the accurate ages lying between 38 and 32 Ma. Several petrological observations suggest that this stage probably represents (partial) re-equilibration upon decompression, rather than the maximum depth reached by the Monte Rosa nappe. Late Alpine thermal overprinting is evidenced by only very few monazite ages of <30 Ma obtained, and no precise P-T-brackets could be obtained for that retrograde stage.

This research demonstrates the potential of 'in-situ' chemical micro-dating applied to monazite from amphibolite facies pelites, notably in conjunction with the petrological analysis of a polymetamorphic history.

Keywords: Monte Rosa nappe, western Central Alps, polymetamorphic pelites, Th-U-Pb dating, monazite, P-T evolution, exhumation, low temperature eclogite facies, amphibolite facies

1. Introduction

The Monte Rosa nappe is a classic crystalline basement nappe situated at the critical tectonic junction between the Central and the Western Alps. Despite impressive insights from many eminent Alpine geologists (e.g. ARGAND, 1911; BEARTH, 1939; BEARTH, 1952; DAL PIAZ, 1964; DAL PIAZ, 1966; FRANCHI, 1903; FREY *et al.*, 1976; HUNZIKER, 1970; MATTIROLO *et al.*, 1913; REINHARDT, 1966), the evolution and paleogeographic provenance of the Monte Rosa nappe remain controversial. It contains widespread evidence of a protracted polymetamorphic history:

[1] Mineralogisch-petrographisches Institut, Universität Bern, Baltzerstrasse 1, CH-3012 Bern, Switzerland. <engi@mpi.unibe.ch>

Voluminous Variscan granitoids intruded a high-grade gneiss basement, including deformed migmatites, causing contact metamorphism; also during the Permian, regional metamorphism affected this complex; the Alpine orogeny first produced prominent eclogites and other high-pressure rocks, followed by a widespread Barrovian overprint reaching greenschist facies in the West and amphibolite facies in the eastern portions of the nappe. In terms of tectonic position in the Alpine nappe stack, the Monte Rosa nappe (Fig.1) lies at a level corresponding, to the West, the Gran Paradiso and Dora Maira "massifs" and, further East, the Adula nappe, all of which contain Alpine eclogites as well. For the Adula nappe, for example, rapid exhumation from depths in excess of 70 km during the mid Tertiary is well established (e.g. FREY & MÄHLMANN FERREIRO, 1999; NAGEL, 2000). To what extent the high pressure relics in all of these tectonic units may be interpretable in terms of one coherent subduction/emplacement history is a key question in Alpine geodynamics and is relevant in the context of collisional orogeny in general. Current understanding of the kinematic sequence of events and their thermal consequences, in particular, is certainly far from complete in any orogen, including the Alps.

Progress on these questions depends to no small degree on reliable *temporal* links between several stages of evolution documented by petrological and structural studies for each of these units. For the Monte Rosa nappe, petrographic work by BEARTH (1952, 1958) and DAL PIAZ (1971) documented that, due to localised strain within the nappe, plurifacial assemblages are not just locally preserved, but occur in several km^2-size domains. Previous efforts to constrain the temporal evolution of the Monte Rosa nappe (BEARTH, 1952; CHOPIN & MONIÉ, 1984; DAL PIAZ & LOMBARDO, 1986; FREY *et al*., 1976; HUNZIKER, 1970; HUNZIKER & BEARTH, 1969; HUNZIKER *et al.*, 1992; HUNZIKER & MARTINOTTI, 1984; KÖPPEL & GRÜNENFELDER, 1975; MONIÉ, 1985; ROMER *et al.*, 1996; RUBATTO & GEBAUER, 1999) indicated Alpine, Variscan, and older ages. Substantial disagreement remains regarding the significance of many of the metamorphic ages in these studies and the discrepancies between dates they obtained (e.g. PAQUETTE *et al.*, 1989). The difficulty of interpretation is partly due to problems with some isotopic systems used (e.g. excess argon, partial thermal resetting), but a major shortcoming has to do with the selection and documentation of mineral phases used to date the samples. Unfortunately, the loss of structural context incurred when separating mineral fractions from polymetamorphic samples renders a reliable integration of petrological information impossible. Particularly controversial are age data indicating metamorphism in the Cretaceous, based on Rb-Sr and Ar-Ar dating (CHOPIN & MONIÉ, 1984; HUNZIKER, 1970; MONIÉ, 1985) obtained on samples from peripheral parts of the Monte Rosa nappe, including the Furgg Zone and the Gornergrat Zone. For the latter, recent results by RUBATTO & GEBAUER (1999), who made use of the high spatial resolution of the ion microprobe (SHRIMP) to date multiphase zircons from a metaquartzite, indicated a long sequence of events (from ~700 to 34 Ma), but with no indication of activity leading to zircon growth in the Cretaceous. These authors concluded that the most external zircon zones, dated at 35 Ma, correspond to high pressure conditions for the metaquartzite, estimated at P<14-15 kbar and T<550°C. It is difficult, however, to ascribe the dates obtained on a few individual rims of zircon grains to a specific petrogenetic stage of the metamorphic evolution of their host rock. Furthermore, recent work by ROBYR *et al*. (2000) indicates doubt whether the Gornergrat belongs to the Monte Rosa nappe. For the main part of the Monte Rosa nappe, no corresponding age dates are available, but a high-pressure garnet from Dora Maira gave a Lu-Hf age of 32.8±1.2 Ma (DUCHÊNE *et al*., 1997).

The granitoid rocks predominant in the Monte Rosa nappe were investigated in a pioneering study by FREY *et al*. (1976) that combined petrology, including (isotope) thermometry and geochronology. In terms of thermobarometry, however, metapelites may be more promising. The present investigation thus put its focus on pelitic schists and paragneisses that make up a good part of the pre-Variscan basement complex and occur, more sparsely, within the large granitoid masses as well (BEARTH, 1952). This paper reports on pelitic schists collected from central and southern parts of the Monte Rosa nappe in which paragneiss units had been mapped, notably by MATTIROLO *et al*. (1913), BEARTH (1952) and REINHARDT (1966). Following a brief account of the geological setting,

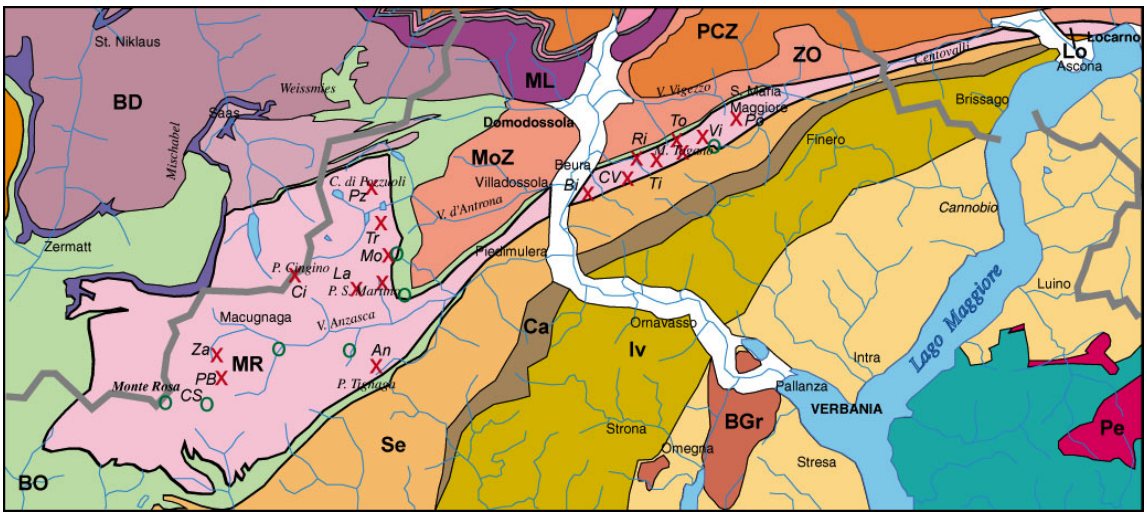

Figure 1: Tectonic overview of the Monte Rosa nappe, showing the sample locations in a regional context. Relevant tectonic units labelled according to the Tectonic Map of Switzerland (Spicher, 1980): BD: Bernhard nappe, BO: Bündnerschiefer-Ophiolite zone, BGr: late Variscan granites, Ca: Canavese zone, Iv: Ivrea zone, MoZ: Moncucco zone, ML: Monte Leone nappe, MR: Monte Rosa nappe, Se: Sesia Zone, ZO: Zone of Orselina.

microstructural and petrologic evidence used to constrain the metamorphic evolution of the metapelites is presented, including thermo-barometric results. For most of these same samples, single grains of monazite were selected and separated from thin section, using a set of consistent selection criteria. Chemical Th-U-Pb dates (SCHERRER *et al.*, 2001a) and isotopic Th-Pb ages (obtained using laser ablation PIMMS; PARRISH *et al.*, 2001) for such grains are presented. Because our approach utilises the full context information about the mineral grains we dated, and because monazite has such a high closure temperature for Pb-diffusion, the results obtained afford a reliable interpretation of several stages of the metamorphic evolution. Implications are addressed in two chapters, first in terms of the polymetamorphism of pelites and the behaviour of monazite in these, and then in terms of the evolution of the Monte Rosa nappe as a whole. Finally, the significance of this nappe in the Alpine collision belt, its emplacement and the exhumation of high-pressure rocks are discussed.

We conclude that the Alpine subduction channel acted as a conduit for extrusion not only of highly attenuated fragments, as in the case of the Southern Steep Belt of the Alps (ENGI *et al.*, 2001), but also to guide the exhumation of rather more massive upper crustal fragments from depths >40 km back to upper crustal levels.

2. Geological framework

Figure 1 shows the Monte Rosa nappe in its present tectonic context, at the same level as the Gran Paradiso nappe of the Western Alps (DAL PIAZ & LOMBARDO, 1995) and the Adula nappe of the Central Alps to the East (PFIFFNER & TROMMSDORFF, 1998). The Monte Rosa nappe is immediately rimmed by several Pennine thrust sheets comprising Mesozoic ophiolites and metasediments, and showing abundant evidence of high-pressure Alpine metamorphism. The pre-Variscan metamorphic basement of the Monte Rosa unit is of sillimanite-Kspar-grade, includes migmatites and was intruded by massive granites (initial $^{87}Sr/^{86}Sr$: 0.712) and granodiorites during late Paleozoic, as interpreted by HUNZIKER (1970; Rb-Sr isochron: 310±50 Ma) and recently confirmed by LANGE *et al.* (2000; U-Pb data on magmatic zircon and monazite). Deformed Monte Rosa granite dated by HUNZIKER (1970; Rb-Sr isochron: 260±10 Ma, initial $^{87}Sr/^{86}Sr$: 0.713) and ages near 250 Ma obtained on the regionally

widespread foliation-forming white micas (HUNZIKER & BEARTH, 1969) lead these authors to propose a late-Variscan (Permian) metamorphic event. Its character remains ill constrained (FREY *et al.*, 1976; HUNZIKER *et al.*, 1992) but it seems to correlate in time with minor magmatic activity that produced acidic dykes, both aplites and pegmatites but no mafic ones. Pervasive changes produced during the Alpine cycle differ in intensity, leaving relics in many areas and rock types. The overprint is strongest near shear zones, in peripheral part ("Schieferhülle"; BEARTH, 1952) of the Monte Rosa granite, and in the easternmost section of the nappe, i.e. the Steep Belt between Valle d'Ossola and Locarno. While in the latter area an amphibolite facies overprint effaced most of the high-pressure characteristics of the earlier Alpine metamorphism, this overprint diminishes in intensity and pervasiveness towards the West. Low-temperature eclogite facies relics thus occur far more frequently to the West of Valle d'Ossola, despite the regionally characteristic postkinematic albitization (BEARTH, 1952) that may be linked to late Alpine hydrothermal activity (PETTKE *et al.*, 1999). Notably, in the widespread undeformed Monte Rosa granites, no evidence has been found of high-pressure breakdown of plagioclase to sodic pyroxene + zoisite + quartz, which is widespread in the adjacent Sesia-Lanzo zone (e.g. Monte Mucrone; COMPAGNONI & MAFFEO, 1973; OBERHÄNSLI *et al.*, 1985). As outlined above, the age of Alpine high-pressure phase in the Monte Rosa nappe is still being debated (mid-Cretaceous or Eo-/Oligocene?), whereas the age of the later thermal overprint is constrained to 34-28 Ma (PETTKE *et al.*, 2000; PETTKE *et al.*, 1999; KÖPPEL *et al.*, 1981; ROMER *et al.*, 1996). Looking at the polymetamorphic history of the entire nappe in some more detail, a number of limits in the present state of knowledge are apparent:

- Peak metamorphic conditions reached during the pre-Variscan evolution have not been quantitatively studied. However, assemblages and local textures were meticulously documented by (BEARTH, 1952) and show the following reaction sequence to be regionally widespread in metapelites: Cordierite first formed at the expense of biotite and was then pseudomorphosed by sillimanite; garnet, sillimanite, and biotite occur as a restite assemblage veined by a quartz-feldspar-metatectites; K-feldspar is abundant, with much of the muscovite (and sericite) appearing texturally late. Jointly, these observations indicate partial melting under upper amphibolite facies conditions at medium to low pressures. The absence of andalusite and orthopyroxene, as well as the sparsity of kyanite indicate temperatures near 700°C and pressures of 3-6 kbar. No regional metamorphic gradients have been documented for this pre-Variscan stage. While early studies ascribed kyanite to a late (but pre-granitic!) stage, more recent work (DAL PIAZ, 1971; DAL PIAZ & LOMBARDO, 1986) has interpreted kyanite to be part of the early Alpine assemblages.

- The Permian event is even less well constrained, presumably because it reached conditions of a lower grade than either the earlier metamorphism or the subsequent Alpine high-pressure stage. In granitoids regionally widespread assemblages include oligoclase, orthoclase, and $2M_1$ muscovite (in contrast to Alpine HP-assemblages with microcline, ($2M_1$ or 3T) phengite, and [albite+epidote] or oligoclase), and oxygen isotope temperatures for the former indicate temperatures between 520 and 560°C (FREY *et al.*, 1976). Pressures estimated in that same study are given as 2-4 kbar, but the precise basis is not clear. No studies of mafic or pelitic rocks have been conducted so far to derive pressure conditions for the Permian metamorphism or to document the spatial variability of its intensity and character, hence possible tectonic implications remain mysterious. Temporally, the relation between Variscan magmatism and the Permian metamorphic overprint is certainly close. Spatially, the situation is not so clear, since no discrete thermal aureoles have been recognized away from the intrusive contacts (e.g. in the W and SW parts of the nappe), which are undisturbed in several areas (BEARTH, 1952)[2]. Evenso, it seems entirely possible that the Permian event essentially represents contact metamorphism, i.e. that heating was due mostly to acid magmatism rather than crustal thinning.

- The early Alpine phase, apart from the age uncertainty mentioned, is fairly well established as

[2] We interpret the high grade gneiss schollen described by Bearth from within undeformed portions of the Monte Rosa granite as fragments of the pre-Variscan metamorphic basement.

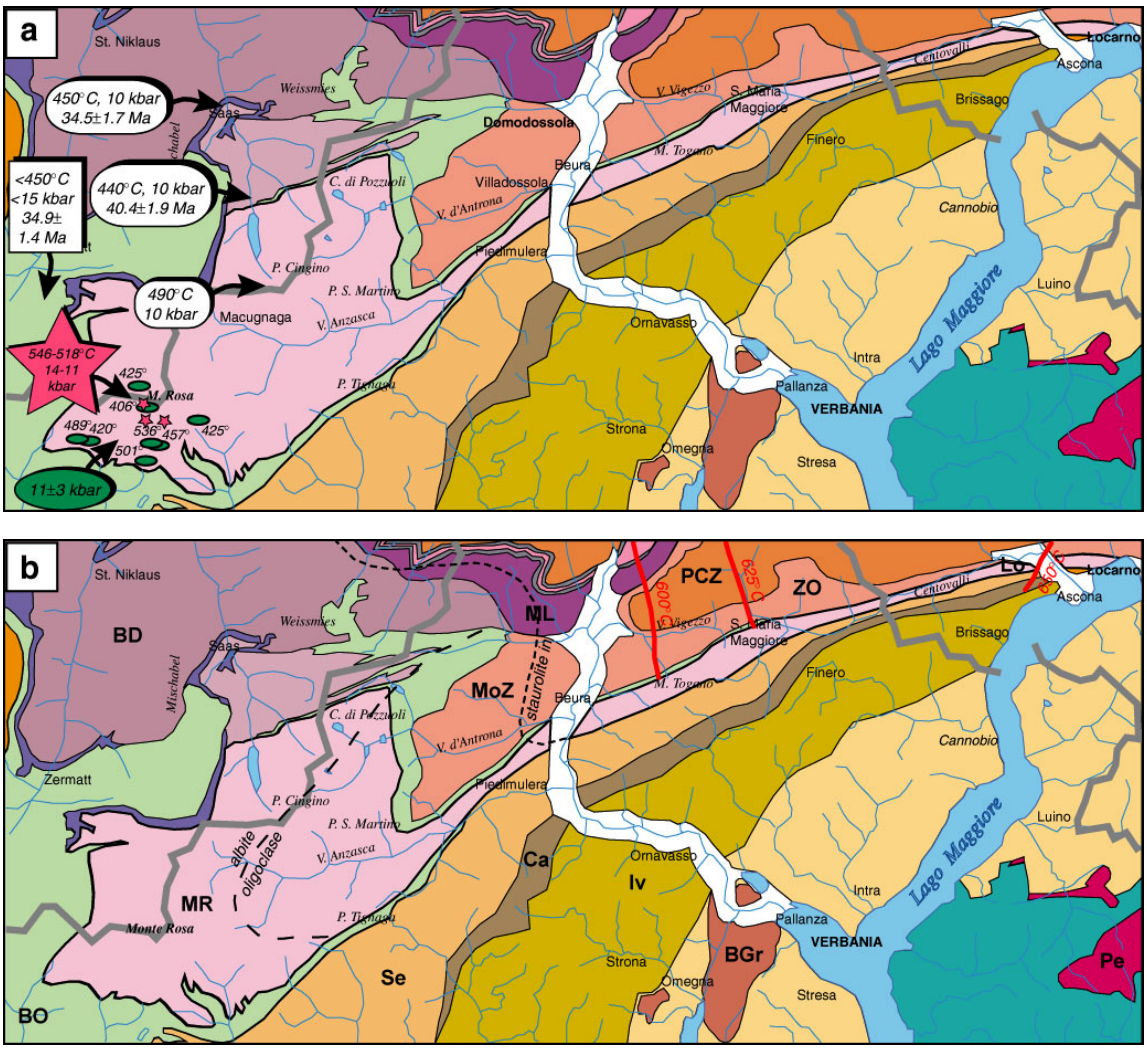

Figure 2: Metamorphic conditions compiled for the Monte Rosa nappe, (a) for the early Alpine high-pressure (eclogite) stage of evolution, and (b) for the Barrovian overprint (the "Meso-Alpine" stage of HUNZIKER *et al.*, 1992).

Data symbols in (a) are for *eclogites*: oval – (DAL PIAZ & LOMBARDO, 1986); star – (BORGHI *et al.*, 1996); for *metagranites*: rounded rectangles – (FREY *et al.*, 1976); and for *quartzite*: rectangle (RUBATTO & GEBAUER, 1999).

In (b) the albite-oligoclase isograd is from BEARTH (1958), the staurolite zone boundary from NIGGLI (1970), and isotherms are from TODD & ENGI (1997).

a high pressure overprint. Evenso, the number of samples documented by modern methods is quite limited: (FREY *et al.*, 1976) derived oxygen isotope temperatures of 440-490°C from five phengites samples of the Monte Rosa metagranite. Using this range and the compositions of phengite (Si=3.3-3.4) reported in that same study, the calibration by MASSONNE & SCHREYER (1987) indicates maximum pressures of 9-10 kbar. A similar range, bracketed between 9±1 and <14 kbar was delimited from low-temperature eclogites by DAL PIAZ & LOMBARDO (1986), with temperatures between 402

and 536°C based on garnet-clinopyroxene thermometry[3]. For three garnet mica schists studied by BORGHI *et al*. (1996), thermobarometry gave 515-545°C and 11-14 kbar for what these authors identified to be "first generation assemblages" on textural grounds, but with no mineral age data available. On the basis of three samples from each of the Internal Pennine "Massifs" (Monte Rosa, Gran Paradiso, and Dora Maira), these authors also inferred a PT-path for the Alpine HP-evolution, supposed to be valid for all of the units. The regional distribution of all of the PT-data available so far for this stage is shown in Figure 2a. It is not straightforward to infer a metamorphic field gradient from these data, owing to likely systematic differences between the methods used and the possibility of partial re-equilibration under post-emplacement conditions.

- Conditions for this meso-Alpine lower-pressure overprint reached only greenschist facies in the western portion of the Monte Rosa nappe, with a well defined albite-oligoclase isograd (Bearth, 1958) and, further to the NE, the staurolite zone boundary (DAL PIAZ, 1971; NIGGLI, 1970) indicating a field gradient (Fig.2b) that mimics the pattern of regional isotherms for the Central Alps by TODD & ENGI (1997). To be sure, only for this last overprint is it clear that P-T-conditions within the Monte Rosa nappe are comparable to those of neighbouring tectonic units; for the early Alpine and previous phases of the polymetamorphic evolutions, this has not been established and indeed appears unlikely to be the case. The age and duration of this last thermal overprint are difficult to delimit precisely. It probably decreased in intensity and age from East to West, but the time interval over which mineral transformations took place probable increased in the same direction. This pattern is indicated by available isotopic and fission track ages (discussed by ZINGG & HUNZIKER, 1990, HUNZIKER, 1992, and ROMER *et al*., 1996), and such a pattern is also expected on the basis of thermal models (ENGI *et al*., 2000; ROSELLE *et al*., 2000) for the thermal relaxation following peak regional metamorphism.

Paleogeographic reconstructions for the Monte Rosa nappe have come to widely differing conclusions, with some authors attributing the slice of continental crust to paleo-Africa, to the Briançonnais, or to the European margin. Though the debate is ongoing, recent suggestions favour the latter scheme, based on the high pressure metamorphism (FROITZHEIM, 1997; GEBAUER, 1999; RUBATTO & GEBAUER, 1999) having reached its maximum depth on subduction during Eo- to Oligocene times.

3. Selection and analysis of single grain monazite

Samples collected for the present study are listed in Table 1, which also gives summary of minerals observed. Monazite occurs in most of the paragneiss samples of the Monte Rosa nappe, but its abundance, grain size, and structural context are quite variable (SCHERRER *et al*., 2001a).

Distinction by context, i.e. inclusions in garnet versus single grains or clusters within the matrix, permits a clear separation of two phases of monazite growth (Fig.3) in the metapelites. Well shielded monazite inclusions in garnet are compositionally homogeneous and range in size from <10 μm to >100 μm. Such inclusions are found in large garnet porphyroblasts. A texturally different type of monazite inclusions also occurs, displaying symplectitic textures (SCHERRER *et al*., 2001a), and these have been attributed to rapid decompression following high pressure conditions during Eo- to Oligocene times (SCHERRER *et al*., 2001b). Far more abundant than either of these types are monazite grains in the matrix, occurring either at grain boundaries or, quite commonly, within biotite, white mica, or one of the aluminosilicate phases. These matrix monazites display many different morphologies, from fine grained trails or single grains to porphyroblastic relics. Texturally, they commonly appear partially recrystallised in between matrix minerals or fully recrystallized with these.

For the purpose of dating specific stages of the polymetamorphic evolution, we selected samples with sufficiently large monazite grains (>50 μm if possible) from texturally interpretable contexts, i.e. inclusions in garnet porphyroblasts, equilibrated metamorphic assemblages within the matrix, or reaction textures attributable to a specific breakdown reaction. The methodological approach

[3] We note that these temperatures were obtained using the calibration by ELLIS & GREEN (1979). The more recent version by KROGH (1988). yields 337-488°C.

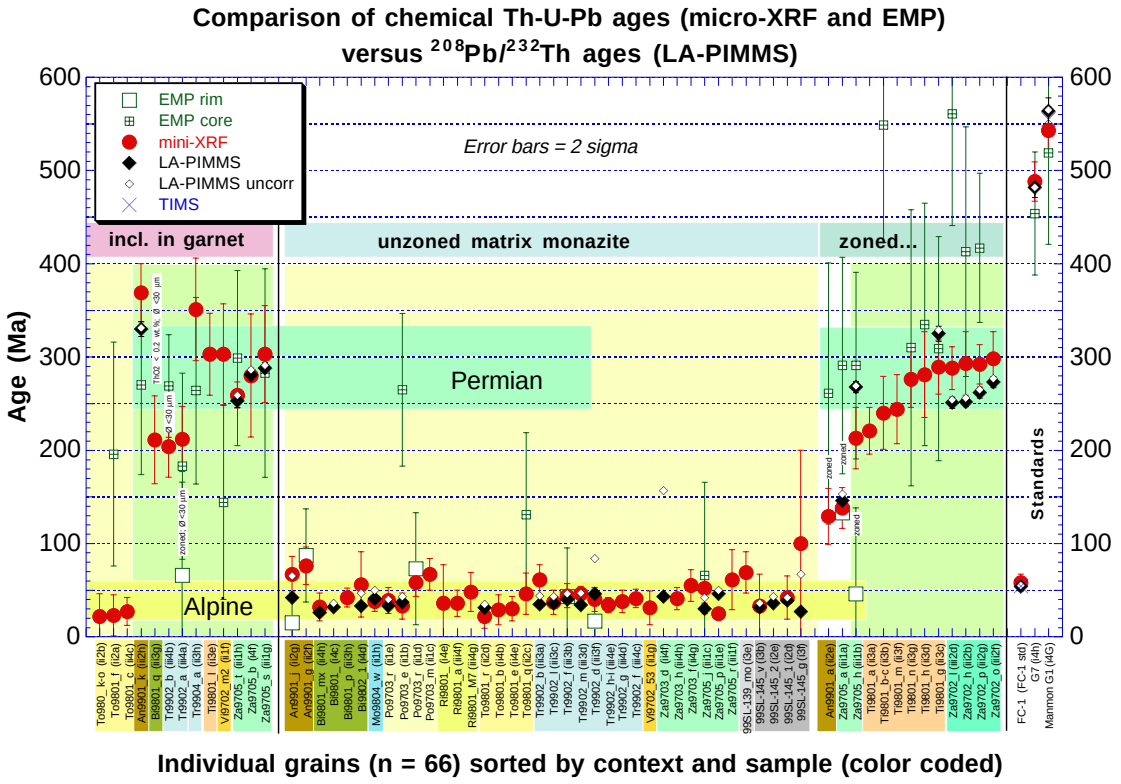

Figure 3: Comparison of monazite ages of separated single grains derived from subsequent analysis on the same grain by non-destructive electron microprobe and XRF-microprobe, and last by laser-ablation multicollector ICP-MS (destructive). Sorting by context provides a picture of two distinct phases of monazite growth: monazite inclusions in garnet, as well as inherited cores of large matrix grains grew during Permian metamorphism; homogenous monazite within the matrix and rims of heterogenous matrix grains indicate monazite growth during Alpine metamorphism. There is no evidence of another distinct phase of monazite growth between Permian and Alpine times. Intermediate ages can all be explained by insufficient spatial (µ-XRF or LA-PIMMS) or temporal (EMP) resolution of the analytical technique applied.

concerning Th-U-Pb dating of monazite in this study is described by SCHERRER *et al.* (2000, 2001a). A combination of techniques was applied to document microstructures and select grains for dating. Besides the petrographic microscope, SEM and electron microprobe images (BSE and X-ray maps) proved most useful. The selection criteria required by the geochronological methods available set limits on what types of monazite could be dated and did not allow, for example, the analysis of certain fine grained reaction products, such as symplectitic monazite. Where the size and homogeneity criteria were satisfied, however, single monazite grains were first analysed by electron microprobe and then painstakingly extracted from specially prepared thin sections, using techniques detailed by SCHERRER *et al.* (2000). Drilled out monazite grains were then analysed (SCHERRER *et al.*, 2001a) by XRF microprobe (at University of Bern) to obtain chemical Th-U-Pb ages, and a subset of the samples was subsequently dated by LA-PIMMS (laser-ablation Plasma-Ionisation Multi-collector Mass Spectrometry, at NIGL, British Geological Survey).

Chemical and isotopic age data obtained from monazite grains extracted from our metapelite samples of the Monte Rosa nappe fall into three classes (Fig. 3, 4; Tab. 1): Chemically homogeneous monazite inclusions in large garnet porphy-

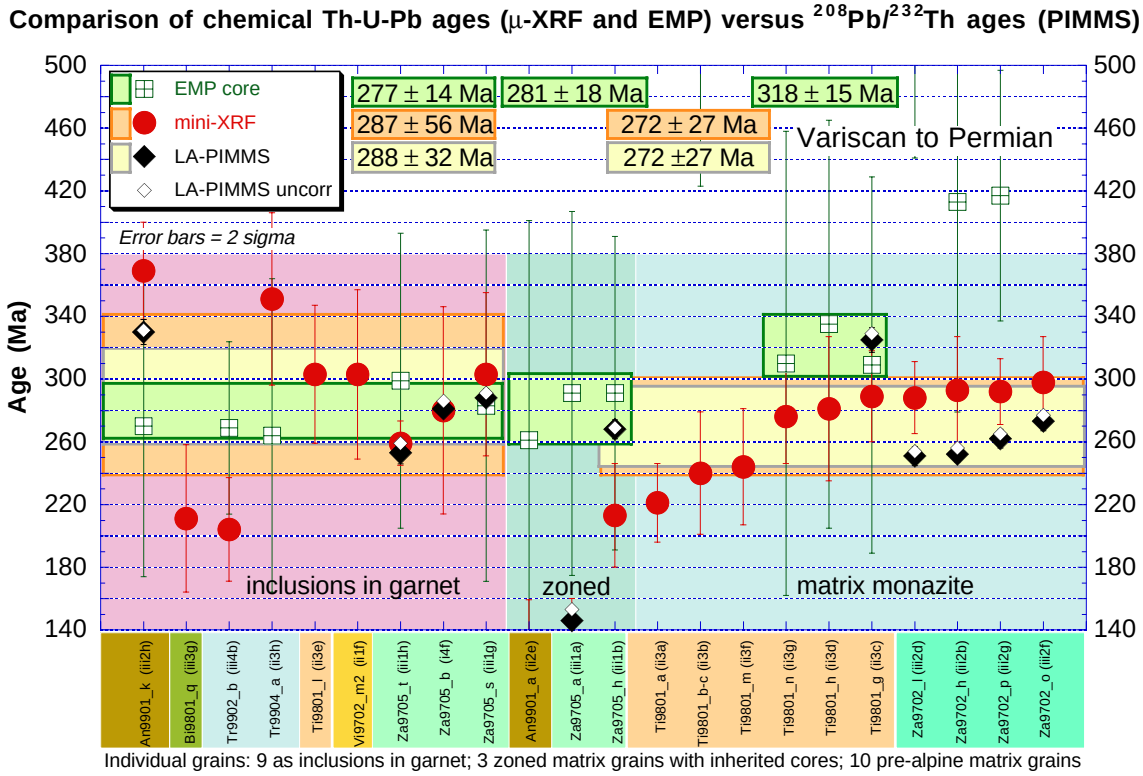

Figure 4a: Same data as presented in Fig. 3, concentrating on Permian monazite population.

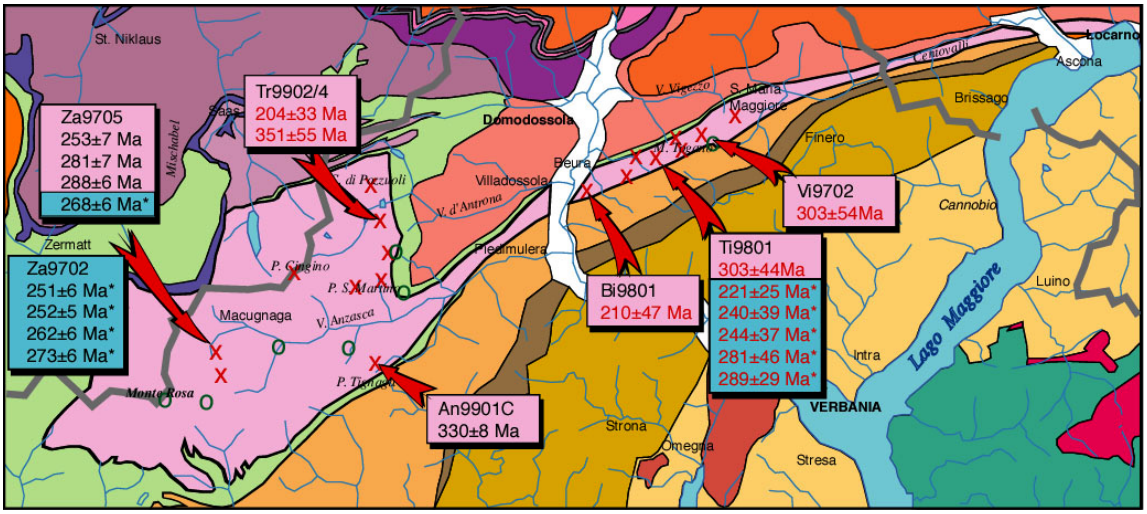

Figure 4b: Regional distribution of Permian ages. Black numbers denote isotopic ages (PIMMS) and numbers in red denote chemical ages (μ-XRF). Numbers with an asterisk * refer to cores of matrix monazite grains (blue background).

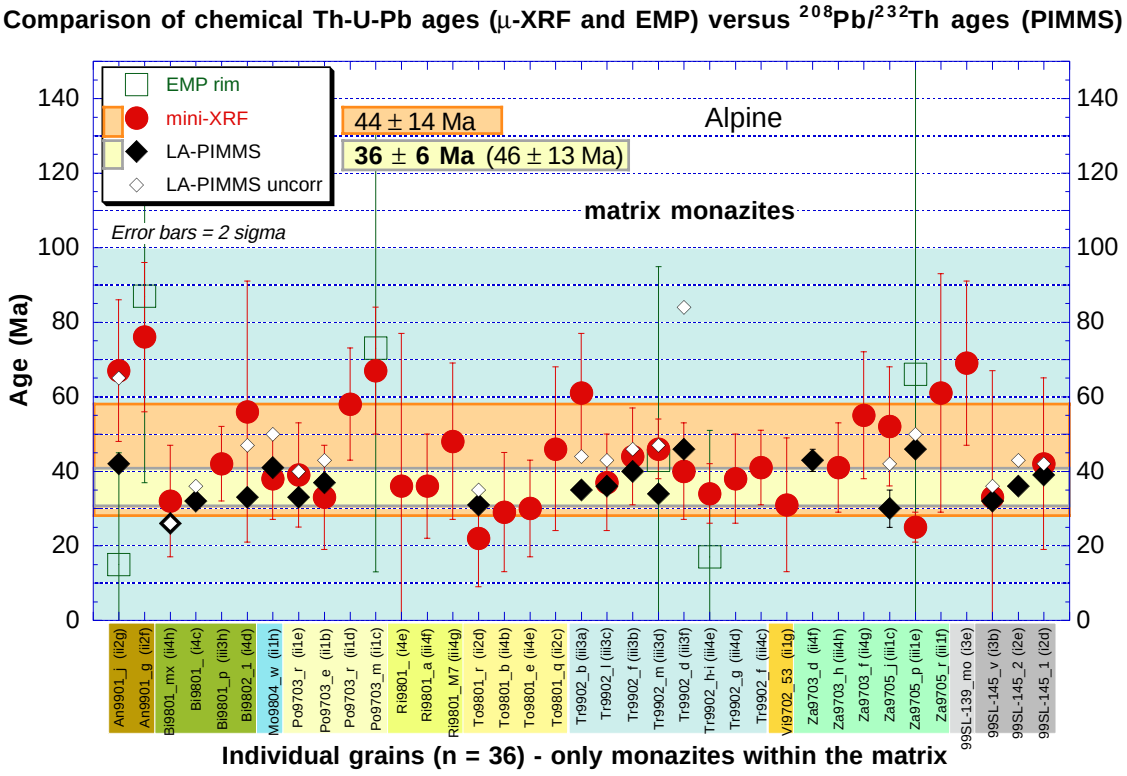

Figure 4c: Same data as presented in Fig. 3, concentrating on Alpine monazite population.

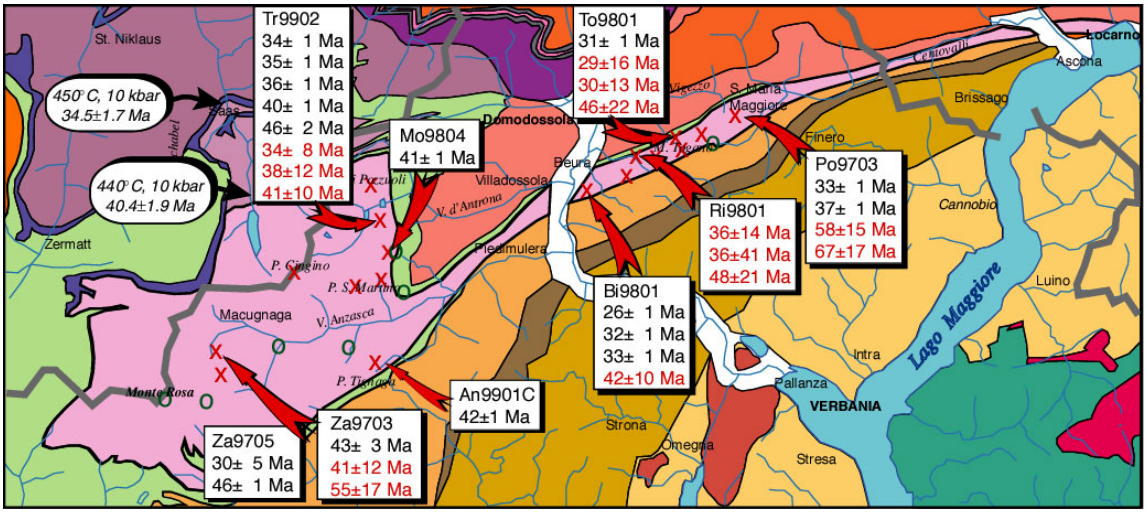

Figure 4d: Regional distribution of Alpine ages. Black numbers denote isotopic ages (PIMMS) and numbers in red denote chemical ages (μ-XRF). The round boxes refer to ages of zircon rims from ophiolitic rocktypes adjacent to the Monte Rosa nappe (Rubatto & Gebauer, 1999).

Permian monazite ages

P-T data	Sample (grain)	µ-XRF age	±2 σ	208Pb/232Th age (Ma)	±2 σ	uncorrected 208Pb/232Th	EMP core	±2 σ	EMP rim	±2 σ	Textural type of grain
-	An9901_k (iii2h)	369	31	330	8	331	270	96			monazite inclusion in garnet
-	Bi9801_q (iii3g)	211	47								monazite inclusion in garnet
-	Tr9902_b (iii4b)	204	33				269	55			monazite inclusion in garnet
-	Tr9904_a (ii3h)	351	55				264	100			monazite inclusion in garnet
-	Ti9801_l (ii3e)	303	44								monazite inclusion in garnet
-	Vi9702_m2 (ii1f)	303	54								monazite inclusion in garnet
	Za9705_t (iii1h)	259	14	253	7	259	299	94			monazite inclusion in garnet
	Za9705_b (i4f)	280	66	281	7	286					monazite inclusion in garnet
-	Za9705_s (iii1g)	303	52	288	6	291	283	112			monazite inclusion in garnet
-	An9901_a (ii2e)	129	30				261	140	133	124	single matrix monazite
	Za9705_a (iii1a)	138	22	146	5	153	291	116			single matrix monazite
-	Za9705_h (iii1b)	213	33	268	6	269	291	100	46	92	single matrix monazite
	Ti9801_a (ii3a)	221	25								single matrix monazite
	Ti9801_b-c (ii3b)	240	39				549	126			single matrix monazite
	Ti9801_m (ii3f)	244	37								single matrix monazite
	Ti9801_n (ii3g)	276	30				310	148			single matrix monazite
	Ti9801_h (ii3d)	281	46				335	130			single matrix monazite
-	Ti9801_g (ii3c)	289	29	325	8	329	309	120			single matrix monazite
	Za9702_l (iii2d)	288	23	251	6	254	561	120			single matrix monazite
	Za9702_h (iii2b)	293	34	252	5	256	413	134			single matrix monazite
	Za9702_p (iii2g)	292	21	262	6	265	417	80			single matrix monazite
-	Za9702_o (iii2f)	298	29	273	6	277					single matrix monazite

Alpine monazite ages

P-T data	Sample (grain)	µ-XRF age	±2 σ	208Pb/232Th age (Ma)	±2 σ	uncorrected 208Pb/232Th	EMP core	±2 σ	EMP rim	±2 σ	Textural type of grain
	An9901_j (ii2g)	67	19	42	1	65			15	30	single matrix monazite
No P-T data	An9901_g (ii2f)	76	20						87	50	single matrix monazite
	Bi9801_mx (ii4h)	32	15	26	1	26					single matrix monazite
	Bi9801_ (i4c)			32	1	36					single matrix monazite
	Bi9801_p (iii3h)	42	10								single matrix monazite
9-10 kb, 600°C	Bi9802_1 (i4d)	56	35	33	1	47					single matrix monazite
No P-T data	Mo9804_w (ii1h)	38	11	41	1	50					monazite reaction texture
	Po9703_r (ii1e)	39	14	33	1	40					single matrix monazite
	Po9703_e (ii1b)	33	14	37	1	43	265	82			single matrix monazite
	Po9703_r (ii1d)	58	15								single matrix monazite
8 kb, 600 °C	Po9703_m (ii1c)	67	17						73	60	single matrix monazite
	Ri9801_ (i4e)	36	41								single matrix monazite
	Ri9801_a (iii4f)	36	14								single matrix monazite
No P-T data	Ri9801_M7 (iii4g)	48	21								single matrix monazite
	To9801_r (ii2d)	22	13	31	1	35					single matrix monazite
	To9801_b (ii4b)	29	16								monazite inclusion in tourmaline
	To9801_e (ii4e)	30	13								single matrix monazite
No P-T data	To9801_q (ii2c)	46	22				131	88			single matrix monazite
	Tr9902_b (iii3a)	61	16	35	1	44					cluster matrix monazite
	Tr9902_l (iii3c)	37	13	36	1	43					monazite reaction texture
	Tr9902_f (iii3b)	44	13	40	1	46					monazite reaction texture
	Tr9902_m (iii3d)	46	8	34	1	47			43	52	monazite reaction texture
	Tr9902_d (iii3f)	40	13	46	2	84					monazite reaction texture
	Tr9902_h-i (iii4e)	34	8						17	34	monazite reaction texture
	Tr9902_g (iii4d)	38	12								monazite reaction texture
9 kb, 600 °C	Tr9902_f (iii4c)	41	10								monazite reaction texture
No P-T data	Vi9702_53 (ii1g)	31	18								single matrix monazite
	Za9703_d (ii4f)			43	3	157					single matrix monazite
	Za9703_h (iii4h)	41	12								single matrix monazite
No P-T data	Za9703_f (ii4g)	55	17								single matrix monazite
	Za9705_j (iii1c)	52	16	30	5	42					single matrix monazite
	Za9705_p (iii1e)	25	4	46	1	50			66	100	single matrix monazite
No P-T data	Za9705_r (iii1f)	61	32								single matrix monazite
No P-T data	99SL-139_mo (i3e)	69	22								cluster matrix monazite
	99SL-145_v (i3b)	33	34	32	1	36					cluster matrix monazite
	99SL-145_2 (i2e)			36	1	43					cluster matrix monazite
No P-T data	99SL-145_1 (i2d)	42	23	39	1	42					cluster matrix monazite

Table 1: Monazite age dating by chemical XRF-microprobe (and EMP) and isotopic LA-PIMMS.

roblasts are of Permian origin (Fig. 4a,b). Matrix monazite generally indicate Alpine ages (Fig. 4c,d), or they have a Permian core surrounded by an Alpine rim. Heterogeneous grains, some with clear core-rim structures and others with complex resorption features, seem to be more common to the west of the Antrona ophiolite and rare in the easternmost part of the nappe, i.e. the Southern Steep Belt. Monazite of Permian age only was observed in one sample, which apparently has escaped the effects of Alpine metamorphism.

Details of the age distribution in each sample are discussed in the subsequent chapter, in the context of the local textures and metamorphic assemblages to which the dated monazite grains belong. In the following, age results shown are those with the lowest analytical uncertainty available for any monazite grain. As in Table 1, errors are quoted in the text at the 2σ-level and, to identify the technique used, chemical XRF-dates are identified by an asterisk (e.g. 260±25 Ma*), whereas PIMMS-ages are shown without a symbol (e.g. 325±8 Ma).

4. Petrologic evolution

4a. Petrographic characteristics of Monte Rosa metapelites

Thorough petrographic investigations were made by BEARTH (1952), DAL PIAZ (1963), DAL PIAZ (1964), DAL PIAZ (1966), DAL PIAZ (1971), REINHARDT (1966), WETZEL (1972), and BORGHI *et al*. (1996). Typical constituents of Monte Rosa paragneisses include quartz, white mica (phengite and/or muscovite), biotite, garnet, ilmenite, rutile, apatite, monazite and zircon, with staurolite, kyanite and/or sillimanite, chlorite, plagioclase (albite or oligoclase), and allanite occurring in some samples only. Local textural and mineralogical observations indicate that some metapelites retain partial evidence of their polymetamorphic history, whereas others apparently reset completely at some stage of their evolution. Hence it is essential to characterise assemblages at the grain scale, to check for local mineral (dis)equilibria and interpret the state of resetting prior to performing thermobarometry or mineral chronometry.

Within most of the samples analysed, garnet is Fe-rich (Alm_{60-85}) and commonly occurs in (at least) two generations and with some grains showing typical prograde zonation or multiple overgrowth profiles (Fig.5).

At a regional scale, it is observed that staurolite is most abundant east of Val d'Ossola, particularly in the Southern Steep Belt, where generally few relics of high pressure metamorphism have been reported for the Monte Rosa nappe. However, staurolite of an earlier generation is present also in several samples from further West, outside the staurolite zone boundary of NIGGLI (1970), NIGGLI & NIGGLI (1965), in samples retaining high pressure assemblages. On the other hand, chloritoid, phengitic mica (3.3-3.4 Si p.f.u.), rutile, plus kyanite or sillimanite, have been found only to the west of the Antrona trough (Fig.2). Plagioclase is sparse and where analysed is of oligoclase composition (~An_{30}). Three types of white mica could be distinguished, with paragonitic and phengitic mica being restricted to the western samples, whereas muscovite (<3.1 Si p.f.u.) is widespread throughout the nappe. Where rutile occurs, it is commonly rimmed by ilmenite, except where protected within in porphyroblasts of gar_1 or $stau_1$. Chlorite appears mostly linked to late greenschist facies overprinting, but in some samples it is clearly part of the higher pressure assemblages.

Based on textural relationships, Alpine metamorphic assemblages can be divided into higher and lower pressure assemblages, as previously discussed by (BORGHI *et al.*, 1996). These include Qtz-Ph-Cld-Chl_1-Grt_1-Ky-Rt±Ilm±Pg±St_1 at higher pressure and Qtz-Ms-Bt-Grt_2±St_2±Olig/Ab+Ep at lower pressure.

A select set of individual samples (Table 2, cf. Appendix) and groups thereof are characterised below, presented according to petrological criteria and monazite age data.

4b. Methods used

The characterisation and interpretation of polymetamorphic samples demands particular attention to microstructural characteristics, such as relics and domains containing neoblasts of one or more phases overgrowing older assemblages. Apart from careful petrography and comparison to

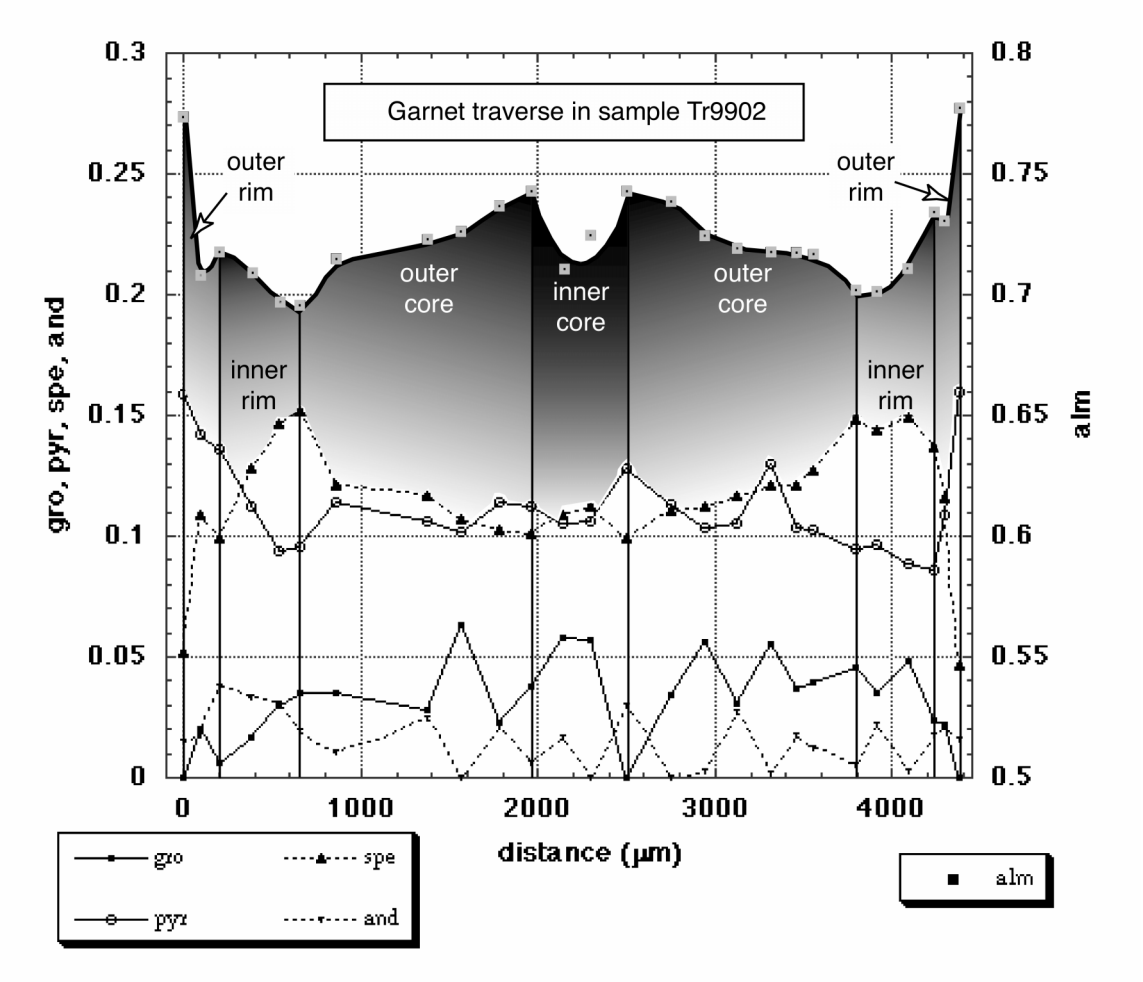

Figure 5: Compositional profile across large garnet porphyroblast in sample Tr9902, arguably representing three generations of garnet. A monazite inclusion within the core of similar Za9705 garnet indicates a uniform age of 259 ± 14 Ma, whereas large matrix grains display a core-rim structure with a Permian core and an Alpine rim.

suitable petrogenetic grids, the availability of monazite ages from several individual structural domains of a sample has proven most helpful. Assemblages used in this study to constrain metamorphic P-T-conditions were selected *after* monazite grains from the same domain had been age-dated with credible results. The aim was thus to obtain thermobarometric data for a particular stage in the metamorphic evolution of the sample. Of course the simultaneity of monazite growth (or complete recrystallisation) and of chemical equilibration of the silicate-oxide assemblage used for P-T-determinations cannot be guaranteed. However, criteria such as the chemical homogeneity of monazite and of the major constituent phases analysed, their alignment in one and the same penetrative foliation, as well as clean boundaries indicative of textural equilibrium, were used to lend support. Despite these precautions, the thermobarometric multiequilibrium approach used indicates that we were not always successful in avoiding disequilibrium assemblages in some cases.

All phases of potential equilibrium assemblages, selected from dated samples, were analysed by electron microprobe (Cameca SX50, 15 kV, 20 nA; WDS mode, using synthetic and natural standards). Analyses were obtained within

small domains selected in thin section, where possible on grains in direct contact. Data were screened to ensure the accuracy of analyses used. These were normalised according to the requirements of the thermodynamic analysis, using TWQ (BERMAN, 1991) with the dataset by BERMAN & ARANOVICH (1996). In addition, an ideal activity model was used for Mg-Fe-chlorite, and the improved thermodynamic properties by NAGEL *et al.* (2000) were adopted for staurolite. To avoid large uncertainties in activities, we excluded mineral species present in very low concentration, i.e. $X_{species}<0.05$ (TODD, 1998).

To evaluate the P-T-conditions preserved in any analysed assemblage we considered all of the (fluid-absent) equilibria computed to be stable anywhere in the P-T-domain [200-1200°C, 1-20 kbar]. The intersection pattern of all of the stable and metastable branches of these possible equilibria was inspected as a first indication of the suitability of the complete assemblage. Depending on the number of phase components involved, the number of independent equilibria turned out usually between 4 and 2. In the latter case, a unique P-T-intersection results, reflecting merely the paucity of the assemblage, the quality of which obviously cannot be evaluated using TWQ alone. In such cases, it was sometimes possible to check the quality of the P-T-result by comparing the observed assemblage against a suitable petrogenetic grid and by performing the following experiment: Assume that the activity of TiO_2 and/or Al_2SiO_5 equals unity, i.e. that the assemblage was in fact saturated in rutile and/or kyanite (or sillimanite), compute the P-T-diagram again. Then evaluate all of the additional equilibria generated as *limiting* the space for which $a(TiO_2)<1$ and/or $a(Al_2SiO_5)<1$. This approach thus utilises not only the phases present, but also includes the observed absence of the respective titanium or aluminosilicate phases. Judging by the consistency of P-T-intersections and the narrow P-T-fields obtained using this approach, we conclude that many of the metapelites investigated appear to be only very slightly undersaturated in the respective phases. In such cases, this experiment sets very useful additional limits in thermobarometry. Its application is, of course, not restricted to "poor" assemblages, i.e. with only two independent reactions. In diagrams presented below, the additional information gained from this approach is shown as grey areas labelled, for example, "kyanite-absent field". – Where 3 or 4 equilibria were independent, the dispersion of invariant points in P-T-space was inspected and, in some cases, overall equilibrium appeared to be well preserved (e.g. Fig.6, 7). In other cases, all but a few equilibria seemed well behaved, and outliers involved one particular phase component. This was commonly found to be siderophyllite or rutile. In the former case, the discrepant results may well be caused by an inadequacy in the thermodynamic model, whereas for rutile petrographic evidence indicated an irreversible reaction, such as partial replacement by ilmenite. In either case the hypothesis of a completely intact equilibrium assemblage could not be maintained, the violating mineral species or component was eliminated, and TWQ analysis continued without it. Results shown in the subsequent paragraphs indicate that fairly convincing equilibrium assemblages are indeed rather rare in the samples we investigated, but reliable thermobarometric constraints can be derived from a few of them.

4c. Permian metamorphism

In several areas, including the central portion of the nappe to the West of Macugnaga, BEARTH (1952) had mapped metasediments showing little or no Alpine overprint. A suite of metapelites, sandwiched between the main mass of Macugnaga augengneiss and granitic tectonites of the Stelli zone, was sampled near Alpe Pedriola, NW of Pizzo Bianco. Most of these samples (Za-suite in Tables 1 and 2; cf. Fig.1) show the early stages well preserved. In particular, Za9702 displays no signs of a high pressure or retrograde greenschist facies overprint, i.e. the sample appears to have largely escaped Alpine metamorphism. In contrast to samples of chloritoid bearing garnet-mica gneisses (Za9703, Za9705) from the same area, Za9702 also lacks a penetrative foliation. It contains exceptionally abundant fibrolite and K-feldspar, three generations of garnet, and unusual textural characteristics of biotite and white mica. The earliest generation of garnet is present as subidiomorphic grains (~5 mm in diameter), with no evidence of corrosion or overgrowth on them, but with random needles (sillimanite? up to 3 mm in length) crosscutting the grains. Surrounding this earliest generation of garnet is a fine grained felt of

fibrolite plus quartz. This sillimanite-rich felt is thickest at opposing ends of garnet porphyroblasts, suggesting the replacement of previous pressure shadows. A dense cluster of roundish garnet grains overgrew the felt and partially replaced it. The only hint at a weak foliation in this sample is given by corroded platelets of coarse biotite that surround the felt rimming the first generation garnet. Biotite is conspicuously reddish-brown, may show delicate symplectitic fringes and was replaced, near its margin to fibrolite, by elongate poikilitic garnet containing quartz, K-feldspar, and abundant tiny ilmenite grains as inclusions. These textural and mineralogical features, notably the extreme enrichment in sillimanite, lead us to interpret this sample as a restitic metapelite. In view of the regional homogeneity of the metapelites (BEARTH, 1952), it appears that a significant portion of the leucosome was lost from its pelitic protolith during or following partial melting. Millimetre-size pockets dominated by quartz and K-feldspar, containing some 30% randomly oriented muscovite and biotite, with only traces of sillimanite, may represent seggregates of such leucosome.

Four monazite grains from the matrix of sample Za9702 were dated, yielding a median age of 252±9 Ma (PIMMS data, Table 1). These ages are but slightly younger than those obtained from monazite enclosed in garnet in sample Za9705 taken a few hundred meters away, for which 281±16 Ma resulted. These data represent maximum ages for the garnet from which the respective monazite inclusions were extracted, hence no significant age difference between the porphyroblasts and the matrix monazite can be detected. In sample Za9705, however, monazite grains in the matrix indicate that it has been partially reset, probably due to recrystallisation of monazite in the matrix. Ages obtained gave a bimodal distribution: Four monazite grains within the matrix evidently recrystallised at Alpine times (30±5, 36±16*[4], 46±1, 61±32 Ma*); at least two grains are zoned, one of which gives an intermediate age (145±5 Ma) clearly attributable to mixing of age zones (Permian core vs Alpine rim) due to insufficient spatial resolution, whereas the other one could be resolved analytically indicating a Permian core (268±6 Ma) and an Alpine aged rim (46±46 Ma[5]). In a third sample of that suite (Za9703), all of the monazites from the matrix show Alpine ages between 43±3 and 55±17 Ma. Evidently this suite of high-grade metapelites experienced unequal amounts of recrystallisation in post-Permian times, with some samples showing Alpine chloritoid ±staurolite ±chlorite, but Za9702 is indeed remarkably unaffected.

Even more exceptional is sample Ti9801 from taken just SW of Pizzo Tignolino, some 8 km SE of Domodossola. Despite the strong strain evident in the Southern Steep Belt portion of the Monte Rosa nappe, this staurolite-chlorite-tourmaline bearing garnet-biotite-muscovite schist indicates the preservation of Permian (and possibly older) ages of monazite within garnet porphyroblasts and in the matrix! For the latter, the median age is 260±25 Ma* from XRF chemical dating, whereas one grain dated by PIMMS gave 325±8 Ma; only one monazite inclusion in garnet could be dated, yielding 303±44 Ma*. As in the previous suite, we infer that the Alpine metamorphism, which in this locality reached lower amphibolite facies conditions, did not reset the Permian ages even in the matrix. Yet the silicate assemblage in this case does not look particularly different from those in neighbouring samples, many of which demonstrably did equilibrate during Alpine times (below). We cannot be sure whether the silicate assemblage in Ti9801 does retain the characteristics of the Permian metamorphism. However, since this sample as well as Za9702 discussed above were taken but a few hundred meters away from intrusive contacts to major granitic bodies, it seems likely that the assemblages were formed by Variscan contact metamorphism and not by a Permian regional event. The P-T-conditions of formation or equilibration were not investigated further.

In several other samples (Tr9902, Tr9904, Va9702) monazite inclusions in garnet indicate Permian ages, but in all of these the matrix assemblages, including monazite, had evidently recrystallised in Alpine times. Though garnet (gar_1) in these samples typically contains numerous inclusions, none of them had sufficiently complete inclusion assemblages to warrant thermo-barometry. For those reasons, no precise P-T-

[4] Where no or failed PIMMS-data are available, XRF-data are quoted and denoted by an asterisk.

[5] EMP age with large error due to young age of rim (rim spatially unresolved by PIMMS and XRF techniques).

conditions could be determined for the Permian regional metamorphism.

4d. Alpine high pressure overprint

A group of our samples shows complex zoning in garnet porphyroblasts and characteristic overgrowth textures that document the transition from pre-Alpine to early-Alpine conditions. Typical in metapelites is a mica-rich matrix dominated by white mica – commonly muscovite and phengite – but with only subordinate biotite, kyanite overgrowing and partially replacing fibrolite, small and commonly roundish garnet of a second generation, stubby to long-prismatic staurolite, bands of mosaic quartz with sporadic oligoclase and, in mica-free domains, K-feldspar.

In samples showing tectonite fabrics, however, the high-pressure overprint is extensive and obvious. In Monte Rosa metagranites (DAL PIAZ & LOMBARDO, 1986; FREY *et al.*, 1976), phengite has Si-contents of 3.35-3.41 atoms per formula unit, Ti-biotite typically shows $Mg/(Mg+Fe^{2+})=0.36\pm0.06$, and assemblages include albite+epidote (or oligoclase), microcline, quartz, as well as accessory titanite, garnet, tourmaline, and magnetite. Phengite in metapelites show Si-contents similar to these, except where subsequent exsolution (discussed below) lead to a new generation of low-celadonite micas. Thermobarometric and age data for metagranitoids, based on FREY *et al.* (1976), are shown in Figure 2a. Included are only those samples, for which Fe/Mg exchange data for phengite and biotite, as well as oxygen isotope temperatures, indicate the attainment and preservation of equilibrium (i.e. #366, 377, 405) are included; pressure values shown for these samples are based the calibration of MASSONNE & SCHREYER (1987) and Si-values reported by FREY *et al.* (1976); all ages shown from that study are Rb-Sr isochron results. Results from metabasites studied by DAL PIAZ & LOMBARDO (1986) and BORGHI (1996) are also shown. All three studies indicate a low temperature eclogite stage, with preserved equilibria showing mostly 500±50°C, 10±2 kbar, dated at 35-40 Ma.

In the metapelites we studied, assemblages differ somewhat from eastern to western parts of the Monte Rosa nappe. In the East, two samples from Valle Vigezzo (Po9703 and Bi9801; cf. Fig.1, 3; Tab.1, 2) deserve detailed characterisation:

- Po9703 is a banded, tightly foliated garnet-biotite-muscovite-staurolite-schist sampled NE of Porcella. Grain boundaries are clean and commonly straight, aligned monazite grains occur abundantly throughout the matrix that contains recrystallized intergrowths of muscovite and minor biotite. Roundish grains of garnet do not appear to represent more than one generation; similarly pale staurolite is present only in one idiomorphic habitus, as stubby prisms. The Ti-phase is ilmenite only, neither rutile nor titanite have been found. Aluminosilicates are missing, but adjacent samples commonly contain kyanite. TWQ analysis indicates equilibration at conditions close to 600°C and 9 kbar (Fig.6) which appear consistent with the assemblage observed, and the field delimited by the location of equilibria involving kyanite includes the three invariant points computed for the observed assemblage. Hence the P-T-result appears credible. Matrix monazite dated from this assemblage indicates an age of 35±2 Ma, which is interpreted as the age of equilibration.

- Bi9801 was collected at Alpe Bisoggio, SE of Beura (E of Villadossola) and is very similar to Po9703, both texturally and mineralogically, except that a few larger grains of garnet (gar_1) occur and minor fibrolitic sillimanite (but no kyanite) is observed in the mica-rich matrix. Calculated equilibration conditions (Fig.6) are shown for two sets (a and b) of mineral compositions; siderophyllite equilibria were eliminated in both cases. The remaining three independent reactions indicate similar P-T-conditions, between 550-600°C and 9-10.5 kbar, reflecting conditions well within the kyanite field. A single monazite grain from a garnet porphyroblast could be extracted and dated, giving an age of 211±47 Ma*, i.e. indicating that gar_1 may represent a Permian relic. Monazite from the matrix occurs in two textural types, as single grains and clusters (SCHERRER *et al.*, 2001a). Ages indicate recrystallisation at 33±1 and 32±1 Ma, and possibly (partial?) resetting at 26±1 Ma. One way to interpret all of these data is to invoke decompression from ~10 kbar, starting around 34-31 Ma, into the fibrolite field (~5 kbar, assuming isothermal conditions) by 27-25 Ma, but this is of course only a permissible scenario, not the only one possible.

Samples studied from part of the Monte Rosa nappe to the West of Valle d'Ossola include those

to the North and South of the upper Val d'Antrona (localities labelled Pz, Tr, and Mo; Fig. 1&3; Tables 1&2). Many of these contain overgrowth textures and mineralogical evidence of their polymetamorphic evolution, e.g. chloritoid + kyanite near sillimanite+K-feldspar. Attempts to use TWQ for any of these samples produced highly dispersed patterns with P-T-intersections commonly outside the stability fields of the observed assemblages. Two samples do appear well equilibrated, however:

- Tr9902 is a fine-grained micaschist containing garnet (gar_1) porphyroblasts of >5 mm diameter, sprinkled with tiny inclusions of epidote(?) and with coarse biotite+phengite+quartz in adjacent pressure shadows. Abundant roundish, small grains of garnet (gar_2) with dark cores appear in the mica matrix, which contains subordinate quartz, K-feldspar, chlorite, apatite, and rutile rimmed by ilmenite. The matrix and the rock as a whole are not foliated, and the mica assemblage displays pale biotite as rims around muscovite and lamellar patches within the white mica. These are interpreted as exsolution features from phengite breakdown, and the microstructural evidence does not suggest extensive recrystallisation during or following that process. Thermobarometric results (Fig.7) for three sets of mineral compositions suggest equilibration conditions between 550-600°C and 9±1 kbar. The stability field of the observed assemblage and the kyanite-absent field appear to be consistent with the TWQ-intersections, but with only two independent mineral equilibria being useable, the control on the P-T-data is not great. – Monazite occurs both as discrete grains in the matrix and as inclusions in gar_1. Ages obtained for the former indicate a range (from XRF-data only) of 34±8 to 50±17 Ma*, consistent with the only PIMMS date of 46±2 Ma. Monazite inclusions in early garnet yielded 204±33 and 212±35 Ma* as a maximum age for gar_1 – again seen as evidence of the persistence of Permian (or Jurassic?) garnet. In an adjacent sample (Tr9904) early garnet porphyroblasts contain monazite suggesting an even older age (Table 2), as well as xenotime too small to be dated by the techniques used in this study.

- Pz9905 is a staurolite bearing garnet-biotite-white mica gneiss collected on the ridge N of Cime di Pozzuoli. It shows similar characteristics to Tr9902 and TWQ indicates similar equilibration conditions as well, 570±30°C and 10±1 kbar (Fig.8). No monazite grains from this sample have been dated, but the consistency between ages obtained for similar samples (Tr9902, Tr9904, and Mo9804) from the NE-portion of the Monte Rosa nappe indicates that these P-T-conditions probably pertain to a similar time segment, i.e. ~40-35 Ma ago.

In many samples from the northeastern and central parts of the Monte Rosa nappe, including those of the Mo- and PB-suites (Fig. 1&2, Tables 1&2), phengite breakdown textures such as those described above have been observed, leading us to interpret the calculated P-T-data as representing some stage along the Alpine decompression path of the respective sample. Though none of the assemblages documented indicate the preservation of pressures beyond 11 kbar, these textures make it likely that the nappe had in fact reached somewhat higher pressure conditions previously. The lack of complete recrystallisation during the decompression stage is thought to be responsible for the dispersion of thermobarometric results of other samples than those described here.

4e. Thermal overprint and retrograde features

Many samples from the portion of the Monte Rosa nappe to the East of Valle d'Ossola are dominantly characterised by extensive reequilibration under medium pressure amphibolite facies conditions, as evidenced by the abundance of muscovite and the appearance of a new generation of idiomorphic staurolite and/or small almandine-rich garnet. Relic phengite is but locally preserved in masses of celadonite-poor muscovite that contain ill defined patches or lamellae of pale biotite in minor amounts, presumably again due to exsolution from phengite. In more recrystallized samples, such intergrowths developed discrete grain boundaries between muscovite and biotite; thin lamellae (<1 to 5 μm) of biotite are observed even in idiomorphic muscovite grains >200 μm in size. Kyanite is the stable aluminosilicate polymorph, by contrast to some pelites in tectonic units adjacent to the Monte Rosa nappe, especially in eastern parts of Valle Vigezzo and in Centovalli, where sillimanite occurs (NIGGLI & NIGGLI, 1965; TODD & ENGI, 1997). As outlined for sample Bi9801 (see previous section), the Monte Rosa nappe may have been exhumed rapidly enough, such that eastern

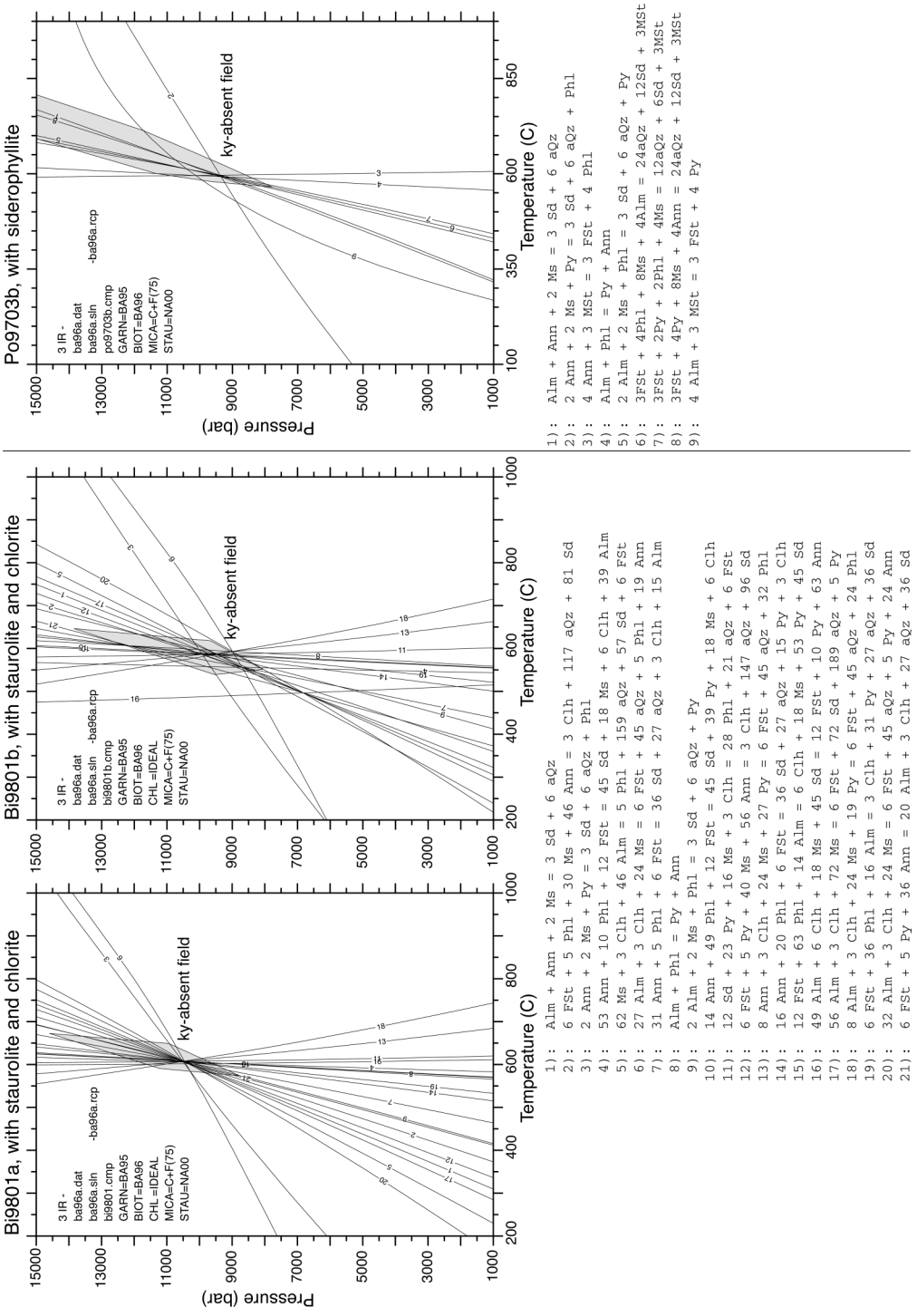

Figure 6: P-T-diagram showing location of fluid-absent equilibria computed using TWQ for phase compositions measured in samples Po9703 and Bi9801. Models used and restrictions applied discussed in text. The grey area labelled "ky-absent field" delimits the are for which the activity $a(Al_2SiO_5)<1$ in kyanite – a phase considered just slightly metastable in the observed assemblages.

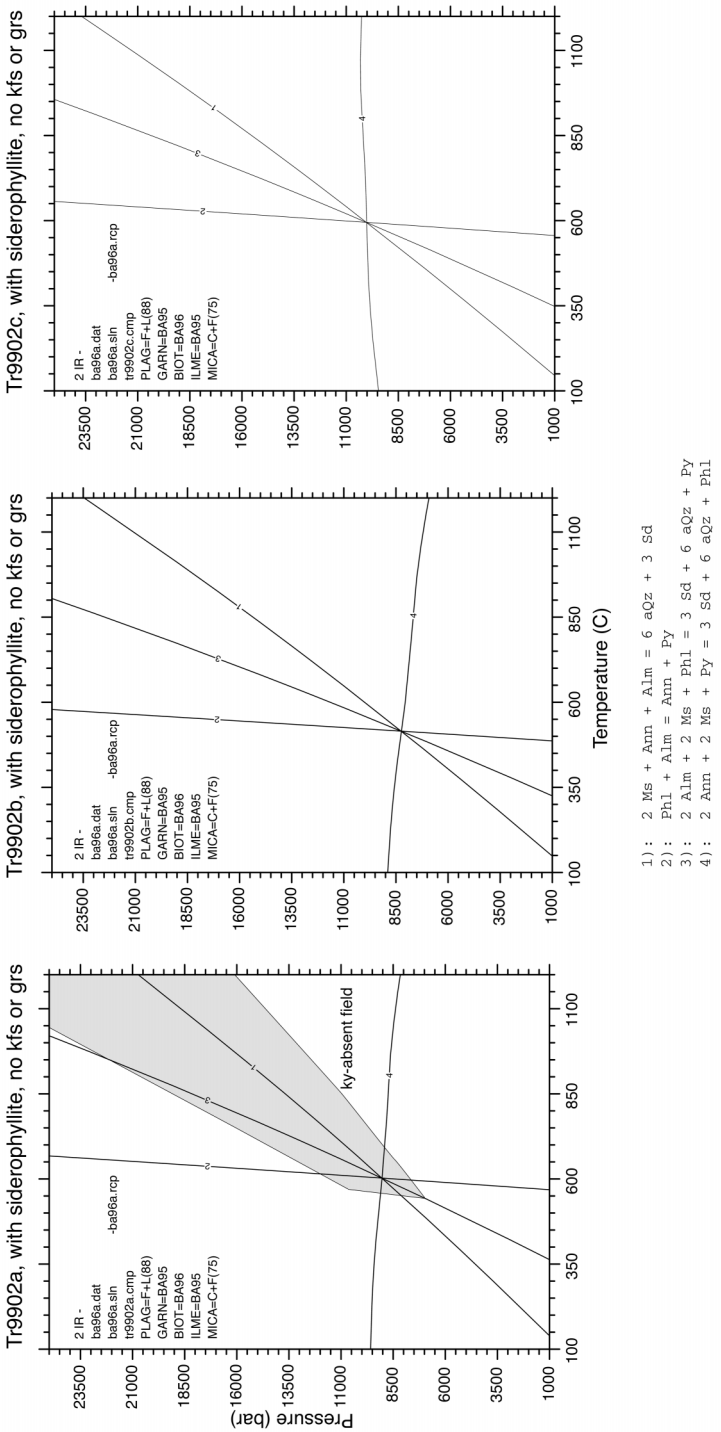

Figure 7: P-T-diagram showing location of fluid-absent equilibria computed using TWQ for three sets of phase compositions measured in sample Tr9902. See text and Fig.6 for further explanations.

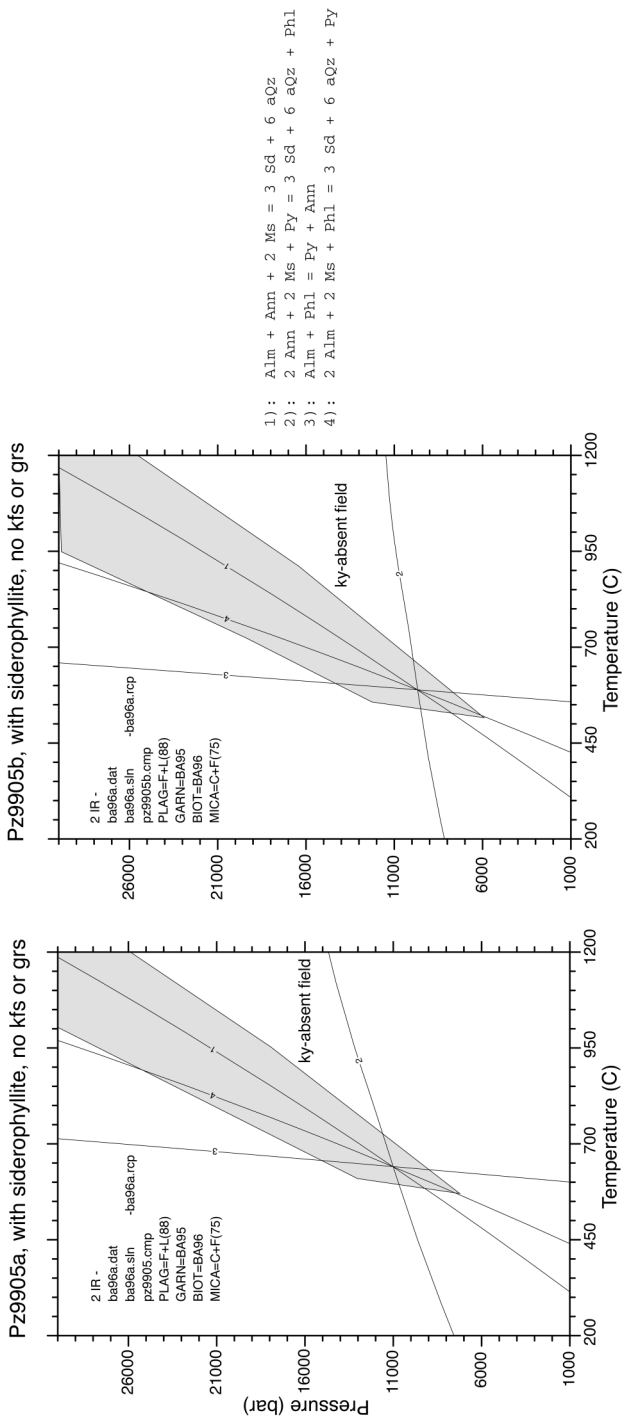

Figure 8: P-T-diagram showing location of fluid-absent equilibria computed using TWQ for phase compositions measured in sample Pz9905. See text and Fig.6 for further explanations.

portion of the nappe experience decompression in the sillimanite field, leading to the local formation of fibrolite (around 26 Ma ago?).

In addition some metapelites show late greenschist facies retrogression, both East and West of Valle d'Ossola. In the former case, this is probably linked to a late imprint after the amphibolite facies thermal maximum, bot outside the Alpine staurolite field, it is impossible to discern two stages. Neither P-T-data nor monazite ages interpretable as a specific stage of retrogression could be documented.

5. Implications

5a. Tectono-metamorphic evolution of the Monte Rosa nappe

The pre-Variscan metamorphic evolution cannot be defined clearly on the basis of the present results. Sporadic monazite ages found along the southern margin of the nappe (yielding 325±8 Ma in the matrix of Ti9801; 330±8 Ma in An9901 inclusions from texturally old garnet porphyroclasts) agree, within error, with the Rb-Sr isochron age of 310 Ma (±50 Ma according to HUNZIKER, 1970; ±20 Ma according to FREY *et al.*, 1976), interpreted as the age of formation or emplacement of the Monte Rosa granodiorite pluton. Present knowledge, unfortunately, does not constrain the depth of emplacement of this major magmatic body. The isolated garnet grains containing the oldest monazite dated here are interpreted as contact-metamorphic in origin.

The late Variscan phase of magmatism, dated by HUNZIKER (1970) and HUNZIKER & BEARTH (1969) at 260±10Ma, produced widespread but lesser volumes of granitic magmas. Permian contact metamorphism is thought to have caused well equilibrated assemblages to form in metapelites such as the Za-suite described in this study. In most samples of that suite sillimanite and K-feldspar are abundant, and only samples demonstrably affected by the Alpine event contain texturally younger kyanite, an approximate pressure bracket of 5±2 kbar may be estimated for the intrusive activity around 260 Ma. Monazite grains from many garnet porphyroblasts and a few matrix assemblages, covering a very large portion of the Monte Rosa nappe, indicate ages within error of this magmatic phase. It appears likely, therefore, that one cannot separate the thermal effects of contact metamorphic from those of a regional metamorphic phase with associated penetrative deformation (HUNZIKER, 1970; HUNZIKER & BEARTH, 1969). In view of the indicated intrusive depth of 10-20 km, advective heating during the extended Variscan magmatic activity may well have raised the geothermal gradient regionally. Upper amphibolite facies assemblages, such as those documented in the present study, including restitic migmatite portions, would thus have possibly resulted from partial melting during that phase. This is not to suggest that the granitic magmatism in the nappe at that time resulted from in-situ partial melting, but the absence of thermal aureoles, the paucity of skarn-like features, and the high grade overprint evident in metapelites at least suggest a close link in space and time.

For the Alpine time period, no early subduction-related prograde metamorphism is evident in metapelites, except possibly in a few chloritoid-bearing assemblages in the central part of the nappe (Za 9705). It seems unlikely that the P-T-t-relations derived from the Alpine assemblages correspond to the deepest subduction stage, given the widespread evidence of phengite (partial) breakdown observed. Probably, partial re-equilibration occurred during ascent or extrusion of the Monte Rosa nappe. Remarkably, however, the pressures obtained are almost always around 9-10 kbar, and for a time segment near 35-40 Ma. No significant regional pressure gradient could be documented for the high pressure stage of the metamorphic history of the nappe (Fig.9). Certainly we have found no evidence that the ultra-high pressure (UHP) conditions reported from the Lago di Cignana area (REINECKE, 1998; VAN DER KLAUW *et al.*, 1997), at the SW rim of the Monte Rosa nappe, have a continuation within the nappe. Similarly, no regional age progression is discernible, within the uncertainty of the available data for the exhumation stage (Fig.4d).

In samples taken to the East of Valle d'Ossola, the Barrovian overprint is strong and has traditionally been assumed to have obliterated most of the earlier high-pressure effects. However, the P-T-conditions indicated by the best-equilibrated of the samples presented in this study indicate a clear discrepancy to the Barrovian conditions

(TODD & ENGI, 1997) established for metapelites of adjacent tectonic units (cf. Fig.2b vs. Fig.9), for which pressures are at least 2-3 kbar lower. Assuming that the conditions documented by the multi-equilibrium thermobarometry correspond approximately to T_{max} and $P(T_{max})$, this discrepancy in pressure indicates that the Monte Rosa nappe reached its T_{max}-conditions during emplacement into the surrounding units, and somewhat earlier (i.e. at a deeper level) than these. Because the temporal constraints are not tight for this phase in adjacent units, no precise constraints on the dynamics of emplacement can be derived. However, this scenario provides a tempting explanation for the remarkable "protrusion" of the isotherms to the SW of the Lepontine dome, in that the rapid extrusion/emplacement of the Monte Rosa nappe may have introduced advective heat and possibly generated additional shear heating. This heat source would then have perturbed the simple geometry of the regional thermal anomaly depicted by the isotherm pattern further east (ENGI *et al*., 1995; TODD & ENGI, 1997). The temporal constraints available for the transition from high-pressure to Barrovian conditions in the Monte Rosa nappe certainly permit such an interpretation.

Relevant in this respect are also recent age data by ROMER *et al.* (1996) for a suite of dykes from eastern parts of the Monte Rosa nappe, which were very accurately dated for two localities. U-Pb ages were obtained from zircon at 30 to 28 Ma, and from xenotime at 26 Ma, all interpreted as dating the postkinematic emplacement of late magmatic aplites and pegmatites under waning metamorphic conditions.

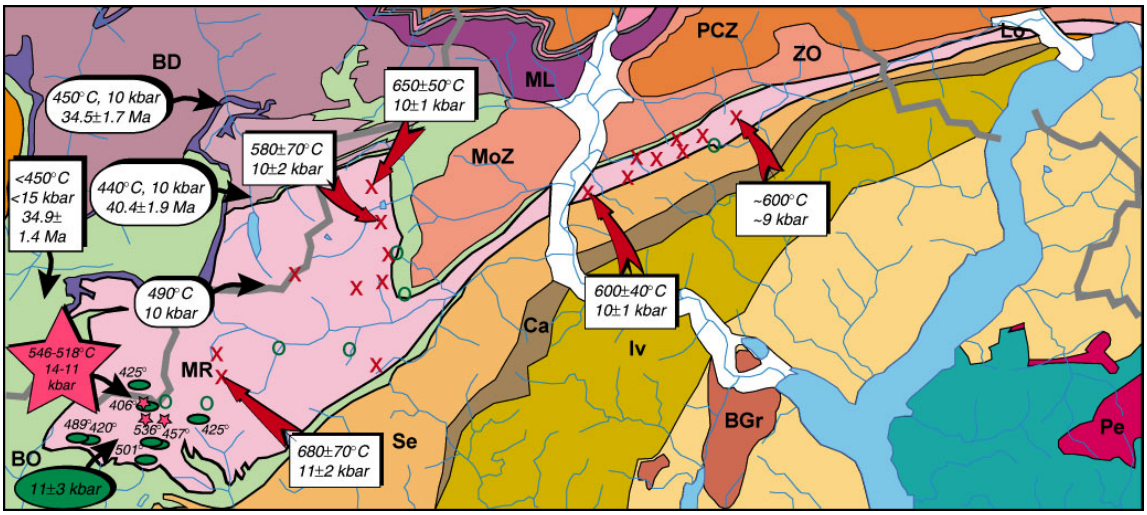

Figure 9: Comparison of metamorphic conditions derived for Alpine high-pressure (exhumation) stage in present study of metapelites, with data from the literature for other rock types. New data shown in rectangular boxes with broad arrows indicating sample locations; other symbols as in Figure 2.

5b. Behaviour of metapelites and monazite within these during polymetamorphism

One of the samples studied retains only Permian characteristics, presumably because it was not exposed to significant deformation or fluid-rock interaction during the Alpine cycle. In this case, both the assemblage of the rock forming minerals (see previous section) and the U-Th-Pb system in monazite are interpreted as having preserved a Variscan state (Table 2). These are remarkable results, as there is no doubt that these samples experienced subsequent subduction to at least lower crustal depth, involving reheating to 550-650°C and rapid extrusion in a convergent setting. We note that the classical study by KÖPPEL & GRÜNENFELDER (1975) reported dates on monazite separates from Monte Rosa granite and one of the metapelites (from Camplicciolli), and that both of these gave U-Pb ages of 260±5 Ma!

Many other samples retain partial Permian characteristics, including undisturbed monazite in porphyroblasts and –clasts, even where matrix recrystallisation caused complete resetting of the monazite grains in the micaschist portion of these samples. Rather few monazite grains indicate "mixed" ages, presumably due to old cores or domains having been overgrown by Alpine monazite. Such intragrain zoning in monazite has commonly been visualised by means of backscatter images in the EMP, and the main chemical cause is due to heterogeneity in Th contents. However, because EMP techniques are inadequate to date young monazite chemically (the limit being <100-200 Ma, depending on Th contents), and the spatial resolution of the μ-XRF and LA-ICPMS instruments is insufficient to resolve different age zones (Fig. 3) in single grains of the size available, “mixed ages” cannot be avoided in some cases.

The occurrence of old monazite inclusions in garnet is best explained if the garnet cores are also assumed to be of Permian age. This hypothesis is supported by chemical zoning patterns observed in some of the large garnet grains that show a homogeneous core surrounded by one or more growth rims (chemical profile in Fig.5). We thus think that the cores of such garnet grains are Permian in age, with the rim being due to Alpine metamorphism. It is not impossible, of course, that the entire garnet might be Alpine in age, but with its core portion simply having included old monazites. This interpretation would require garnet growth at an early Alpine stage prior to the recrystallisation of monazite. Because garnet shows a compositional change between core and the overgrowth rim, the Alpine growth of garnet would have had to be polyphase. The observed zoning patterns are thus more in agreement with a Permian origin.

Even in a sample with strong retrogression (Ti9801), monazite in a garnet retains a Permian age, whereas monazite in the chlorite-mica matrix yield mixed ages (Table 2; Fig. 2). The preservation of Permian monazites in matrix (see also sample Za9702), as well as the occurrence of mixed ages in a "Alpine" chlorite-mica matrix indicate that the presence of fluid and certain metamorphic conditions are not the only factors controlling the "resetting" of monazite. A process related to growth and/or recrystallisation of monazite is necessary to reset the monazite. Understanding monazite forming reactions is needed to use such data in deciphering the P-T-t evolution. Reactions of monazite are indicated by symplectites described in SCHERRER et al. (2001b) and can be also inferred from element compositions. For example, zoning patterns of yttrium in monazite, with enriched cores and depleted rims within the heterogeneous grains, support the observation and idea put forward by PYLE and SPEAR (1999) and FOSTER et al. (2000), i.e. that high yttrium monazite growth precedes garnet growth, whereas monazite growing after garnet nucleation tends to be depleted in yttrium. Xenotime has been observed in a few samples of the metapelite suite investigated here, but its grain size is insufficient for single grain dating by the methods employed.

6. Conclusions

New P-T-t data have been derived from the polymetamorphic basement rocks of the Monte Rosa nappe. ‘In-situ’ micro-dating of monazite by PIMMS and μ-XRF technology combined with thermobarometry has been successfully applied to improve the understanding of the complex polymetamorphic history of the Monte Rosa nappe. Two distinct phases of monazite growth emerged, first in the Permian (around 260 Ma ago), related to the intrusion of the Monte Rosa granite; then during Alpine orogeny, around 35 Ma ago, associated with high pressure metamorphism during Tertiary subduction/obduction.

As in other internal units of the Eastern, Central, and Western Alps, a prominent high pressure phase of Alpine age has been documented in the Monte Rosa nappe, reaching eclogite facies conditions during a narrowly constrained period of 40-35 Ma. The record is remarkably similar to that in the adjacent Zermatt-Saas Fee zone, to the Adula nappe, Cima Lunga complex, and the Mergoscia-Arbedo zone further East, and to the Gran Paradiso and Dora Maira further to the Southwest. These units show substantial differences in the internal structure, rock contents, and their pre-Alpine evolution. Similarities in the tectonic and temporal setting of the Alpine metamorphism does, however, suggest a coherent Alpine evolution. The present study contributes new constraints for its reconstruction. Given the present tectonic situation of the Monte Rosa nappe

with respect to the Southern Steep Belt and the Insubric Line, it appears that this lineament, or its precursor, acted as a guiding structural element in the hangingwall of the Alpine subduction channel, along which the nappe stack was exhumed. Unlike the highly fragmented and internally attenuated character of other units extruded from eclogite facies depth, such as the Adula nappe, the Cima Lunga complex, and the Mergoscia-Arbedo zone including Alpe Arami (ENGI et al., 2001), the Monte Rosa nappe shows that a rather massive, coherent tectonic body could be also exhumed along this same channel within the same time segment and, most likely, a similar overall transpressional regime.

Acknowledgements

This study is part of a PhD project supported by Schweizerischer Nationalfonds (Credit 20-49671.96/1 and 2000-055306.98/1). The EMP laboratory at the MPI Bern has been funded by Schweizerischer Nationalfonds (Credit 21-26579.89). Access to and support at the facilities of NIGL Nottingham, U.K., was made possible by R. Parrish and is gratefully acknowledged.

References

ARGAND, E., 1911. Les nappes de recouvrement des Alpes Pennines et leurs prologements structuraux. Matériaux pour la Carte Géologique de la Suisse; nouvelle série, 31.

BEARTH, P., 1939. Über den Zusammenhang von Monte Rosa- und Bernhard-Decke. Eclogae geologicae Helvetiae, 32(1), 101-111.

BEARTH, P., 1952. Geologie und Petrographie des Monte Rosa. Beiträge zur Geologischen Karte der Schweiz, Neue Folge, 96. Lieferung, 94.

BEARTH, P., 1958. Ueber einen Wechsel der Mineralfazies in der Wurzelzone des Penninikums. Schweizerische Mineralogische und Petrographische Mitteilungen, 38, 363-373.

BERMAN, R. G., 1991. Thermobarometry using multi-equilibrium calculations: a new technique, with petrological applications. Canadian Mineralogist, 29, 833-855.

BERMAN, R. G. & ARANOVICH, L. Y., 1996. Optimized standard state and mixing properties of minerals: I. Model calibration for olivine, orthopyroxene, cordierite, garnet, and ilmenite in the system FeO-MgO-CaO-Al2O3-SiO2-TiO2. Contributions to Mineralogy and Petrology, 126, 1-24.

BORGHI, A., COMPAGNONI, R. & SANDRONE, R., 1996. Composite P-T paths in the internal Penninic massifs of the western Alps: Petrological constraints to their thermo-mechanical evolution. Eclogae Geol Helv, 89(1), 345-367.

CHOPIN, C. & MONIÉ, P., 1984. A unique magnesiochloritoid-bearing, high-pressure assemblage from the Monte Rosa, Western Alps; petrologic and 40Ar-39Ar radiometric study. Contributions to Mineralogy and Petrology, 87, 388-398.

COMPAGNONI, R. & MAFFEO, B., 1973. Jadeite-bearing metagranites s.l. and related rocks in the Mount Mucrone area (Sesia-Lanzo Zone, western Italian Alps). Schweizerische Mineralogische und Petrographische Mitteilungen, 53, 355-378.

DAL PIAZ, G. V., 1964. Il cristallino antico del versante meridionale del Monte Rosa. Paraderivati a prevalente metamorfismo alpino. Rendiconti della Società Italiana di Mineralogia e Petrologia, 20, 101-136.

DAL PIAZ, G. V., 1966. Gneiss ghiandoni, marmi ed anfiboliti antiche del ricroprimento Monte Rosa nell'alte Val d'Ayas. Bolletino della Società Geologica Italiana, 85, 103-132.

DAL PIAZ, G. V., 1971. Nuovi ritrovamenti di cianite alpina nel cristallino antico del Monte Rosa. Rendiconti della Società Italiana di Mineralogia e Petrologia, 27(2), 437-477.

DAL PIAZ, G. V. & LOMBARDO, B., 1986. Early Alpine eclogite metamorphism in the Penninic Monte Rosa-Gran Paradiso basement nappes of the northwestern Alps. In: Blueschists and eclogites (eds Evans, B. W. & Brown, E. H.), pp. 249-265, Geological Society of America, Boulder, CO.

DAL PIAZ, G. V. & LOMBARDO, B., 1995. Alpine Tectonics and Metamorphism of the Western Alps. Guidebook for the Pre-Symposium Field Excursion. In: VII International Symposium on Antarctic Earth Sciences, pp. 61 p., Siena (Italy).

DUCHÊNE, S., BLICHERT-TOFT, J., LUAIS, B., TELOUK, P., LARDEAUX, J.M., ALBAREDE, F.1997. The Lu-Hf dating of garnets and the ages of the Alpine high-pressure metamorphism. Nature, 387, 586-589.

ELLIS, D. J. & GREEN, D. H., 1979. An experimental study of the effect of Ca upon garnet-clinopyroxene exchange equilibria. Contributions to Mineralogy and Petrology, 71, 13-22.

ENGI, M., BERGER, A. & ROSELLE, G. T., 2001. The role of the tectonic accretion channel (TAC) in a collisional orogen. Geology, (submitted).

ENGI, M., BERGER, A., ROSELLE, G. T., GRANDJEAN, V. & SCHERRER, N.C., 2000. Metamorphic evolution of the Central Alps: Significance of the subduction channel. International Geological Congress, Rio de Janeiro, Extended Abstract, 4.

ENGI, M., TODD, C. S. & SCHMATZ, D. R., 1995. Tertiary metamorphic conditions in the eastern Lepontine Alps. Schweizerische Mineralogische und Petrographische Mitteilungen, 75(3), 347-369.

FOSTER, G., KINNY, P., VANCE, D., PRINCE, C., HARRIS, N., 2000. The significance of monazite U-Th-Pb age data in metamorphic assemblages; a combined study of monazite and garnet chronometry. Earth and Planetary Science Letters, 181, 327-340.

FRANCHI, S., 1903. Sul rinvenimento di nuovi giacimente di roccie giadeitiche nelle Alpi occidentali e nell'Appennino ligure. Bolletino della Società Geologica Italiana, 22, 130-134.

FREY, M., HUNZIKER, J. C., O'NEIL, J. R. & SCHWANDER, H., 1976. Equilibrium-disequilibrium relations in the Monte Rosa granite, Western Alps: Petrological, Rb-Sr and stable isotope data. Contrib. Mineral. Petrol., 55, 147-179.

FREY, M. & MÄHLMANN FERREIRO, R., 1999. Alpine metamorphism of the Central Alps. Schweizerische Mineralogische Petrographische Mitteilungen, 79, 135-154.

FROITZHEIM, N., 1997. Mesozoic paleogeography and Alpine tectonics along transects in Eastern and Western Switzerland - consequences for the origin of the Monte Rosa nappe. In: Quaderni di Geodinamica Alpina e Quaternaria; 3rd Workshop on Alpine Geological Studies, pp. 53-54.

GEBAUER, D., 1999. Alpine geochronology of the Central and Western Alps: new constraints for a complex geodynamic evolution. Schweizerische Mineralogische und Petrographische Mitteilungen, 79, 191-208.

HUNZIKER, J. C., 1970. Polymetamorphism in the Monte Rosa, Western Alps. Eclogae geologicae Helvetiae, 63(1), 151-161.

HUNZIKER, J. C. & BEARTH, P., 1969. Rb-Sr-Altersbestimmungen aus den Walliser Alpen; Biotitalterswerte und ihre Bedeutung fuer die Abkühlungsgeschichte der alpinen Metamorphose. Eclogae Geologicae Helvetiae, 62, 205-222.

HUNZIKER, J. C., DESMONS, J. & HURFORD, A. J., 1992. Thirty-two years of geochronological work in the Central and Western Alps; a review on seven maps. Mém. Géol. Lausanne, 13.

HUNZIKER, J. C. & MARTINOTTI, G., 1984. Geochronology and evolution of the Western Alps: a review. Memorie della Società Geologica Italiana, 29, 43-56.

KÖPPEL, V. & GRÜNENFELDER, M., 1975. Concordant U-Pb ages of monazite and xenotime from the Central Alps and the timing of high temperature metamorphism, a preliminary report. Schweizerische Mineralogische und Petrographische Mitteilungen, 55, 129-132.

KÖPPEL, V., GÜNTHERT, A. & GRÜNENFELDER, M., 1981. Patterns of U-Pb zircon and monazite ages in polymetamorphic units of the Swiss Central Alps. Schweizerische Mineralogische und Petrographische

Mitteilungen, 61, 97-120.

KROGH, E. J., 1988. The garnet-clinopyroxene Fe-Mg geothermometer – a reinterpretation of existing experimental data. Contributions to Mineralogy and Petrology, 99, 44-48.

LANGE, S., NASDALA, L., POLLER, U., BAUMGARTNER, L. P. & TODT, W., 2000. Crystallization age and metamorphism of the Monte Rosa Granite, Western Alps. In: 17th Swiss Tectonic Studies Group Meeting, ETH Zürich.

MASSONNE, H.-J. & SCHREYER, W., 1987. Phengite geobarometry based on the limiting assemblage with K-feldspar, phlogopite, and quartz. Contributions Mineralogy Petrology, 96, 212-224.

MATTIROLO, E., NOVARESE, V., FRANCHI, S. & STELLA, A., 1913. Carta Geologica d'Italia, Foglio 29 Monte Rosa (1:100'000), Servizio Geologico Italiano.

MONIÉ, P., 1985. La methode 39Ar-40Ar appliquée au metamorphisme alpin dans le massif du Mont-Rose (Alpes occidentales); chronologie detaillée depuis 110 Ma. Eclogae Geologicae Helvetiae, 78, 487-516.

NAGEL, T., 2000. Metamorphic and structural history of the southern Adula nappe (Graubünden, Switzerland). Unpub. Ph.D. Thesis, University of Basel, Basel.

NAGEL, T., DE CAPITANI, C. & FREY, M., 2000. Isograds and PT-evolution in the eastern Lepontine Alps, Switzerland. Journal of Metamorphic Geology, (in print).

NIGGLI, E., 1970. Alpine Metamorphose und alpine Gebirgsbildung. Fortschritte Mineralogie, 47, 16-26.

NIGGLI, E. & NIGGLI, C., 1965. Karten der Verbreitung einiger Mineralien der alpidischen Metamorphose in den Schweizer Alpen (Stilpnomelan, Alkali-Amphibol, Chloritoid, Staurolith, Disthen, Sillimanit). Eclogae geologicae Helvetiae, 58, 335-368.

OBERHÄNSLI, R., HUNZIKER, J. C., MARTINOTTI, G. & STERN, W. B., 1985. Geochemistry, geochronology and petrology of Monte Mucrone: an example of eo-alpine eclogitization of Permian granitoids in the Sesia-Lanzo zone, western Alps, Italy. Chemical Geology, 52, 165-184.

PAQUETTE, J.-L., CHOPIN, C. & J.-J., P., 1989. U-Pb zircon, Rb-Sr and Sm-Nd geochronology of high- to very-high-pressure meta-acidic rocks from the western Alps. Contributions to Mineralogy and Petrology, 101, 280-289.

PARRISH, R.R. et al., 2001

PETTKE, T., DIAMOND, L.W. & KRAMERS, J.D. (2000): Mesothermal gold lodes in the north-western Alps: A review of genetic constraints from radiogenic isotopes. European Journal of Mineralogy, 12, 213-230.

PETTKE, T., DIAMOND, L. & VILLA, I., 1999. Mesothermal gold veins and metamorphic devolatilisation in the NW Alps: The temporal link. Geology, 27, 641-644.

PFIFFNER, M. & TROMMSDORFF, V., 1998. The high-pressure ultramafic-mafic-carbonate suite of Cima Lunga-Adula, Central Alps: Excursions to Cima di Gagnone and Alpe Arami. Schweizerische Mineralogische und Petrographische Mitteilungen, 78, 337-354.

PYLE, J.M. & SPEAR, F.S., 2000. An empirical garnet (YAG) - xenotime thermometer. Contributions to Mineralogy and Petrology, 138, 51-58.

REINECKE, T., 1998. Prograde high- to ultrahigh-pressure metamorphism and exhumation of oceanic sediments at Lago di Cignana, Zermatt-Saas Zone, western Alps. Lithos, 42(3-4), 147-189.

REINHARDT, B., 1966. Geologie und Petrographie der Monte-Rosa Zone, der Sesia-Zone und des Canavese im Gebiet zwischen Valle d'Ossola und Valle Loana. Schweizerische Mineralogische und Petrographische Mitteilungen, 46, 553-678.

ROBYR, M., MASSON, H. & STECK, A., 2000. The Gornergrat - Stockhorn area: a new geological interpretation. Abstract volume (unpubl.): Annual meeting of the Swiss Society for Mineralogy and Petrology, Winterthur, 12-13 October 2000.

ROMER, R. L., SCHÄRER, U. & STECK, A., 1996. Alpine and pre-Alpine magmatism in the root-zone of the western central Alps. Contrib Mineral Petrol, 123(2), 138-158.

ROSELLE, G. T., THÜRING, M. & ENGI, M., 2000. MELONPIT: A finite element code for simulating tectonic mass movement and heat flow within subduction zones. American Journal of Science, xxx.

RUBATTO, D. & GEBAUER, D., 1999. Eo/Oligocene (35 Ma) high-pressure metamorphism in the Gornergrat Zone (Monte Rosa, Western Alps): implications for paleogeography. Schweizerische Mineralogische und Petrographische Mitteilungen, 79, 353-362.

SCHERRER, N. C., ENGI, M., CHEBURKIN, A., PARRISH, R. R. & BERGER, A., 2001a. Non-destructive micro-dating of monazite by XRF technology. (in preparation).

SCHERRER, N. C., ENGI, M., GNOS, E., JAKOB, V. & LIECHTI, A., 2000. Monazite analysis; from sample preparation to microprobe age dating and REE quantification. Schweizerische Mineralogische und Petrographische Mitteilungen, 80(1), 93-105.

SCHERRER, N. C., GNOS, E. & CHOPIN, C., 2001b. Retrograde monazite-forming reactions in bearthite bearing high pressure rocks. Schweizerische Mineralogische und Petrographische Mitteilungen, (submitted).

SPICHER, A., 1980. Tektonische Karte der Schweiz, 1:500'000, Schweizerische Geologische Kommission.

TODD, C. S., 1998. Limits to GASP- thermobarometry in Ca-poor rocks such as metapelites. American Mineralogist, 83, 1161-1167.

TODD, C. S. & ENGI, M., 1997. Metamorphic field gradients in the Central Alps. Journal of Metamorphic Geology, 15(4), 513-530.

VAN DER KLAUW, S. N. G. C., REINECKE, T. & STOCKHERT, B., 1997. Exhumation of ultrahigh-pressure metamorphic oceanic crust from Lago di Cignana, Piemontese zone, western Alps: the structural record in metabasites. Lithos, 41(1-3), 79-102.

ZINGG, A. & HUNZIKER, J. C., 1990. The age of movements along the Insubric Line West of Locarno (northern Italy and southern Switzerland). Eclogae geol Helv, 83, 629-644.

APPENDIX A: TABLE 2. SAMPLE LIST

Samples collected by Nadim Scherrer, MPI Uni Bern

Sample	X-Coord	Y-Coord.	Alt.(m)	Location	Zone	Rocktype	Major components	Minor	Accessories	Reference
An9901	649,850	87,200	2095	SW of A. Ancium, W of P. Tignaga, just to the E of the little lake at 2103 m. Grt-bearing paragneisses bedded parallel to the Augengneisses. Apparently belonging to the MRZ	MRZ	Grt-bearing mica gneiss	Qtz, Bt, Ms, Grt, Chl	Tur	Ilm, Rt, Mnz	
Bi9801	667,200	102,600	640	Alpe Bisoggio, SE Beura	MRZ	Grt±St-Bt-Ms gneiss	Grt, St, Bt, Ms, Chl, Qtz, Kfs, Pl,		Ilm, Tu, Mnz	Reinhardt, B.
Bi9802	667,200	102,600	640	Alpe Bisoggio, SE Beura	MRZ	Grt±St-Bt gneiss	Grt, ± St, Bt, Ms, Chl, Qtz, Kfs, Pl		Ilm, Tu, Mnz, Zrn	
Bo9701	642,950	89,600	1250	Fornalei	? MoZ	Grt-amphibolite				
Ci9901	644,500	97,050	2920	between Ofentalpass and P. Cingino Sud	MRZ	Grt-bearing Ms gneiss				
CM9901	648,050	89,400	1410	S of Ceppo Morelli and N of P. Tignaga, just below A. Corte di Sotto where the trail crosses the creek (in the creek bed as well as along the trail on the NW side of the creek). The blocks (not in situ!!!) are most likely to originate off the flanks of Pt 1963	MRZ	Grt-amphibolite				
CN9701	675,750	104,850	2135	Costa Nera	SZ	Grt±St±Ky-Bt gneiss				Reinhart, B., 1966
CN9702	675,750	104,850	2135	Costa Nera	SZ	Grt±St±Ky-Bt gneiss				Reinhart, B., 1966
CS9701	636,100	84,900	2800	SW Colle d. Loccie, not in situ	MRZ	Grt-amphibolite				Bearth, P.
CS9702	636,100	84,900	2800	SW Colle d. Loccie, not in situ	MRZ	Grt-amphibolite				
CS9801	636,500	86,000	3380	E of Pta Tre Amici	MRZ	Grt-amphibolite	Amph, Grt, Qtz, Rt, Ilm, Zo,			Bearth, P.
CS9802	636,500	86,000	3380	E of Pta Tre Amici	MRZ	Grt-amphibolite	Amph, Grt, Qtz, Zo, Rt, Ilm, Spn, Cal			Bearth, P.
CS9803	635,700	86,175	3640	Rif. Resegotti	MRZ	Grt-amphibolite	Amph, Grt, Qtz, Pheng			
CV9801	670,400	103,050	1785	NE A. Corte Vecchia	MRZ	Grt±St-Bt gneiss				Reinhart, B., 1966
La9901	648,300	94,550	2645		MRZ	Grt-Bt-Ms schist				Bearth, P.
La9902	648,300	94,550	2645		MRZ	Grt-Bt-Ms schist				Bearth, P.
La9903	649,900	95,650	2690	between points 2657 and 2713 along Cresta di Lareccio. The band outcrops just SW of Pt 2713 trending NW-SE	MRZ	Grt-Bt-Ms schist				
La9904	649,900	95,650	2690	between points 2657 and 2713 along Cresta di Lareccio. The band outcrops just SW of Pt 2713 trending NW-SE	MRZ	Grt-Bt-Ms schist				
La9905	650,025	95,600	2635	collected not in situ but obviously within a few meters of its original position, overlaying the Grt-mica schist	MRZ	Grt-bearing Ms gneiss				
La9906	650,350	95,700	2620	SE of P. San Martino on the southern face of the SW ridge off Pt. 2733. Interesting for structural studies.	MRZ	Grt-bearing mica gneiss				
La9907	647,900	94,750	2785	between P. Lame (2792) and Psso delle Lonze along the ridge.	MRZ	Grt-Bt-Ms schist				Bearth, P.
La9908	647,800	94,700	2707	Psso delle Lonze	MRZ	Grt-Bt-Ms schist				Bearth, P.
Ma9711	709,075	115,850	320	Gordola	OZ	Grt-amphibolite				
Ma9712	709,175	115,600	226	Pt. 226, E side	LZ?	Grt-amphibolite				
Ma9713	709,170	115,605	226	Pt. 226, N side	LZ?	Grt-amphibolite				
MC9701	652,700	94,450	1510	N Min. d'oro dei Cani, not in situ	AZ	Grt-bearing Ep-amphibolite				
MC9702	652,700	94,450	1510	N Min. d'oro dei Cani, not in situ	AZ	Grt-Ep-amphibolite				
MC9703	652,800	94,600	1600	N Min. d'oro dei Cani	MoZ	Grt-Bt-Ms schist				
MC9704	652,800	94,650	1620	N Min. d'oro dei Cani	MoZ	Grt-bearing Sil-Bt gneiss				
MC9705	653,750	94,475	1430	NW Cingora	MoZ	Grt-Bt-Ms schist				
Mo9801	652,250	97,600	2385	W Pso. del Mottone	MRZ	Grt-bearing mica gneiss	Grt, tz, Ms, Bt, Chl, Ilm, Plag, Kfs,	Aln	Rt, Mnz	
Mo9802	652,250	97,600	2385	W Pso. del Mottone	MRZ	Grt-bearing mica gneiss	Grt, Qtz, Ms, Chl, Plag, Kfs, Ilm, Rt, Bt	Hem	Mnz, Aln	
Mo9803	651,000	95,950	2265	E P. San Martino	MRZ	Grt-bearing mica gneiss	Ms, Qtz, Bt, Grt, Ap,			Bearth, P.
Mo9804	651,050	95,950	2120	E P. San Martino	MRZ	Grt-bearing mica gneiss	Qtz, Bt, Ms, Chl, Grt, Kfs,		Ilm, Rt, Mnz	
Mo9805	651,050	95,950	2120	E P. San Martino	MRZ	amphibolite				
Pa9804	633,750	85,450	4385	E of Parrot Spitze	MRZ	Grt-amphibolite	Hbl, Bt, Qtz, Grt, Rt, Ilm, Spn,	Ap, Zo,		
PB9901	638,850	87,750	3175	Just below Pt 3180 (NW) on Pizzo Bianco	MRZ	Grt±St-Bt gneiss				Bearth
PB9902	638,850	87,750	3175	Just below Pt 3180 (NW) on Pizzo Bianco	MRZ	Grt±St-Bt gneiss				Bearth
PB9903	638,850	87,750	3175	Just below Pt 3180 (NW) on Pizzo Bianco	MRZ	Grt-Amphibolite				Bearth
PB9904	638,350	88,400	2610	Just SE of Pta C. Battisti on the northern side of Loccieciuse	MRZ	Grt±St-Bt gneiss				Bearth
Pi9701	670,900	104,800	1860	NW Pta I Pisoui, collected along the steep section of the trail just below the peak. According to Reinhardt, the location belongs to the outer shell of the antiform defined by the paragneisses (Grt-Bt-Ms schists)	MRZ	Grt-Bt-Ms schist	Qtz, Plag, Ms, Bt, Grt1, Grt2, Ilm, Ap		Zr, Mz, Rt, Aln	Reinhardt, B., 1966
Po9701	678,300	105,950	1750	NE La Porcella	MRZ	Grt-St-Bt-Ms schist				Reinhart, B., 1966
Po9702	678,300	105,950	1750	NE La Porcella	MRZ	Grt-St-Bt-Ms schist				Reinhart, B., 1966
Po9703	678,300	105,950	1750	NE La Porcella	MRZ	Grt-St-Bt-Ms schist	Qtz, Grt, Bt, Ms, St		Mnz, Zr	Reinhart, B., 1966
Pz9701	650,175	100,975	1270	NE L. di Antrona	MRZ	Grt-amphibolite	Hbl, Bt, Grt, Qtz, Ilm, Rt,		Hem	Bearth, P. 1957
Pz9702	650,350	100,750	1080	NE L. di Antrona	MRZ	Grt-bearing Sil-Bt gneiss				Bearth, P. 1957
Pz9703	651,250	103,200	1940	E of Forcola	MRZ	Grt-bearing Sil-Bt gneiss				Bearth, P. 1957
Pz9704	651,250	103,200	1940	E of Forcola	MRZ	Grt-bearing Sil-Bt gneiss				Bearth, P. 1957
Pz9905	649,325	103,075	2490	N of Cime di Pozzuoli (Pt 2602) on the northwards leading ridge at about 2490 m. Appearance is clearly distinctive from the monotonous light colored granit-gneisses.	MRZ	Grt±St-Bt gneiss				Bearth
Pz9906	649,325	103,075	2490	N of Cime di Pozzuoli (Pt 2602) on the northwards leading ridge at about 2490 m. Appearance is clearly distinctive from the monotonous light colored granit-gneisses.	MRZ	Grt±St-Bt gneiss				Bearth
Pz9907	650,200	100,350	1080	Along the SW corner of Lago di Antrona along the trail round the lake. The outcrop is just where the trail bends northwards after the bridge coming round clockwise.	MRZ	Grt±St-Bt gneiss				Bearth
Ra9701	675,600	105,550	2200	S side P. Ragno-Nona	MRZ	Grt-St-Bt-Ms schist				Reinhart, B., 1966
Ra9702	675,600	105,550	2200	S side P. Ragno-Nona	MRZ	Grt-St-Bt-Ms schist				Reinhart, B., 1966
Ra9703	675,250	105,050	2200	S P. Nona, W Costa Nera	MRZ	Grt-Hbl-Bt schist				Reinhart, B., 1966
Ra9704	675,900	105,750	2220	W of P. Ragno	MRZ	amphibolite				
Ra9705	675,900	105,750	2220	W of P. Ragno (next to Ra9704)	MRZ	amphibolite				Reinhardt, B.
Ra9706	675,300	105,450	2270	P. Nona, a few meters to the S along Costa Nera	? S of MRZ	Grt-bearing amphibolite				Reinhardt, B.
Ra9707	675,300	105,450	2270	P. Nona, a few meters to the S along Costa Nera	? S of MRZ	Grt-bearing amphibolite				Reinhardt, B.
Ra9708	675,300	105,450	2270	P. Nona, a few meters to the S along Costa Nera	? S of MRZ	Grt-bearing amphibolite				Reinhardt, B.
Ri9801	670,600	104,300	1450	NW A. Rina	MRZ	Grt±St-Bt gneiss	Bt, Ms, Chl, Grt, Qtz, Kfs, Ilm		Ap, Tur, Mnz	Reinhart, B., 1966
Ri9802	670,600	104,300	1450	NW A. Rina	MRZ	Grt±St-Bt gneiss	Qtz, Kfs, Chl, Ms, Bt, Chl, Grt, Pl	St, Ap	Ilm, Mnz, Aln	Reinhart, B., 1966
Ti9701	672,125	103,900	2110	S P. Tignolino	MRZ	Grt-Bt-Ms schist				Reinhart, B., 1966
Ti9801	671,300	103,550	1740	SW P. Tignolino	MRZ	Grt±St-Bt gneiss	Qtz, Ms, Chl, Grt, St, Ilm	Bt	Zr, Mz, Aln,	Reinhart, B., 1966
To9801	673,750	105,650	1895	NE of M. Togano, S of P. Marcio	MRZ	Grt-Tur-Bt-Ms schist	Qtz, Bt, Ms, Tur, Grt, Ilm, Pl	Hem	Zr, Mz,	Reinhart, B., 1966
To9802	673,850	104,550	2190	S of M. Togano	MRZ	Grt±St-Ms gneiss	Qtz, Ms, Ilm, Grt, St, Chl, Pl		Zr, Mz,	Reinhart, B., 1966

APPENDIX A: TABLE 2. SAMPLE LIST

Samples collected by Nadim Scherrer, MPI Uni Bern (continued)

Sample	X-Coord	Y-Coord.	Alt.(m)	Location	Zone	Rocktype	Major components	Minor	Accessories	Reference
Tr9801	652,025	95,800	2101	E L. di Trivera	AZ	Grt-bearing Ep-amphibolite				
Tr9902	651,000	99,050	1800	east of A. Larticcio at 1800 m where the trail crosses the gully with the main creek.	MRZ	Grt-Bt-Ms schist	Qtz, Ms, Bt, Grt, Ap	Ilm, Chl	Rt, Mnz,	Bearth, P.
Tr9903	651,800	98,800	2247	Point 2247 north of Psso di Trivera and SW of Punta di Trivera	MRZ	Grt-Bt-Ms schist				Bearth, P.
Tr9904	651,900	98,150	2300	just to the NE of Psso di Trivera	MRZ	Grt-bearing mica gneiss				Bearth, P.
VD9601	663,310	102,080	275	T. Ovesca, Villadossola	MRZ	Augengneiss				
VD9602	663,310	102,080	274	T. Ovesca, Villadossola	MRZ	Gabbro, ultramafic lens				
Vi9702	674,220	104,900	2195	SE M. Togano	MRZ	Grt-bearing mica schist	Grt, ±St, Bt, Ms, Pl, Qtz, Chl	Aln, Ilm, Tur	Xen, Zrn, Rt, Mnz	Reinhart, B., 1966
VL9601	681,450	106,400	1790	NW La Cima	SZ	Flasergabbro?				
VL9602	681,550	106,250	1790	SE La Cima	SZ	??				
Za9701	637.500	89,300	2140	E A. Pedriola, n.i.s.	MRZ	Ky-bearing Grt-Ms schist	Grt, Cld, Qtz,		Mnz	Bearth, P.
Za9702	637,300	89.450	2070	E A. Pedriola	MRZ	Grt-bearing Sil-Bt gneiss	Sil, Phe,Qtz, Grt (1+2)		Mnz	Bearth, P.
Za9703	637,350	89,675	2045	NE A. Pedriola, n.i.s.	MRZ	Ky-bearing Grt-Ms schist	Sil, St?, Phe->Bt		Rt, Ilm, Chl, Pl	Bearth, P.
Za9704	637,650	89,925	2060	NE A. Pedriola, n.i.s.	MRZ					Bearth, P.
Za9705	637,900	89,900	2070	NE A. Pedriola, n.i.s.	MRZ	Ky-bearing Grt-Ms schist				Bearth, P.

Monte Rosa samples collected by Sabine Pawlig, Uni Mainz

Sample	X-Coord	Y-Coord.	Alt.(m)	Location	Zone	Rocktype	Major components	Minor	Accessories	Reference
99SL-139				Monte Rosa, Val d'Ayas, Sabine Lange		Gneis am Rand der Scherzone				
99SL-145				Monte Rosa, Val d'Ayas, Sabine Lange		Ky-Ctd-Chl-Phen-Qz aus der Karbonatlinse				
99SL-148				Monte Rosa, Val d'Ayas, Sabine Lange		Ky-Ctd-Chl-Phen-Qz aus der Karbonatlinse				
99SL-159				Monte Rosa, Val d'Ayas, Sabine Lange		undeformierter Monte Rosa Granit				

Standards

FC-1	Canada	Monazite age standard (R. Parrish)
G1	Madagascar	Manangotry monazite standard (Poitrasson)
G1b	Madagascar	Manangotry monazite standard (Poitrasson)
G1c	Madagascar	Manangotry monazite standard (Poitrasson)
G7	Sri Lanka	Sri Lanka monazite standard (Reusser)

APPENDIX B: AGE LIST

Note: These data should be interpreted only on the basis of the information contained within the Grain Database on CD

Samples collected by Nadim Scherrer, Uni Bern (Monte Rosa nappe)

Sample	Grain	Code	µ-XRF Age	± 2s	208/232 cor	±2s	208/232 unc.	EMP core	±2s	EMP rim	TIMS	±2s	Context
An9901	An91C_a	ii2e	129	30				261	140	133			single matrix monazite
An9901	An91C_g	ii2f	76	20				87	50				single matrix monazite
An9901	An91C_j	ii2g	67	19	42.4	1	64.5	15	30				single matrix monazite
An9901	An91C_o	ii2h	102	38									single matrix monazite
An9901	An9901C_k in grt	iii2h	369	31	330.1	8.2	331.4	270	96				monazite inclusion in garnet
Bi9801	Bi9801a	i4c			32.1	0.8	35.6						cluster matrix monazite
Bi9801	Bi9801a mx25-4	ii4h	32	15	26	0.6							single matrix monazite
Bi9801	Bi9801a_p	iii3h	42	10									single matrix monazite
Bi9801	Bi9801a_q in grt	iii3g	211	47									monazite inclusion in garnet
Bi9802	Bi9802b1.sp	i4d	56	35	32.6	1.1	46.8						single matrix monazite
Mo9804	Mo9804_w	ii1h	38	11	40.7	1.1	50.4						monazite reaction texture
Po9703	Po73_b2	ii1a											zircon
Po9703	Po73_e	ii1b	33	14	36.6	0.8	42.8	265	82				single matrix monazite
Po9703	Po73_m	ii1c	67	17									single matrix monazite
Po9703	Po73_q	ii1d	58	15				73	60				single matrix monazite
Po9703	Po73_r	ii1e	39	14	32.8	0.8	39.9						single matrix monazite
Ri9801	Ri9801a	i4e	36	41									single matrix monazite
Ri9801	Ri9801a_a	iii4f	36	14							35.6	1	single matrix monazite
Ri9801	Ri9801a_M7	iii4g	48	21							33.5	1	single matrix monazite
Ti9801	Ti81_a	ii3a	221	25									single matrix monazite
Ti9801	Ti81_b-c	ii3b	240	39				549	126				single matrix monazite
Ti9801	Ti81_g	ii3c	289	29	325.4	7.9	329.2	309	120				single matrix monazite
Ti9801	Ti81_h	ii3d	281	46				335	130				single matrix monazite
Ti9801	Ti81_l in grt	ii3e	303	44									monazite inclusion in garnet
Ti9801	Ti81_m	ii3f	244	37									single matrix monazite
Ti9801	Ti81_n	ii3g	276	30				310	148				single matrix monazite
To9801	To81_f in grt	ii2a	23	22				196	120				monazite inclusion in garnet
To9801	To81_k-o in grt	ii2b	22	24									monazite inclusion in garnet
To9801	To81_q	ii2c	46	22				131	88				single matrix monazite
To9801	To81_r	ii2d	22	13	30.9	0.7	34.6						single matrix monazite
To9801	To81zus_a in tur	ii4a											zircon
To9801	To81zus_b in tur	ii4b	29	16									monazite inclusion in tourmaline
To9801	To81zus_c in grt	ii4c	27	15									monazite inclusion in garnet
To9801	To81zus_d matrix	ii4d											single matrix monazite
To9801	To81zus_e matrix	ii4e	30	13									single matrix monazite
Tr9902	Tr92_b	iii3a	61	16	34.7	0.8	43.9						cluster matrix monazite
Tr9902	Tr92_f	iii3b	44	13	39.9	1	45.8	43	52				monazite reaction texture
Tr9902	Tr92_l	iii3c	37	13	35.5	0.8	43.4						monazite reaction texture
Tr9902	Tr92_m	iii3d	46	8	33.6	0.9	47.4						monazite reaction texture
Tr9902	Tr9902_a in grt	iii4a	212	35				183	100	66			monazite inclusion in garnet
Tr9902	Tr9902_b in grt	iii4b	204	33				269	55				monazite inclusion in garnet
Tr9902	Tr9902_f	iii4c	41	10									monazite reaction texture
Tr9902	Tr9902_g	iii4d	38	12									monazite reaction texture
Tr9902	Tr9902_h-i	iii4e	34	8									monazite reaction texture
Tr9902	Tr9902a_d	iii3f	50	17	46.4	1.8	83.9	17	34				monazite reaction texture
Tr9904	Tr9904_a in grt	ii3h	351	55				264	100				monazite inclusion in garnet
Tr9904	Tr9904_d_xe	iv1a											xenotime
Tr9904	Tr9904_e xe	iii3e											xenotime
Vi9702	Vi9702a_m2 in grt	ii1f	303	54				144	104				monazite inclusion in garnet
Vi9702	Vi9702a mo25-3	ii1g	31	18									single matrix monazite
Za9702	Za72_d	iii2a											zircon
Za9702	Za72_h	iii2b	293	34	251.6	5.3	255.9	413	134				single matrix monazite
Za9702	Za72_j	iii2c											single matrix monazite
Za9702	Za72_l	iii2d	288	23	251.2	5.6	253.5	561	120				single matrix monazite
Za9702	Za72_m	iii2e											monazite intergrown with ilmenite
Za9702	Za72_o	iii2f	298	29	273.4	6.2	276.7						single matrix monazite
Za9702	Za72_p	iii2g	292	21	262.1	5.8	265.4	417	80				single matrix monazite
Za9703	Za9703b_d	ii4f			42.9	3	156.7						single matrix monazite
Za9703	Za9703b_f	ii4g	55	17									single matrix monazite
Za9703	Za9703b_h	iii4h	41	12									single matrix monazite
Za9705	Za75_a zoned	iii1a	138	22	145.5	5	152.9	291	116				single matrix monazite
Za9705	Za75_h zoned	iii1b	213	33	268.3	5.7	269.1	291	100	46			single matrix monazite
Za9705	Za75_j	iii1c	52	16	30.4	4.5	42.3	66	100				single matrix monazite

Samples collected by Nadim Scherrer, Uni Bern (Monte Rosa nappe) continued

Sample	Grain	Code	µ-XRF Age	± 2s	208/232 cor	±2s	208/232 unc.	EMP core	±2s	EMP rim	TIMS	±2s	Context
Za9705	Za75_o	iii1d	36	16	289.6	120.4	348	72	61				single matrix monazite
Za9705	Za75_p	iii1e	25	4	46.1	1.1	50						single matrix monazite
Za9705	Za75_r	iii1f	61	32									single matrix monazite
Za9705	Za75_s in grt	iii1g	303	52	287.9	6.2	291.2	283	112				monazite inclusion in garnet
Za9705	Za75_t in grt	iii1h	259	14	252.7	6.5	259.3	299	94				monazite inclusion in garnet
Za9705	Za9705_b qg_28/11/99	i4f	281	24	280.8	7.2	285.8						monazite inclusion in garnet

Monazite age standards, MPI, Uni Bern

Sample	Grain	Code	µ-XRF Age	± 2s	208/232 cor	±2s	208/232 unc.	EMP core	±2s	EMP rim	TIMS	±2s	Context
FC-1	FC-1 std	FC-1 std	55.3	2.3	54.4	1.5	55.1				54.3	1	standard
G1	G1_std	i4G	542.9	24.6	564.4	14.3	564.7	519	98		555	10	standard
G7	G7_std	i4h	487.9	20.8	482	10.8	482.2	454	66				standard

Samples collected by Sabine Pawlig of Uni Mainz (SW Monte Rosa nappe, Italy)

Sample	Grain	Code	µ-XRF Age	± 2s	208/232 cor	±2s	208/232 unc.	EMP core	±2s	EMP rim	TIMS	±2s	Context
99SL-139	99SL-139_mo	i3e	69	22									cluster matrix monazite
99SL-139	99SL-139_xe	i3c											xenotime
99SL-139	99SL-139_zi	i3d											zircon
99SL-145	99SL-145_1	i2d	42	23	39	0.9	41.9						cluster matrix monazite
99SL-145	99SL-145_2	i2e			36.1	0.9	43						cluster matrix monazite
99SL-145	99SL-145_3	i2f											cluster matrix monazite
99SL-145	99SL-145_g	i3f	100	100	27	2.4	67.2						cluster matrix monazite
99SL-145	99SL-145_h	i3g	98	32	102	3.1	110.8						cluster matrix monazite
99SL-145	99SL-145_i	i3a											cluster matrix monazite
99SL-145	99SL-145_s	i2g			137.1	5.8	173.3						cluster matrix monazite
99SL-145	99SL-145_v	i3b	33	34	31.6	0.7	36.1						cluster matrix monazite
99SL-145	99SL-145_w	i2h											cluster matrix monazite
99SL-148	99SL-148_j	i3h											cluster matrix monazite
99SL-159	99SL-159_b	i4a			222.9	5.4	283						single matrix monazite
99SL-159	99SL-159_e	i4b			222.4	5.3	237						single matrix monazite

Samples collected by Tivadar Toth (Carpathians, Hungary)

Sample	Grain	Code	µ-XRF Age	± 2s	208/232 cor	±2s	208/232 unc.	EMP core	±2s	EMP rim	TIMS	±2s	Context
1131	1131_g	i1a	361	38									single matrix monazite
1131	1131_m	i1b	369	43	328.5	7.1	353.8	257	122				single matrix monazite
1131	1131_n	i1c	303	74									single matrix monazite
4960	4960	i1f	353	50									single matrix monazite
5176	5176_i	i1d	347	57									single matrix monazite
5176	5176_j	i1e	377	50	332.6	7	344.7	243	72				single matrix monazite

Sample collected by Ph. Häuselmann (Val Vergeletto, Switzerland)

Sample	Grain	Code	µ-XRF Age	± 2s	208/232 cor	±2s	208/232 unc.	EMP core	±2s	EMP rim	TIMS	±2s	Context
PD79	PD79_1	i1g	268	20	295.6	6.3	298.1						single matrix monazite
PD79	PD79_2	i1h	344	52									monazite inclusion in garnet
PD79	PD79_e	i2c											single matrix monazite
PD79	PD79_j	i2a	298	24	289	6.2	289.7	165	100				single matrix monazite
PD79	PD79_n	i2b	282	57	279.5	6	281.4	161	100				single matrix monazite

Poster presentation at The Allan White Symposium: 'S-type granites and related rocks'
La Trobe University, Melbourne, Australia, 11.-12. January 2001

Micro-dating of monazite by new XRF-microprobe technology applied to polymetamorphic rocks of the Monte Rosa nappe

by N.C. Scherrer[1], A. Cheburkin[2], M. Engi[1] & R. Parrish[3]

Abstract

A newly developed XRF-microprobe at the Institute of Mineralogy and Petrology, University of Bern, Switzerland, has been applied for precise chemical Th-U-Pb dating of individual monazite grains separated from Pb-free polished petrographic thin sections.

The instrument performance was tested on a dataset of over 70 monazite grains individually drilled from 25 thin sections characterised by electron microprobe. 14 samples were selected so as to regionally represent the pre-granitic basement rocks (garnet-mica gneiss) of the Monte Rosa gneiss nappe (western Central Alps).

Summarising the geological results, there are two distinct phases of monazite growth in these polymetamorphic rocks apparent: one during Permian times (280 ± 40 Ma), and a younger phase of Alpine age (35 ± 10 Ma). The two age groups occur side by side at thin section scale but they are clearly separated by context: the younger ones are restricted to grains within the matrix, and the older ones to monazite inclusions in garnet, or, more rarely, inherited cores of large matrix grains. Of all sampled sites there are two exceptions to this rule, i.e. where all dated grains (matrix and inclusions) fall into the older category. Monazite in these two rocks must have largely escaped the effects of Alpine metamorphism, which included eclogite facies conditions (Eocene) followed by amphibolite facies conditions (Oligocene).

The non-destructive nature of the XRF-microprobe permitted a comparative study of dating methods by sequentially applying chemical dating by electron microprobe analysis (EMPA), chemical dating by XRF-microprobe analysis, and isotopic $^{208}Pb/^{232}Th$ dating by LA-PIMMS (Laser-Ablation Plasma Ionisation Multi Mass Spectrometry) analysis.

As an example, the precision achieved with the XRF-microprobe for a well characterised monazite age standard FC-1 (TIMS age 54.3 Ma; µ-XRF age 55.3 ± 2.6 Ma), doubly polished to 30 µm in thickness, is below 5 % (2 sigma) after 90 minutes integration time (50 kV; 30 mA) at a spatial resolution of 90 µm. The sample characteristics are: 200-300 ppm of Pb (µ-XRF), 3.8-5.1 wt% of Th (EMPA) and 0.4-1.4 wt% U (EMPA).

Combined with an electron microprobe and conventional optical microscopy, the XRF-microprobe is thus a competitive low-cost and non-destructive alternative to more costly isotopic methods. The XRF-microprobe is easy to use and maintain.

[1] Institute of Mineralogy and Petrology, University of Bern Switzerland. <scherrer@mpi.unibe.ch>; <engi@...>
[2] Dept. of Earth Sciences, Laurentian University, Canada <acheburkin@nickel.laurentian.ca>
[3] NIGL, British Geological Survey, Nottingham, U.K. <rrp@nigl.nerc.ac.uk>

MICRO-DATING OF MONAZITE BY NEW XRF-MICROPROBE TECHNOLOGY APPLIED TO POLYMETAMORPHIC ROCKS OF THE MONTE ROSA NAPPE, WESTERN CENTRAL ALPS, ITALY.

N.C. Scherrer1, A. Cheburkin2, M. Engi1 & R. Parrish3

1 Institute of Mineralogy and Petrology, University of Bern Switzerland <scherrer@mpi.unibe.ch>, <engi@mpi.unibe.ch> ;
2 Dept. of Earth Sciences, Laurentian University, Canada <acheburkin@nickel.laurentian.ca>;
3 NIGL, British Geological Survey, Nottingham, U.K. <rrp@nigl.nerc.ac.uk>

http://www.earthsci.unibe.ch/groups/xrf/XRF.html

The XRF-microprobe...

micro-XRF analyser
of the
Institute of Mineralogy and Petrology
University of Bern, Switzerland

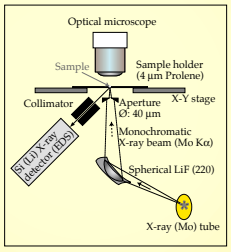

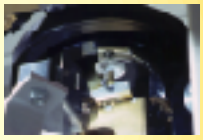

EDS-spectra suitable for chemical Th-U-Pb dating

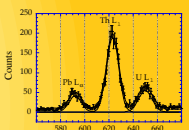

roughly

Pbtotal/Thtotal = 208Pb/232Th = f(t) since Th/U in monazite is >100

$$Pbtotal = \frac{Thtotal * [\exp(1232*t)-1]*208}{232} + \frac{0.9928 * Utotal * [\exp(1238*t)-1]*206}{238} + \frac{0.0072 * Utotal * [\exp(1235*t)-1]*207}{238} = f(t)$$

XRF-microprobe performance in non-destructive chemical Th-U-Pb age determination...

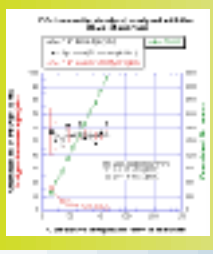

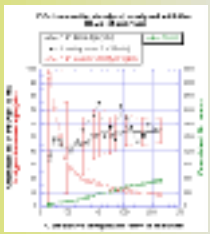

Standard monazites:

	FC-1 Manangotry Mnz	
µ-XRF	55.3 ± 2.3 Ma	554 ± 13 Ma
TIMS	54.3 ± 1.5 Ma	555 ± 6 Ma (NIGL)
TIMS	552 ± 4 Ma (KU)	

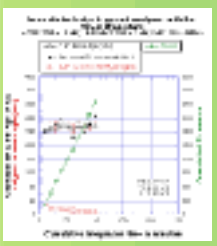

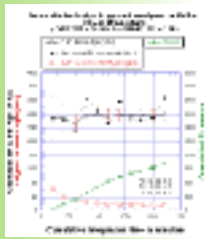

Dating monazite in polymetamorphic pelites. What are we analysing? We'd like to know...

Finding monazite made easy...

Polymetamorphic rocks may have a long history with multiple stages of monazite growth.
Unlike with conventional heavy liquid separation techniques, staying with doubly polished petrographic thin sections is far more informative, since...
there often is a clear distinction of multiple monazite generations by textural context: monazite occurring...

... as shielded inclusions in garnet

... as porphyroblastic relics

... as newly formed matrix grains

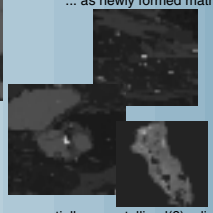

...as partially recrystallised(?) relics ...with inherited(?) components

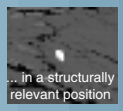

... in a structurally relevant position

...as symplectitic monazite

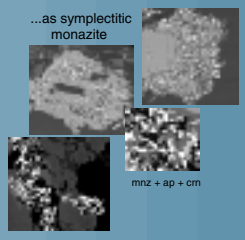

mnz + ap + crn

...with complex internal heterogeneity

...with no apparent polyphase growth

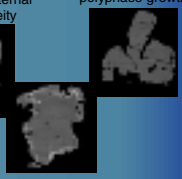

...with distinct core to rim morphology

Searching, mapping and quantifying monazite by EMP analysis...

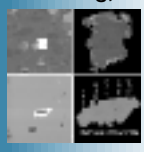

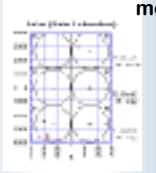

Za9705 h CORE		Za9705 h RIM	
average of n =	3	average of n =	2
Y2O3	2.197	Y2O3	0.342
La2O3	13.768	La2O3	9.881
Ce2O3	27.411	Ce2O3	25.963
Nd2O3	11.292	Nd2O3	13.827
PbO	0.085	PbO	0.027
ThO2	4.987	ThO2	6.786
UO2	0.553	UO2	1.212
Age Ma	291 ± 98	Age Ma	47 ± 66

Drilling out single grains from Pb-free polished thin sections...

Perform µ-XRF analysis, followed by an independent technique, e.g. LA-ICPMS and compare...

Application to polymetamorphic pelites of the Monte Rosa nappe, western Central Alps, Italy

Geologic overview of the Monte Rosa nappe

Ages of monazites in the matrix

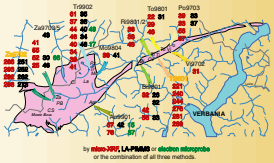

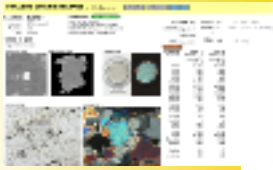

monophase growth matrix monazite

< polyphase growth with core and rim

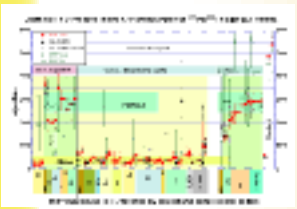

Ages of monazite inclusions in garnet

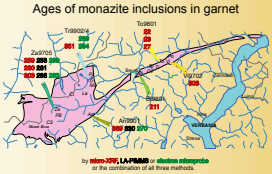

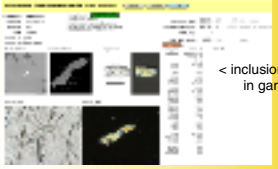

< inclusion in garnet >

Brief educational resume of Nadim Cornelius Scherrer

2 February 1971	born in Wattwil SG, Switzerland, son of Albert and Anita Scherrer-Keller
1972 - 1975	resident of São Paolo, Brasil, with Pascal, Erica and Margrit joining the family
1975 - 1977	Kindergarten in Rothrist AG, Switzerland
1978 - 1984	Primary school in Rothrist AG (1. - 3.) und Herisau AR (3. - 6.)
1984 - 1985	Secondary school in Herisau AR
1985 - 1991	High school in Appenzell AI with completion of Matura Type B
1992 - 1994	Bachelor of Science, University of New England, Armidale, NSW, Australia.
1994	Naturalization to become an Australian citizen
1995 - 1996	Bachelor of Science with Honours, University of New England, Australia, awarded with a University medal. Thesis title: "The Application of Palaeomagnetic Techniques to Speleothems".
1997 - 2000	PhD and part-time research assistant at the Institute of Mineralogy and Petrology, University of Bern, Switzerland. Dissertation: "Behaviour of Monazite and Evolution of Polymetamorphic Pelites from the Monte Rosa Nappe, Western Central Alps, Italy", funded by the Swiss National Fonds.